CONIDIO-FORMS: IDENTIFYING AND CHARACTERIZING NATURAL MORPHOLOGICAL VARIATION IN *NEUROSPORA CRASSA* CONIDIOPHORES

by

EMILY KRACH

(Under the Direction of Jonathan Arnold)

ABSTRACT

The classic filamentous fungus *Neurospora crassa* propagates asexually through the dissemination of conidia. These spores are produced through specialized structures called conidiophores. While the genetic, environmental, and circadian cues guiding conidiophore development are well understood, little is known about the morphological variation of these structures, particularly in wild populations. In other filamentous fungi, conidiophore architecture has been shown to impact both spore dispersal patterns and pathogenicity. This dissertation utilizes a wild population collection of 21 strains from Louisiana, USA to explore natural conidiophore morphological variation. We identified three novel and distinct architectural phenotypes, named Wild-Type (WT), Wrap, and Bulky, that are upheld throughout conidiophore development. We show that these phenotypes have ecological implications through sporulation and germination behavior, particularly in different environments. To screen morphology in a high-throughput manner, we developed an automatic image classifier specifically designed to assign conidiophore phenotype. After conducting crosses, this tool was used to classify progeny conidiophores to fit a genetic model for heritability. Lastly, we performed RNA-

Sequencing to identify genes differentially expressed in the mycelia and conidiophores of strains representing each conidiophore phenotype, finding that the Bulky strain exhibits a unique transcriptional profile from that of WT and Wrap. Together, this work lends novel insight to phenotypic variation of the conidiophore and its robustness to environmental perturbations, as well as genetic differences underlying this variation in a natural population.

INDEX WORDS: Neurospora crassa, conidiophore, natural variation, sporulation, germination, convolutional neural network, generalized linear model, transcriptomics

CONIDIO-FORMS: IDENTIFYING AND CHARACTERIZING NATURAL MORPHOLOGICAL VARIATION IN *NEUROSPORA CRASSA* CONIDIOPHORES

by

EMILY KRACH

BS, University of Maryland, 2016

A Dissertation Submitted to the Graduate Faculty of The University of Georgia in Partial Fulfillment of the Requirements for the Degree

DOCTOR OF PHILOSOPHY

ATHENS, GEORGIA

2021

CONIDIO-FORMS: IDENTIFYING AND CHARACTERIZING NATURAL MORPHOLOGICAL VARIATION IN *NEUROSPORA CRASSA* CONIDIOPHORES

by

EMILY KRACH

Major Professor:	Jonathan Arnold
Committee:	Alexander Bucksch
	Jonathan Eggenschwiler
	Zachary Lewis
	Leidong Mao

Electronic Version Approved:

Ron Walcott
Vice Provost for Graduate Education and Dean of the Graduate School
The University of Georgia
December 2021

ACKNOWLEDGEMENTS

First, I must thank Jonathan Arnold for his unwavering patience, support, and guidance in my scientific training. I am incredibly grateful for his encouraging me to carve out my own area of research and explore professional interests outside the laboratory. Jonathan has cultivated a lab environment that is kind, collaborative, and genuinely fun, and it has been an absolute privilege to learn there. I thank Arnold Lab members past and present for their vibrant scientific discussion and friendship, especially Michael Judge, James Griffith, Mary Case, Michael Skaro, and Jia Hwei-Cheong. My committee members have also been instrumental in propelling this project forward. I am thankful to Alex Bucksch, Jonathan Eggenschwiler, Zack Lewis, and Leidong Mao for providing their time and expertise.

I would also like to acknowledge xPD and the Innovation Gateway at UGA. Their programming and professional development opportunities have diversified my graduate training and undoubtedly advanced the trajectory of my career.

I am indebted to my friends, new and old, for their love, encouragement, and patience. The friendships I have built in Athens will last far beyond my time here. I am so thankful to them for making this experience a whole lot of fun. Despite being hundreds of miles away, my friends from home have always felt like they're right here. I thank them for keeping me close and lifting me up. My life is made substantially richer by having such fiercely loyal and loving people in it.

My DanceFX family has made Athens feel like home. I thank them for providing me with a place to let loose and move freely, both literally and figuratively. It has been an absolute honor and inspiration to be their teacher, student, teammate, and friend.

Lastly, and most importantly, I acknowledge my family, Mom, Dad and Michelle. I simply would not be here without them. I thank them for always supporting me, pushing me, and assuring me that anything is achievable with hard work and perseverance. I owe this accomplishment to them.

TABLE OF CONTENTS

LIST OF TABLES

Page

LIST OF FIGURES

Page

CHAPTER 1

INTRODUCTION AND LITERATURE REVIEW

Introduction to *Neurospora crassa*

Neurospora crassa has served as a model eukaryote in laboratories for over 100 years. The pink bread mold was initially identified as a contaminant in French bakeries in the 1840s and has since proven integral for foundational studies in molecular genetics, population genetics, biochemistry, cell biology, photobiology, circadian biology, ecology, evolution, and development (Davis, 2000). In nature, the heterothallic ascomycete typically grows on burned vegetation in tropical and subtropical regions but has been detected into northern conifer forests (Perkins and Turner 1988; Jacobson et al. 2004). *N. crassa* is particularly useful for genetic studies, as it has a relatively short generation time, and a complete knockout collection is readily available through the Fungal Genetics Stock Center (Colot et al 2006). Many genes in the Neurospora genome do not have homologues in the unicellular model *Saccharomyces cerevisiae*, suggesting it serves as a better model for higher order eukaryotes (Osiewacz, 2002). While *N. crassa* is not pathogenic, close filamentous fungal relatives such as *Aspergillus*, *Magnaporthe,* and *Fusarium* are pathogenic. Principles learned by studying *N. crassa* are often conserved between ascomycetes and could provide critical insight into these pathogenic relatives.

N. crassa is an attractive model for developmental studies due to its complex yet easily traceable life cycle, depicted in Figure 1.1. This life cycle consists of at least 28 morphologically distinguishable cell types (Bistis et al. 2003). While it does have a sexual

life cycle, *N. crassa* spends the majority of its life cycle developing in the following vegetative process. Haploid spores called conidia germinate and give rise to filamentous hyphae. Hyphae exhibit polarized growth, branch, and fuse with nearby compatible filaments to form a complex filamentous network called a mycelium (Riquelme et al. 2011). Incomplete cross walls called septa allow movement of cytoplasm and organelles between multinucleate compartments throughout the filament. Environmental stressors such as nutrient deprivation and desiccation stimulate the conidiation pathway, beginning with the development of aerial hyphae (Ruger-Herreros and Corrochano 2020). These specialized filaments undergo a series of buddings and constrictions to generate macroconidiophores, structures responsible for the production of new multinucleate macroconidia (Springer 1993). *N. crassa* also generates uninucleate microconidia through the development of microconidiophores, though these spores do not germinate and likely exclusively serve to fertilize the female protoperithecia in nature (Maheshwari, 1999). Microconidiophore development is independent and unique from that of macroconidiophores. Conidiophore development is more thoroughly reviewed below in next section.

As previously mentioned, *N. crassa* also undergoes a more complex sexual life cycle when strains of opposite mating types, A and a, meet (Shear and Dodge, 1927). Low-nitrogen and carbon environmental conditions induce development of the protoperithecium, which is fertilized by a conidium through specialized hyphae called trichogynes (Westergaard and Mitchell 1947; Bistis 1981). Fusion of nuclei is followed by two meiotic divisions and an additional mitotic division, yielding eight haploid ascospores within a sac called an ascus (Springer 1993; Davis, 2000). Ascospores are then

ejected from the ascus and able to germinate after heat or chemical activation (Dodge 1912; Emerson 1948). Germinated ascospores give rise to vegetative hyphae, allowing the asexual life cycle described above to continue. This mating process takes roughly three weeks to conduct in the laboratory, allowing relatively quick generation of and high-throughput selection of recombinant progeny.

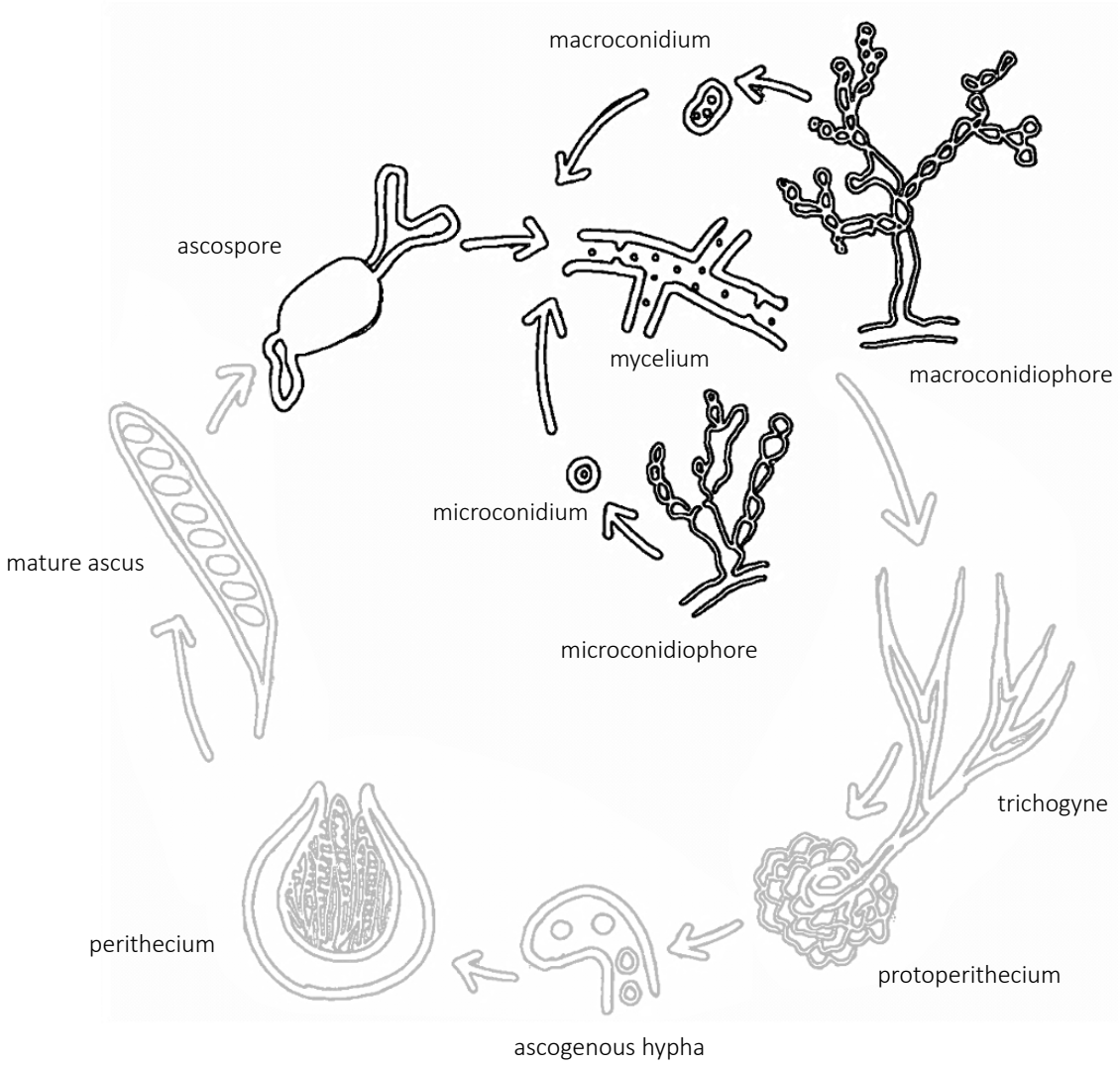

Figure 1.1. ***Neurospora crassa*** **life cycle.** The vegetative life cycle is depicted in black and the sexual cycle in gray.

Conidiophore Development

Macroconidiophore development is induced by aeration, desiccation, nutrient deprivation, low carbon dioxide levels, and exposure to light (Sargent and Kaltenborn 1972; Nelson et al. 1975) for reproduction, dispersal, and survival under harsh environmental conditions (Springer 1993). *N. crassa* develops functionally, morphologically, and developmentally distinct macro- and microconidia, where macroconidia are multinucleate and microconidia are small, uninucleate, lesser in abundance, and later to develop (Springer and Yanofsky 1989). When discussing conidia and development of conidiophores, I am hereon referring to the macroconidiation process, as this is the developmental process around which this dissertation work is based.

Development of the conidiophore is initiated by differentiation into aerial hyphae that grow perpendicularly from the surface mycelium. Many genes have been identified that reduce aerial hypha growth (*vad-5, ve-1, cmd*), alter aerial hypha morphology (*cpt, cr-1, fr*), and inhibit aerial hypha development altogether (*sk*) (Ruger-Herreros and Corrochano 2020; Laxmi and Tamuli 2017; Springer and Yanofsky 1989). This process takes 1-2 hours, after which the organism switches to a budding form of growth to develop proconidial chains (Springer and Yanofsky 1989). First, minor constriction budding occurs, requiring genes *aconidiate-2* (*acon-2*) and *fluffyoid* (*fld*), followed by a switch to major constriction budding involving genes *aconidiate-3* (*acon-3*) and *fluffy* (*fl*) (Springer and Yanofsky 1989). The organism often reverts to hyphal growth during minor constriction budding; however, this switch no longer occurs once major constriction budding begins. *Fluffy* is considered the major regulator of conidiation in *N. crassa* and is the most thoroughly characterized of the previously mentioned genes. The gene encodes

a zinc cluster protein that activates downstream conidiation-specific (*con*) genes *con-6* and *con-10* (Bailey and Ebbole 1998). Over-expressing *fl* triggers conidiophore development without the otherwise necessary environmental cues (Bailey-Shrode and Ebbole, 2004). The *fl* mutant inhibits conidiation before major constriction budding and generates a striking cotton-looking phenotype (Bailey-Shrode and Ebbole 2004). This phenotype is also achieved by disruption of *flb-3*, an ortholog to the *Aspergillus nidulans* regulator of conidiation *FlbC* (Boni et al. 2018). Interestingly, the *rca-1* gene complements another regulator of conidiation in *A. nidulans*, *FlbD*, but has no clear role in conidiation in *N. crassa* (Shen et al 1998). Each time a new bud in the conidiophore is formed, it undergoes a subroutine of bud formation and nuclear migration involving genes *gran* and *tng* (Springer and Yanofsky 1989). After this roughly eight-hour process, septa develop between buds and thicken to form double-doublets. Each developing conidium is then further segmented by the formation of connective tissue (Springer and Yanofsky 1989). Conidial separation genes *csp-1* and *csp-2* are required for the subsequent release of conidia for dispersal into the environment, signifying the end to this roughly twelve-hour developmental process (Selitrennikoff et al 1974; Springer and Yanofsky 1989). The morphological stages throughout conidiophore development are shown in Figure 1.2.

Conidiophore development is strictly regulated by the circadian clock (Loros and Dunlap 2001). Light activates the white-collar complex (WCC), a heterodimer of transcription factors WC-1 and WC-2 (Ballario et al 1996; Linden and Macino 1997; Crosthwaite et al 1997). The WCC regulates transcription of *fl*, *con-6*, and *con-10*, binding directly to the promoter region of the major regulator to induce its transcription (Dong et al 2008; Olmedo et al 2010; Olmedo et al 2010). The FL protein is essential for

transcription of the *clock controlled gene ccg-2* (*eas*), which begins roughly one hour into the conidiation process (Lauter, Russo and Yanofsky 1992). To induce *ccg-2* expression, there is transient expression of *fl* during the aerial hyphae stage before its peak at six hours described above (Correa and Bell-Pedersen 2002). The *ccg-2* gene encodes a hydrophobin that coats developing and mature conidia, making the spores highly hydrophobic and air dispersible (Bell-Pedersen et al. 1992). Light has also been observed to regulate expression of conidiation-specific genes *con-5* and *con-13* (Dong et al 2008; Ruger-Herreros and Corrochano 2020). Through this rhythmic conidiation cycle, the clock is easily marked by a visible switching of cell type, making *N. crassa* an incredibly valuable tool through which to study circadian biology.

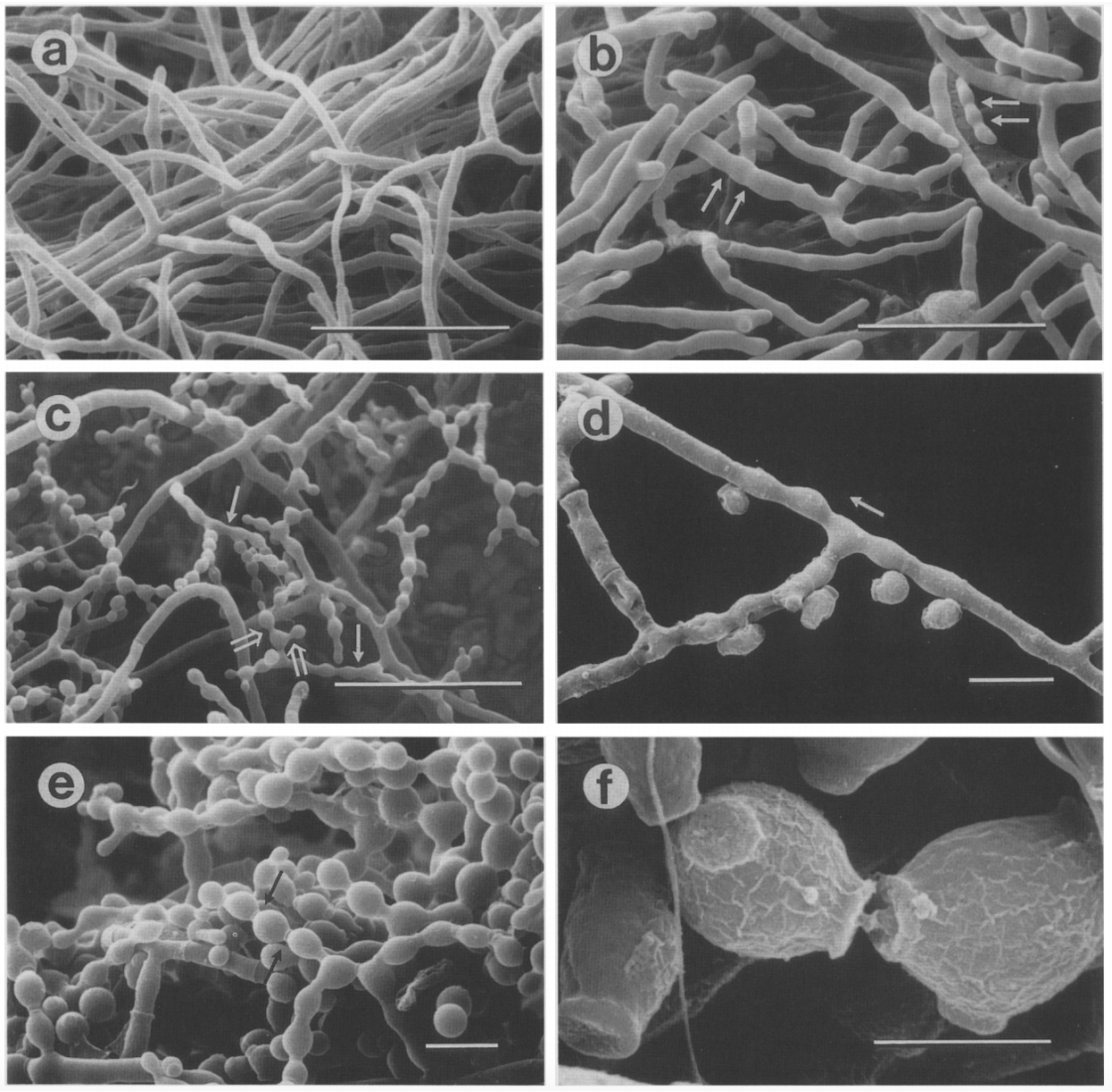

Figure 1.2. Scanning electron micrographs of developing wild-type conidiophores. (a) Vegetative hyphae, 0 hours. (b) Minor constriction chains, 4 hours. Arrows point to constrictions. (c) Major constriction chains, 8 hours. Double-line arrows point to major constrictions; small arrows point to minor constrictions. (d) Minor constriction chain reverting to hyphal growth, 4-8 hours. Arrow denotes direction of growth. (e) Conidiophore with cross-walls (arrows), 12 hours. (f) Connective tissue between two mature conidia, 16 hours. Scale bar lengths are as follows: (a-c), 50 μm; (d-e), 10 μm; (f) 5 μm. Adapted from Springer and Yanofsky, 1989.

Wild Isolates of *N. crassa*

Widespread collection of wild *Neurospora* species began in 1968 in tropical and subtropical regions around the world (Perkins et al 1976). Today, there are over 5,000 wild isolates of *N. crassa* readily available through the Fungal Genetics Stock Center (FGSC). Conidia from visible colonies were collected primarily from burned substrates, sampling seven to ten isolates from each site whenever possible. *Neurospora* is capable of growing prolifically on the burned remnants of many plant species. The organism especially thrives on succulents and monocots with pithy stems and sugary sap, but it is also commonly found on freshly burned wood (Perkins and Turner 1988). Because of this diversity, collection substrates were recorded in general terms such as "burned grass" instead of identifying the particular plant species from which an isolate originated (Perkins and Turner 1988).

N. crassa was most abundantly found in the state of Louisiana, which is where the conventional laboratory reference strain, OR74A (FGSC2489) originated. Subsequent phylogenomic work has revealed that the 20 Louisiana isolates show no population subdivision, unlike other wild collections from a region, making them an ideal tool and appropriately sized collection for studies on a single population (Ellison et al 2011). All isolates in the Louisiana population collection were gathered from burned substrates, offering a point of consistency to their life histories (Perkins and Turner 1988). For these reasons, the Louisiana strains were used for the studies presented in this dissertation (Krach et al 2020). It is possible that these wild isolates may be heterokaryotic, containing nuclei of different genotypes. However, when harvested from an undisturbed burned substrate, each colony should theoretically be derived from a single heat-activated ascospore and thus

be homokaryotic (Perkins and Turner 1988). Regardless, it is important to consider the possibility of heterogeneity when conducting studies with these wild populations.

The use of wild *Neurospora* populations has both provided genetic variants for laboratory studies as well as offered insight into the population biology and evolutionary history of the organism (Gladieux et al 2020). For example, studies on wild isolates have revealed variants in genes encoding proteins such as tyrosinase, trehalase and cellulase, and elucidated key genetic differences governing vegetative incompatibility and ascus morphology (Perkins et al 1976). More recently, genomic approaches have been applied to further characterize evolutionary history and genetic variation both within and between wild populations. The Louisiana isolates were used to characterize the evolution of *het* loci, genes known to control self-recognition (Zhao et al 2015). Comparing *N. crassa* isolates from Louisiana and the Caribbean revealed diverged genomic regions containing genes known to protect against cold temperatures, suggesting that populations had adapted to the climate from which they originated (Ellison et al 2011). This hypothesis was confirmed by measuring the growth rates of strains from each region at different temperatures, where strains from the cooler Louisiana had increased fitness at lower temperatures (Ellison et al 2011).

RNA-sequencing (RNA-seq) has also been a tool successfully employed to explore transcriptomic variation in the Louisiana population collection. Mycelia from this population was genotyped by RNA-seq to elucidate a novel locus involved in germling communication (Palma-Guerrero et al 2013). The same transcriptomic dataset was later used to reveal functions in four unannotated genes related to hyphal morphology, carbon and nitrogen metabolism, and amino acid starvation resistance (Ellison et al 2014).

Notably, these studies were based on gene expression in the hyphal filaments, and no work has yet been done to explore transcriptomic variation in other cell types of a wild population.

Study Motivation and Summary

Conidiophore development and the subsequent dissemination of conidia is critical for propagation of the *N. crassa* vegetative life cycle, a process that is fairly conserved throughout filamentous fungi. The environmental, genetic, and circadian cues guiding conidiophore development are well understood; however, little is known about the morphological variation of these structures, particularly in natural populations. So, what? Why bother studying morphology? Though morphology merely refers to the shape, size, and patterning of a structure, it provides a crucial foundation for the understanding of function, development, taxonomy, heredity, and evolution of that structure and/or organism. Natural selection acts on morphological traits to influence evolution, enabling multicellular organisms with dynamic life cycles and complex morphologies to thrive (Bonner 1974). The *N. crassa* life cycle alone contains 28 morphologically distinct cell types (Bistis et al. 2003). Fungi adapt their form to accommodate constantly changing environments, boasting an astounding ability to maximize fitness throughout a wide array of environmental perturbations (Brown et al. 2021). Such morphological adaptations often have profound implications on the growth, proliferation, virulence, and population dynamics of the organism.

Conidiophore architecture has been shown to affect spore dispersing capacity of *Aspergillus niger* and pathogenicity of *Magnaportha grisea* (Wang et al, 2015; Lau and

Hamer, 1998). Though *Neurospora* is not pathogenic, conidiophore morphological variation observed, the environmental and genetic bases for it, and downstream impacts of that variation could very likely be conserved in its pathogenic relatives. Previous work has successfully employed wild isolates of *Cryptococcus neoformans* to explore morphotype-associated pathogenicity (Wang and Lin, 2012). Pathogenicity aside, conidiophore development has critical implications on the evolution of fungi through its effect on dissemination throughout an environment. Wild isolates of *N. crassa* are readily available through the Fungal Genetics Stock Center and provide an excellent tool through which to study naturally occurring conidiophore architectural variation.

It is difficult to survey phenotypic variation of a complex trait in a high-throughput manner. This has been done in other model fungal systems, like *Saccharomyces cerevisiae*, to attribute genes to phenotypic traits (Ohya et al. 2005). Morphological diversity presents an attractive opportunity through which to conduct phenomics, as has been done in yeast and plant root systems (Ohya et al. 2015; Zhao et al. 2019). Tools such as Digital Imaging of Root Traits (DIRT) have been developed to automatically quantify over 70 architectural traits of a root structure in a high-throughput way (Das et al. 2015). Such studies are important for capturing and quantifying the wide spectrum of phenotypic diversity, especially in different environments. Screening populations for phenotypic variation within them also allows downstream omics studies to uncover genes associated with novel and complex phenotypes.

The purpose of this dissertation work is to identify and characterize natural morphological variation in *N. crassa* conidiophores. In Chapter 2, we surveyed a wild population collection of 21 isolates for conidiophore morphological variation, identifying

three novel and distinct architectural phenotypes. We confirmed that conidiophore phenotype is upheld throughout the duration of its development and showed that it impacts subsequent spore dispersal. To estimate heritability of this trait, we conducted crosses between groups and quantified conidiophore phenotypes of the resulting progeny. To execute these quantifications in a high-throughput manner, we developed an automated image classifier uniquely designed to assign conidiophore phenotype. We were able to successfully fit an inheritance model for the trait using these phenotype assignments. To our knowledge, this is the first report examining natural morphological variation in the *N. crassa* conidiophore and developing a high-throughput phenotyping method for this cell type.

Chapter 3 builds upon the findings in Chapter 2, further characterizing the effects of and genes underlying conidiophore morphology in this wild population. We elaborate on the impact of conidiophore phenotype on spore dispersal and show that conidiophore morphology also affects germination in different environments. To increase the robustness of our heritability estimate, we conducted additional crosses between homokaryotic strains and quantified phenotypes of the resulting progeny using the classification method developed in Chapter 2. We used these counts to fit an inheritance model, where the estimated heritability increased from that presented in the previous chapter. To identify genes contributing to the unique morphologies of this cell type, we performed RNA-Sequencing on both mycelia and conidiophores of representative strains from each phenotypic group. Taken together, the work presented in this dissertation reveals three novel conidiophore phenotypes, characterizes downstream ecological impacts of them, and

identifies genes differentially expressed with conidiophore morphology: a complex trait that has not previously been explored in wild *N. crassa* populations.

References

Bailey, L. A., & Ebbole, D. J. (1998). The fluffy gene of Neurospora crassa encodes a Gal4p-type C6 zinc cluster protein required for conidial development. *Genetics, 148*(4), 1813-1820. doi:10.1093/genetics/148.4.1813

Bailey-Shrode, L., & Ebbole, D. J. (2004). The fluffy gene of Neurospora crassa is necessary and sufficient to induce conidiophore development. *Genetics, 166*(4), 1741-1749. doi:10.1534/genetics.166.4.1741

Ballario, P., Vittorioso, P., Magrelli, A., Talora, C., Cabibbo, A., & Macino, G. (1996). White collar-1, a central regulator of blue light responses in Neurospora, is a zinc finger protein. *Embo j, 15*(7), 1650-1657.

Bell-Pedersen, D., Dunlap, J. C., & Loros, J. J. (1992). The Neurospora circadian clock-controlled gene, ccg-2, is allelic to eas and encodes a fungal hydrophobin required for formation of the conidial rodlet layer. *Genes Dev, 6*(12a), 2382-2394. doi:10.1101/gad.6.12a.2382

Bistis, G. N. (1981). Chemotropic Interactions between Trichogynes and Conidia of Opposite Mating-Type in Neurospora crassa. *Mycologia, 73*(5), 959-975. doi:10.2307/3759806

Bistis, G. N., D.D. Perkins, and N.D. Read. (2003). Different Cell Types in Neurospora crassa. *Fungal Genetics Reports, 50*. doi:https://doi.org/10.4148/1941-4765.1154

Boni, A. C., Ambrósio, D. L., Cupertino, F. B., Montenegro-Montero, A., Virgilio, S., Freitas, F. Z., . . . Bertolini, M. C. (2018). Neurospora crassa developmental control mediated by the FLB-3 transcription factor. *Fungal Biol, 122*(6), 570-582. doi:10.1016/j.funbio.2018.01.004

Bonner, J. T. (1974). *On Development: The Biology of Form*: Harvard University Press.

Brown, A. J. P., Cowen, L. E., Pietro, A. d., Quinn, J., Heitman, J., & Gow, N. A. R. (2017). Stress Adaptation. *Microbiology Spectrum, 5*(4), 5.4.04. doi:doi:10.1128/microbiolspec.FUNK-0048-2016

C.L. Shear, B. O. D. (1927). Life histories and heterothallism of the red bread-mold fungi of the monolia sitophila group. *Journal of Agricultural Research, 34*.

Colot, H. V., Park, G., Turner, G. E., Ringelberg, C., Crew, C. M., Litvinkova, L., . . . Dunlap, J. C. (2006). A high-throughput gene knockout procedure for Neurospora reveals functions for multiple transcription factors. *Proc Natl Acad Sci U S A, 103*(27), 10352-10357. doi:10.1073/pnas.0601456103

Correa, A., & Bell-Pedersen, D. (2002). Distinct signaling pathways from the circadian clock participate in regulation of rhythmic conidiospore development in Neurospora crassa. *Eukaryot Cell, 1*(2), 273-280. doi:10.1128/ec.1.2.273-280.2002

Crosthwaite, S. K., Dunlap, J. C., & Loros, J. J. (1997). Neurospora wc-1 and wc-2: Transcription, Photoresponses, and the Origins of Circadian Rhythmicity. *Science, 276*(5313), 763-769. doi:doi:10.1126/science.276.5313.763

Das, A., Schneider, H., Burridge, J., Ascanio, A. K. M., Wojciechowski, T., Topp, C. N., . . . Bucksch, A. (2015). Digital imaging of root traits (DIRT): a high-throughput

computing and collaboration platform for field-based root phenomics. *Plant Methods, 11*(1), 51. doi:10.1186/s13007-015-0093-3

Davis, R. H. (2000). *Contributions of a Model Organism*. New York: Oxford University Press.

Dodge, B. O. (1912). Methods of culture and the morphology of the archicarp in certain species of the

Ascobolaceae. *Bulletin of the Torrey Botanical Club*.

Dong, W., Tang, X., Yu, Y., Nilsen, R., Kim, R., Griffith, J., . . . Schüttler, H. B. (2008). Systems Biology of the Clock in Neurospora crassa. *PLOS ONE, 3*(8), e3105. doi:10.1371/journal.pone.0003105

Ellison, C. E., Hall, C., Kowbel, D., Welch, J., Brem, R. B., Glass, N. L., & Taylor, J. W. (2011). Population genomics and local adaptation in wild isolates of a model microbial eukaryote. *Proc Natl Acad Sci U S A, 108*(7), 2831-2836. doi:10.1073/pnas.1014971108

Ellison, C. E., Kowbel, D., Glass, N. L., Taylor, J. W., & Brem, R. B. (2014). Discovering functions of unannotated genes from a transcriptome survey of wild fungal isolates. *mBio, 5*(2), e01046-01013. doi:10.1128/mBio.01046-13

Emerson, M. R. (1948). Chemical Activation of Ascospore Germination in Neurospora crassa. *J Bacteriol, 55*(3), 327-330. doi:10.1128/jb.55.3.327-330.1948

George N. Bistis, D. D. P., Nick D. Read. (2003). Different cell types in Neurospora crassa. *Fungal Genetics Reports, 50*. doi:https://doi.org/10.4148/1941-4765.1154

Gladieux, P., De Bellis, F., Hann-Soden, C., Svedberg, J., Johannesson, H., & Taylor, J. W. (2020). Neurospora from Natural Populations: Population Genomics Insights

into the Life History of a Model Microbial Eukaryote. *Methods Mol Biol, 2090*, 313-336. doi:10.1007/978-1-0716-0199-0_13

Jacobson, D. J., Powell, A. J., Dettman, J. R., Saenz, G. S., Barton, M. M., Hiltz, M. D., . . . Natvig, D. O. (2004). Neurospora in temperate forests of western North America. *Mycologia, 96*(1), 66-74.

Krach, E. K., Wu, Y., Skaro, M., Mao, L., & Arnold, J. (2020). Wild Isolates of Neurospora crassa Reveal Three Conidiophore Architectural Phenotypes. *Microorganisms, 8*(11). doi:10.3390/microorganisms8111760

Lau, G. W., & Hamer, J. E. (1998). Acropetal: a genetic locus required for conidiophore architecture and pathogenicity in the rice blast fungus. *Fungal Genet Biol, 24*(1-2), 228-239. doi:10.1006/fgbi.1998.1053

Lauter, F. R., Russo, V. E., & Yanofsky, C. (1992). Developmental and light regulation of eas, the structural gene for the rodlet protein of Neurospora. *Genes Dev, 6*(12a), 2373-2381. doi:10.1101/gad.6.12a.2373

Laxmi, V., & Tamuli, R. (2017). The calmodulin gene in Neurospora crassa is required for normal vegetative growth, ultraviolet survival, and sexual development. *Arch Microbiol, 199*(4), 531-542. doi:10.1007/s00203-016-1319-0

Linden, H., & Macino, G. (1997). White collar 2, a partner in blue-light signal transduction, controlling expression of light-regulated genes in Neurospora crassa. *Embo j, 16*(1), 98-109. doi:10.1093/emboj/16.1.98

Loros, J. J., & Dunlap, J. C. (2001). Genetic and molecular analysis of circadian rhythms in Neurospora. *Annu Rev Physiol, 63*, 757-794. doi:10.1146/annurev.physiol.63.1.757

Maheshwari, R. (1999). Microconidia of Neurospora crassa. *Fungal Genet Biol, 26*(1), 1-18. doi:10.1006/fgbi.1998.1103

Ohya, Y., Sese, J., Yukawa, M., Sano, F., Nakatani, Y., Saito, T. L., . . . Morishita, S. (2005). High-dimensional and large-scale phenotyping of yeast mutants. *Proceedings of the National Academy of Sciences of the United States of America, 102*(52), 19015. doi:10.1073/pnas.0509436102

Olmedo, M., Ruger-Herreros, C., & Corrochano, L. M. (2010). Regulation by blue light of the fluffy gene encoding a major regulator of conidiation in Neurospora crassa. *Genetics, 184*(3), 651-658. doi:10.1534/genetics.109.109975

Olmedo, M., Ruger-Herreros, C., Luque, E. M., & Corrochano, L. M. (2010). A complex photoreceptor system mediates the regulation by light of the conidiation genes con-10 and con-6 in Neurospora crassa. *Fungal Genet Biol, 47*(4), 352-363. doi:10.1016/j.fgb.2009.11.004

Osiewacz, H. D. (2002). *Molecular biology of fungal development*. New York; Basel: Marcel Dekker.

Palma-Guerrero, J., Hall, C. R., Kowbel, D., Welch, J., Taylor, J. W., Brem, R. B., & Glass, N. L. (2013). Genome Wide Association Identifies Novel Loci Involved in Fungal Communication. *PLOS Genetics, 9*(8), e1003669. doi:10.1371/journal.pgen.1003669

Perkins, D. D., Radford, A., & Sachs, M. S. (2000). *The Neurospora Compendium: Chromosomal Loci*.

Perkins, D. D., & Turner, B. C. (1988). Neurospora from natural populations: Toward the population biology of a haploid eukaryote. *Experimental Mycology, 12*(2), 91-131. doi:https://doi.org/10.1016/0147-5975(88)90001-1

Perkins, D. D., Turner, B. C., & Barry, E. G. (1976). STRAINS OF NEUROSPORA COLLECTED FROM NATURE. *Evolution, 30*(2), 281-313. doi:https://doi.org/10.1111/j.1558-5646.1976.tb00910.x

R.F. Nelson, C. P. S., R.W. Siegel. (1975). Cell changes in Neurospora. *Results and Problems in Cell Differentiation*, 291-310.

Riquelme, M., Yarden, O., Bartnicki-Garcia, S., Bowman, B., Castro-Longoria, E., Free, S. J., . . . Watters, M. K. (2011). Architecture and development of the Neurospora crassa hypha -- a model cell for polarized growth. *Fungal Biol, 115*(6), 446-474. doi:10.1016/j.funbio.2011.02.008

Ruger-Herreros, C., & Corrochano, L. M. (2020). Conidiation in Neurospora crassa: vegetative reproduction by a model fungus. *International Microbiology, 23*(1), 97-105. doi:10.1007/s10123-019-00085-1

Sargent, M. L., & Kaltenborn, S. H. (1972). Effects of Medium Composition and Carbon Dioxide on Circadian Conidiation in Neurospora12. *Plant Physiology, 50*(1), 171-175. doi:10.1104/pp.50.1.171

Selitrennikoff, C. P., Nelson, R. E., & Siegel, R. W. (1974). Phase-specific genes for macroconidiation in Neurospora crassa. *Genetics, 78*(2), 679-690. doi:10.1093/genetics/78.2.679

Shen, W. C., Wieser, J., Adams, T. H., & Ebbole, D. J. (1998). The Neurospora rca-1 gene complements an Aspergillus flbD sporulation mutant but has no identifiable role in

Neurospora sporulation. *Genetics, 148*(3), 1031-1041. doi:10.1093/genetics/148.3.1031

Springer, M. L. (1993). Genetic control of fungal differentiation: the three sporulation pathways of Neurospora crassa. *Bioessays, 15*(6), 365-374. doi:10.1002/bies.950150602

Springer, M. L., & Yanofsky, C. (1989). A morphological and genetic analysis of conidiophore development in Neurospora crassa. *Genes Dev, 3*(4), 559-571. doi:10.1101/gad.3.4.559

Wang, F., Dijksterhuis, J., Wyatt, T., Wösten, H. A., & Bleichrodt, R. J. (2015). VeA of Aspergillus niger increases spore dispersing capacity by impacting conidiophore architecture. *Antonie Van Leeuwenhoek, 107*(1), 187-199. doi:10.1007/s10482-014-0316-z

Wang, L., & Lin, X. (2012). Morphogenesis in Fungal Pathogenicity: Shape, Size, and Surface. *PLOS Pathogens, 8*(12), e1003027. doi:10.1371/journal.ppat.1003027

Westergaard, M., & Mitchell, H. K. (1947). NEUROSPORA V. A SYNTHETIC MEDIUM FAVORING SEXUAL REPRODUCTION. *American Journal of Botany, 34*(10), 573-577. doi:https://doi.org/10.1002/j.1537-2197.1947.tb13032.x

Zhao, C., Zhang, Y., Du, J., Guo, X., Wen, W., Gu, S., . . . Fan, J. (2019). Crop Phenomics: Current Status and Perspectives. *Frontiers in Plant Science, 10*(714). doi:10.3389/fpls.2019.00714

Zhao, J., Gladieux, P., Hutchison, E., Bueche, J., Hall, C., Perraudeau, F., & Glass, N. L. (2015). Identification of Allorecognition Loci in Neurospora crassa by Genomics

and Evolutionary Approaches. *Mol Biol Evol, 32*(9), 2417-2432. doi:10.1093/molbev/msv125

CHAPTER 2

WILD ISOLATES OF *NEUROSPORA CRASSA* REVEAL THREE CONIDIOPHORE ARCHITECTURAL PHENOTYPES[1]

[1] Krach, E.K., Y. Wu, M. Skaro, L. Mao, and J. Arnold. 2020. *Microorganisms*. 8(11): 1760. Reprinted here with the permission of the publisher.

Abstract

The vegetative life cycle in the model filamentous fungus, *Neurospora crassa,* relies on development of conidiophores to produce new spores. Environmental, temporal, and genetic components of conidiophore development have been well characterized; however, little is known about their morphological variation. We explored conidiophore architectural variation in a natural population using a wild population collection of 21 strains from Louisiana, USA. Our work reveals three novel architectural phenotypes: Wild Type, Bulky, and Wrap, and shows their maintenance throughout the duration of conidiophore development. Furthermore, we present a novel image-classier using a convolutional neural network specifically developed to assign conidiophore architectural phenotypes in a high-throughput manner. To estimate an inheritance model for this discrete complex trait, crosses between strains of each phenotype were conducted and conidiophores of subsequent progeny were characterized using the trained classifier. Our model suggests that conidiophore architecture is controlled by at least two genes and has a heritability of 0.23. Additionally, we quantified the number of conidia produced by each conidiophore type and their dispersion distance, suggesting that conidiophore architectural phenotype may impact *N. crassa* colonization capacity.

Introduction

Neurospora crassa propagates asexually through the dissemination of haploid spores, conidia, which develop via specialized aerial structures called conidiophores (Davis 2000). Macroconidiophores give rise to macroconidia and are morphologically and developmentally distinct from their smaller counterparts, microconidiophores, which give

rise to uninuclear microconidia (Maheshwari 1999). Since macroconidiophores are the subject of this work, they will be hereafter referred to simply as conidiophores. Development of conidiophores is under strict environmental and temporal control, requiring cues such as desiccation, nutrient deprivation, and light exposure for its induction (Sargent and Kaltenborn 1972). After exposure to these environmental triggers, aerial hyphae grow perpendicular to the preceding mycelial mat to stimulate conidiophore development. The organism subsequently undergoes a series of constriction budding followed by crosswall formations until eventual sporulation, roughly 10 hours following the beginning of this process (Springer and Yanofsky 1989). It is through this dissemination of conidia that the vegetative life cycle can propagate, thus allowing new filaments to germinate after a period of dormancy. Conidiophore development is under strict circadian control, requiring activation of the white collar complex (WCC) by light for activation of *fluffy* (*fl*), a necessary regulator of conidiophore development (Olmedo, Ruger-Herreros, and Corrochano 2010; Bailey-Shrode and Ebbole 2004). While environmental, temporal, and genetic components of conidiophore development in *N. crassa* have been well characterized (Greenwald et al. 2010), little is known about morphological variation of these structures, particularly in natural populations.

In other filamentous fungal species, conidiophore architecture has been shown to directly impact the ability of an organism to disseminate throughout an environment and infect host tissues. For example, conidiophore morphology is altered in *Aspergillus niger* following deletion of *velvetA*, directly impacting both spore dispersion and colonization capacity of the organism (Wang et al. 2015). Additionally, mutating the *acropetal* locus of *Magnaporthe grisea* modifies arrangement of the developing spores in a conidiophore,

resulting in spores that are nonpathogenic (Lau and Hamer 1998). Given these known effects in other fungal species, we sought out to characterize natural conidiophore architectural variation in *N. crassa*, estimate heritability of these phenotypes, and examine their potential impact on sporulation. To do this, we employed a wild population collection of 21 *N. crassa* strains collected from Louisiana, USA (Mir-Rashed et al. 2000). These isolates have been used in previous population genetics studies to elucidate local adaptations to cold tolerance and circadian rhythm (Ellison et al. 2011) and characterize novel functions of loci (Ellison et al. 2014; Palma-Guerrero et al. 2013). Our work reveals three novel and distinct conidiophore architectural phenotypes among these wild populations. These phenotypes persist throughout the duration of conidiophore development and are described here as Wild Type (WT), Bulky, and Wrap. By conducting crosses between each phenotype and characterizing subsequent progeny conidiophores, we were able to fit a model for heritability of the discrete complex trait, conidiophore type. Our model suggests at least two genes control conidiophore architectural phenotype and estimates a heritability of 0.23. We explored the potential impact of conidiophore phenotype on sporulation by quantifying the number of conidia produced and their dispersal distance. Furthermore, we present a novel approach with an accurate image-classifier using a convolutional neural network (He et al. 2016) specifically developed to assign conidiophore architectural phenotypes in a high-throughput manner.

Materials and Methods

Strains and Media

Wild Louisiana isolates were obtained from the Fungal Genetics Stock Center (FGSC) (McCluskey 2003) and are listed in Table 2.1. Strains were maintained on 1.8% glucose 1.8% fructose 1.5% agar slants with 1X Vogel's Media and recommended Biotin and trace element supplements. To isolate conidiophores, strains were inoculated on 1.8% glucose 1.8% fructose 1.5% agar plates (100 x 15 mm) with 1X Vogel's Media, Biotin, and trace element supplements and incubated at 30C for 20 hours. Cultures were then harvested onto a 82 mm diameter nitrocellulose membrane with 0.45 um pore size (Whatman Protran BA-85) and inverted onto a new agar plate as described above and placed under light for aerial hyphae to penetrate the membrane. After 30 hours, membranes were removed from the agar and secured on a flat surface for imaging of conidiophores. Method was adapted from Bailey-Shrode & Ebbole, 2004 (Bailey-Shrode and Ebbole 2004).

Cultures for time-course images were grown following the same protocol with nitrocellulose membranes removed at 20, 25, or 35 hours for imaging of conidiophores at different stages of development.

Table 2.1. Wild Louisiana isolates of *N. crassa*. Strains used in this study were obtained from the FGSC.

Strain Number	FGSC	Perkins	Mat	Strain provenance	Collection site	Substrate/Annotation
Wild Strains						
D110	8870	4448	A	Dettman, J.	Franklin, LA	sugarcane
D111	8871	4449	a	Dettman, J.	Franklin, LA	sugarcane
D112	8872	4453	A	Dettman, J.	Franklin, LA	sugarcane
D114	8874	4464	A	Dettman, J.	Franklin, LA	sugarcane
D116	8876	4481	a	Dettman, J.	Franklin, LA	sugarcane
D118	8878	4491	a	Dettman, J.	Franklin, LA	sugarcane
JW09	2229		A	Welch, J.	Welsh, LA	burned grass
JW10	2229		A	Welch, J.	Welsh, LA	burned grass
JW59	3200		a	Welch, J.	Coon, LA	burned stumps
JW66	3211		a	Welch, J.	Sugartown, LA	pine burn
JW70	3199		A	Welch, J.	Coon, LA	burned stumps
JW75	3943		a	Welch, J.	Houma, LA	sugarcane burn
	847		A	Lein	Louisiana	sugarcane burn
D113	8873	4454	a	Dettman, J.	Franklin, LA	sugarcane
D119	8879	4500	a	Dettman, J.	Franklin, LA	sugarcane
JW20	3212		A	Welch,J	Ravenswood, LA	bonfire
JW76	3943		a	Welch,J	Houma, LA	sugarcane burn
JW159	2221		a	Welch,J	Houma, LA	sugarcane burn
JW160	2222		A	Welch,J	Iowa, LA	grass burn
JW162	2223		a	Welch,J	Iowa, LA	grass burn
JW164	2224		a	Welch,J	Marrero, LA	wood burn
JW167	2228		a	Welch,J	Roanoke, LA	grass burn
OR74A	2489		A	FGSC	Marrero, LA	Unknown

Crosses and Progeny Screening

Crosses were performed in the dark on cornmeal crossing medium, after which ascospores were plated on sorbose + fructose + glucose (SFG) media. Colonies were subsequently picked to isolate random ascospore progeny. Strains selected for crossing were FGSC8872 (WT) x FGSC3943 (Bulky), FGSC8872 (WT) x FGSC8876 (Wrap), and FGSC2229 (Bulky) x FGSC8876 (Wrap). Crosses were conducted in duplicate with 25 progeny selected from each. To isolate and image conidiophores in a high-throughput manner while preventing fusion of different progeny sharing a plate, each strain was inoculated on a 1 mL 1.5% agar droplet containing 1.8% glucose 1.8% fructose with 1X Vogel's Media and recommended Biotin and trace element supplements. Each 150 x 15 mm petri dish contained 8 agar droplets evenly spaced roughly 2.5 cm apart. Each droplet

was inoculated with progeny conidia and incubated at 30C for 20 hours to allow sufficient mycelial growth without hyphal fusion between droplets. Each droplet was then harvested onto a separate nitrocellulose membrane with 0.45 um pore size. Each membrane was inverted onto a new agar droplet as described above and placed under light for aerial hyphae to penetrate the membrane. After 25 hours, membranes were removed from the agar and secured on a flat surface for imaging of conidiophores.

Microscopy and Image Deconvolution

Nitrocellulose membranes containing conidiophores were visualized on an inverted microscope (Axio Observer A1, Carl Zeiss Microscopy, LLC, Thornwood, NY) at 20X magnification and brightfield images were taken with a CCD camera (AxioCam HRm, Carl Zeiss Microscopy, LLC, Thornwood, NY). Multiple z-slices were captured and overlaid in ImageJ (Schneider, Rasband, and Eliceiri 2012) to convey a complete representation of each three-dimensional structure. Augmentation including contrast enhancement and noise and background subtraction was conducted on image stacks to isolate conidiophores from underlying mycelia and/or aerial hyphae (Deng et al. 2016).

Automated Phenotype Classification

Residual nets (ResNet) was used to classify brightfield images into the three phenotypic classes by transfer learning (He et al. 2016). After some hyperparameter searching, ResNet-50 pretrained on ImageNet was chosen as the starting neural network for image classification (Russakovsky et al. 2015). Training parameters were as follows: batch size 15; initial learning rate 0.001; stochastic gradient decent as the optimizer. The

training process didn't update parameters before module 3 in the ResNet, and the parameters were only updated for the last 27 convolutional layers and the fully connected layer. Learning rates decay when plateau was used for modifying learning. Augmentation including random rotation, random horizontal flip, and random gray was introduced in the training to simulate realistic diversity and prevent overfitting. Before augmentation, all images went through padding and resize to fit the ResNet input size. All images were converted to tensor and normalized.

We balanced the three classes of conidiophore phenotypes and separated the data set into training (543), validation (66), and test sets (66). An external test set generated from progeny conidiophore images was collected in a separate batch and used for further validation (WT: 40; Bulky: 60; Wrap: 49). The training set was used to train the neural network and update its parameters. The validation set was used for updating learning rates and finding the final model to alleviate overfitting (Supplementary Figure 1). The test set was not used until the final performance evaluation. We calculated accuracy and macro definition of precision and recall for multi-class classification (Sokolova and Lapalme 2009). The model training and inference used PyTorch (Paszke et al. 2019), torchvision, and CUDA. P100 at Sapelo2 of GACRC was used for model training.

Feature importance was also evaluated on the test set. Features were evaluated on integrated gradient (Mukund Sundararajan 2017) and the noise tunnel method (Adebayo et al. 2018) smoothed the result. We chose the maximal value as baseline instead of regular choices (constant black) because in our brightfield images, a lighter background indicates the absence of features (Sturmfels 2020). In noise tunnel, the noise was added 10 times, and the means of squared attributions were used.

The codes for training and visualization are shared on GitHub (https://github.com/michaelSkaro/image_classification/tree/master/src).

Sporulation Quantification

Representative strains for each phenotypic class (FGSC8872, FGSC8876, and FGSC3943) were inoculated on 1.8% glucose 1.8% fructose 1.5% agar plates with 1X Vogel's Media, Biotin, and trace element supplements and incubated at 30C for 20 hours. Three biological replicates of each strain were performed. Cultures were then harvested onto an 82 mm diameter nitrocellulose membrane and inverted onto a new agar plate as previously described above. Plates were placed under light for 32 hours to allow penetration of aerial hyphae, development of conidiophores, and subsequent sporulation. Nitrocellulose membranes were then removed and conidia were suspended into 50 mL water and counted and sized with the Cellometer Auto 2000 (Nexcelom, Inc., Lawrence, MA) (Case et al. 2014; Brunson et al. 2016).

To compare dispersal distance traveled by spores of each phenotype, the same representative strains listed above were inoculated onto the same growth medium. After 20 hours at 30C, cultures were harvested onto a 60 mm diameter nitrocellulose membrane, inverted onto a new plate, and set under light for 30 hours. Membranes were then removed and placed at the center of a 245 mm square bioassay dish, where SFG medium surrounded a 60 mm diameter blank space now occupied by the membrane. The dish was placed under light for 48 hours to allow for sporulation and subsequent colonial growth. At this time, pictures of each plate were taken with an iPhone XS and contrast enhancement was performed in ImageJ. ImageJ was used to measure distance from the center of each

nitrocellulose membrane to the center of each colony. Two biological replicates were conducted for each strain.

Results

Wild N. crassa isolates exhibit three conidiophore architectural phenotypes.

Conidiophores from 21 wild Louisiana populations of *N. crassa* (Table 2.1) were isolated and imaged and we identified striking architectural variation both within and between populations. Conidiophores were classified by their morphology into three groups that are hereafter referred to as Wild Type (WT), Bulky, and Wrap. The WT phenotypic class is characterized by linear chains of developing conidia that extend and branch outward from the aerial hypha. Developing spores in Bulky conidiophores, however, form crowded clusters that inhibit the ability to distinguish linear chains. These spores also display more variation in their size and shape. In the Wrap phenotype, conidia cling to and/or wrap around a hyphal filament rather than extending and branching outward as in the other phenotypic groups (Figure 2.1).

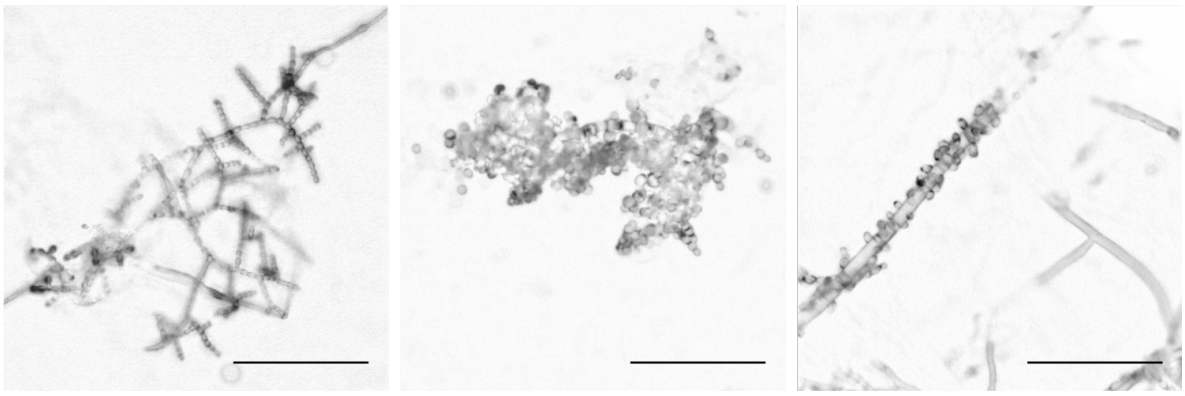

Figure 2.1. The three conidiophore architectural phenotypes. Wild-Type phenotype is depicted in the first panel with FGSC2489, followed by the Bulky phenotype with FGSC8878, and Wrap with FGSC8876. Scale bar, 100 μm.

Each brightfield image was manually classified into one (or two) of the phenotypic classes using the guidelines described above. Many strains had one phenotype demonstrating a clear majority, though every population had representation from at least two of the three phenotypes. All strains developed conidiophores with WT and Wrap phenotypes. Most strains also had Bulky conidiophores, with the exception of five populations (FGSC0847, FGSC2222, FGSC2228, FGSC3199, FGSC8872) lacking such individuals. Among the population set of 21 wild strains, 13 showed a majority of WT conidiophores, while 5 had a majority of Bulky and 3 had a majority of Wrap. Phenotype counts for each strain are tabled in Table 2.2 and phenotype ratios are presented in Figure 2.2.

Table 2.2. Conidiophore phenotype counts for each wild isolate. Individual conidiophore counts vary with each strain. Phenotypes are balanced for classifier training described below. Chi square test for independence: $X^2=380.92$, df=40, $P < 2.2*10^{-16}$.

STRAIN	WT	BULKY	WRAP	TOTAL
FGSC0847	22	0	4	26
FGSC2221	26	1	3	30
FGSC2222	13	0	8	21
FGSC2223	10	2	3	15
FGSC2224	16	23	6	45
FGSC2228	39	0	5	44
FGSC2229	14	54	48	116
FGSC2489	32	7	1	40
FGSC3199	17	0	2	19
FGSC3200	30	5	23	58
FGSC3211	20	16	7	43
FGSC3212	54	2	6	62
FGSC3943	32	80	52	164
FGSC8870	19	2	9	30
FGSC8871	16	6	17	39
FGSC8872	14	0	4	18
FGSC8873	8	11	13	32
FGSC8874	20	3	14	37
FGSC8876	15	21	42	78
FGSC8878	20	26	12	58
FGSC8879	6	12	11	29
TOTAL	443	271	290	

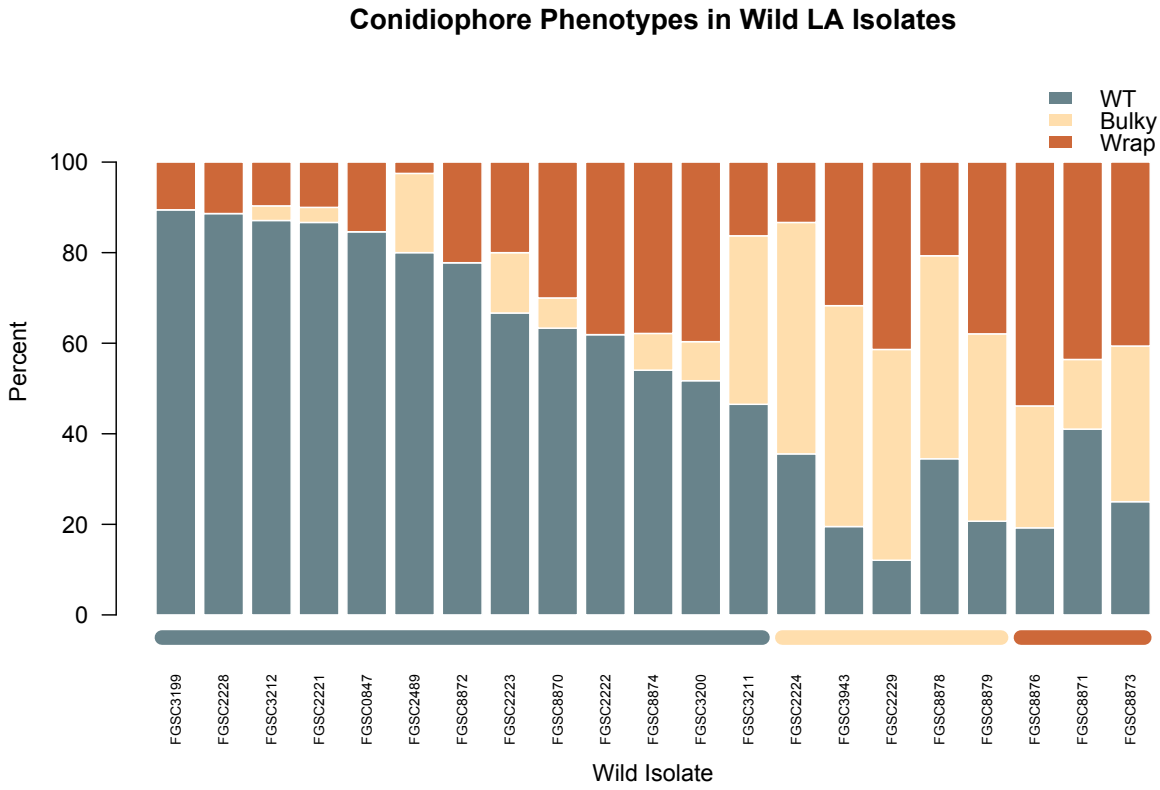

Figure 2.2. Percent of conidiophore phenotypes observed in each wild isolate. The first 13 strains have a majority WT conidiophores, followed by the next 5 strains having a majority of Bulky and the last 3 strains with a majority of Wrap. The majority phenotype within a strain is depicted by the color beneath each bar.

Architectural phenotypes are consistent throughout conidiophore development.

To ensure the three phenotypes were not just representations of different time points along the same developmental trajectory, we captured images of strains strongly representing each phenotype at 20, 25, 30, and 35 hours after transferring cultures to the nitrocellulose membrane, with 30 hours as the initial reference point for mature conidiophore images. It is important to note that each time point was collected from a

separate set of cultures, and these are not time-series images. WT, Bulky, and Wrap phenotypes were presented as early as 20 hours and maintained until sporulation captured at 35 hours, suggesting that the three architectural phenotypes are not a result of temporal disparity along the same developmental trajectory (Figure 2.3).

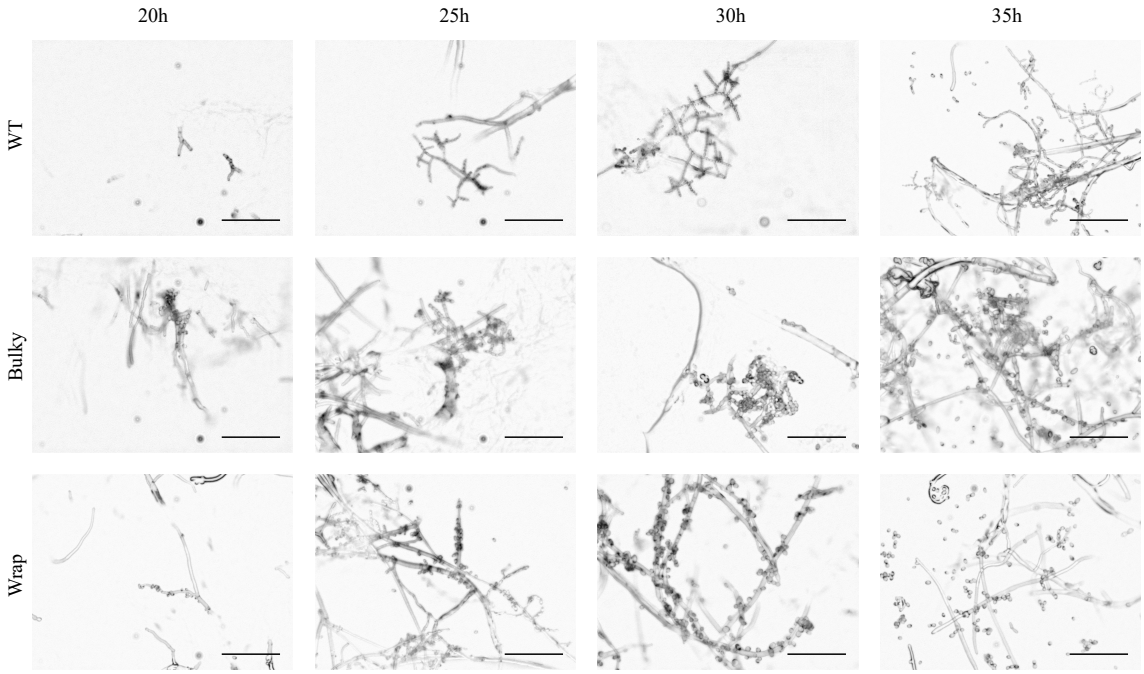

Figure 2.3. Development of conidiophore architectural phenotypes over time. Individual cultures were imaged at 20, 25, 30 and 35 hours after being transferred to a nitrocellulose membrane and placed under light. Development of the conidiophore begins at roughly 20 hours and concludes with sporulation by 35 hours. Representative strains used were: WT: FGSC2489; Bulky: FGSC8879; Wrap: FGSC8876. Scale bar, 100 µm.

There is no dependence of phenotype on strain collection environment.

Next, we investigated whether or not there was a correlation between the environment from which a strain was collected and its most prominent conidiophore phenotype. We found no statistically significant dependence of phenotype on collection substrate as reported by the Fungal Genetics Stock Center (FGSC) (McCluskey 2003) (Chi-square test for independence; X^2=4.9196, df=10, P=0.8965) (Figure 2.4). Interestingly, all strains with a majority of Wrap conidiophores (n=3) were collected from sugarcane, though WT and Bulky strains were also found on this substrate. WT strains were found on all six substrates (sugarcane, grass burn, burned stump, pine burn, bonfire, unknown), and Bulky strains were found on sugarcane, grass burn and pine burn. We also did not find any clear relationship between most prominent phenotype and the town from which each strain was collected, as reported by FGSC (Figure 2.5).

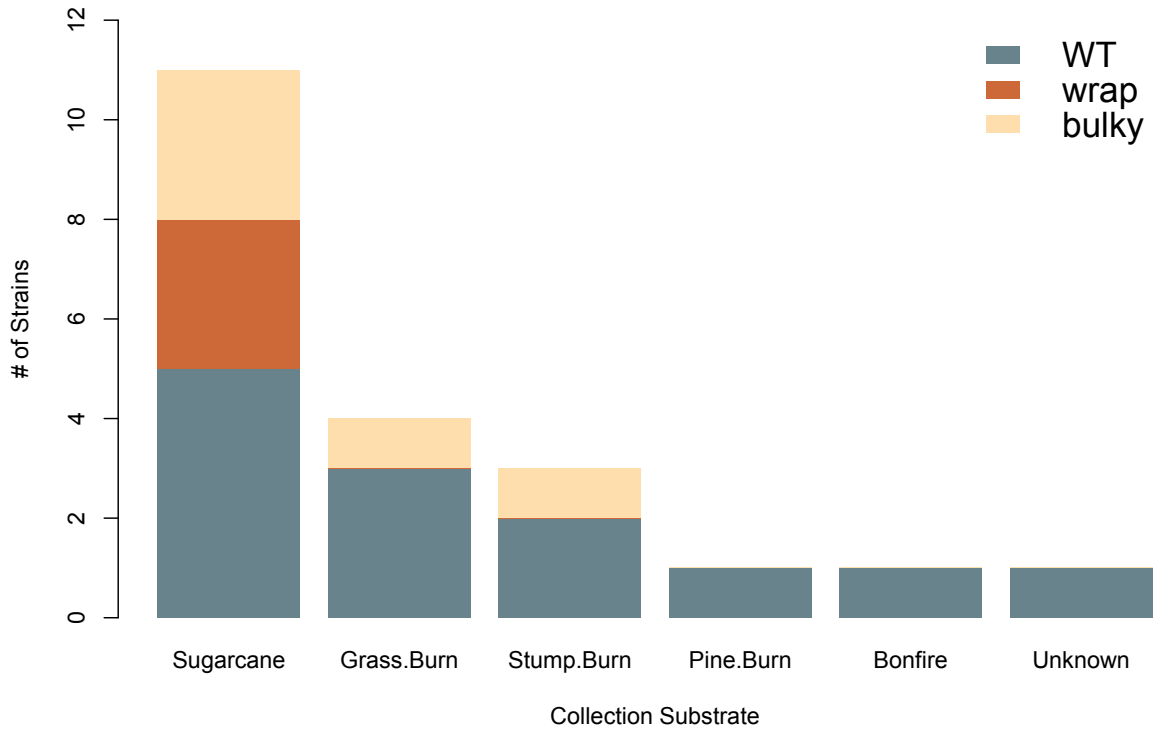

Figure 2.4. Collection substrates of wild isolates. There is no significant correlation between the substrate from which a strain was collected and its most prominent phenotype (X2=4.9196, df=10, P=0.8965). Collection substrate as reported by the Fungal Genetics Stock Center.

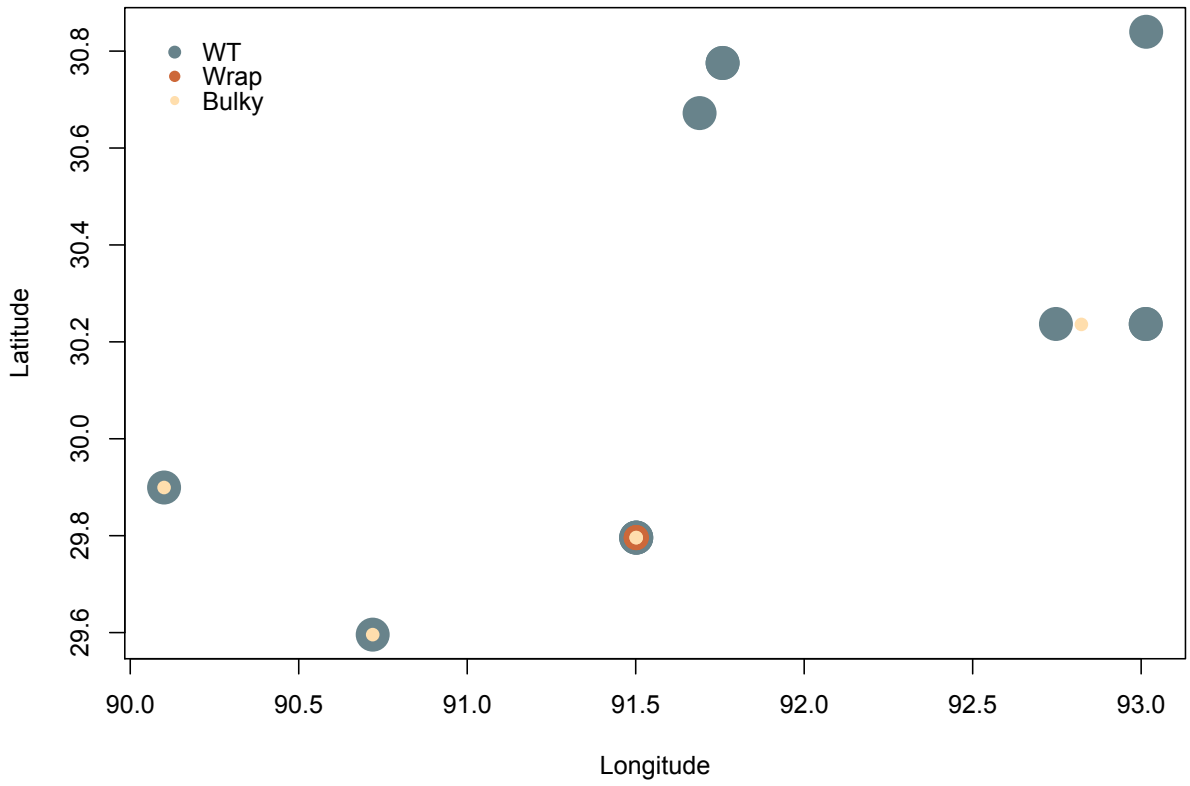

Figure 2.5. Collection sites of wild isolates. There is no clear relationship between most prominent phenotype and collection site. Louisiana town names were reported by FGSC and are depicted here as geographical coordinates. Overlapping datapoints depict multiple strains collected from the same town.

Architectural phenotypes can be automatically classified and corresponding features can be extracted.

Manually categorizing conidiophores into phenotypic classes is time consuming and introduces potential bias. To streamline the future classification of additional conidiophore images, an automated classification process was developed. We demonstrated that an

accurate image classifier could be constructed based on the limited conidiophore image dataset of 543 training samples and presents reasonable performances (Table 2.3).

Table 2.3. Performance of ResNet-50 classification on training, validation, and test sets. Accuracy, precision, and recall is used for evolution.

	Accuracy	**Precision**	**Recall**
Training	0.9632	0.9644	0.9632
Validation	0.7879	0.7890	0.7879
Test	0.7576	0.7540	0.7576
External test set	0.6779	0.6802	0.6639

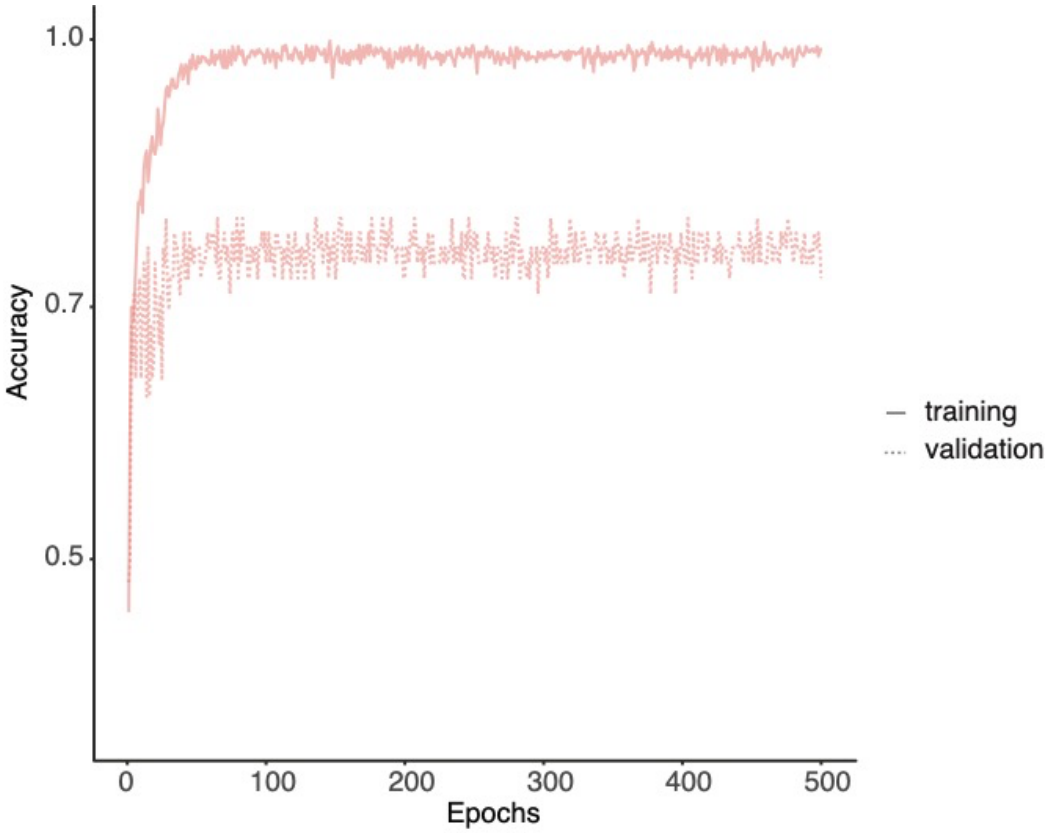

Figure 2.6. Model accuracies through training. Accuracies on training (solid line) and validation (dotted line) set is plotted through epochs. The final model was chosen based on the accuracy of the validation set.

Table 2.4. Confusion table for the test set. Each row indicates different true labels and each column indicates different predictions. In the test set, the accuracies are 0.9545 (Bulky), 0.5909 (Wrap), and 0.7273 (WT).

	BULKY	**WRAP**	**WT**
BULKY	21	1	0
WRAP	4	13	5
WT	2	4	16

Images from both the test and validation set can be accurately classified at rates of 76% and 79%, respectively (Figure 2.7). Testing on an external data set from a separate batch showed slightly worse performance at 68% accuracy. Feature importance is also evaluated (Figure 2.7), confirming that the program is properly identifying the conidiophore within an image for classification. This method was used to classify images of progeny conidiophores in a high-throughput manner to estimate potential heritability of these phenotypes, described below.

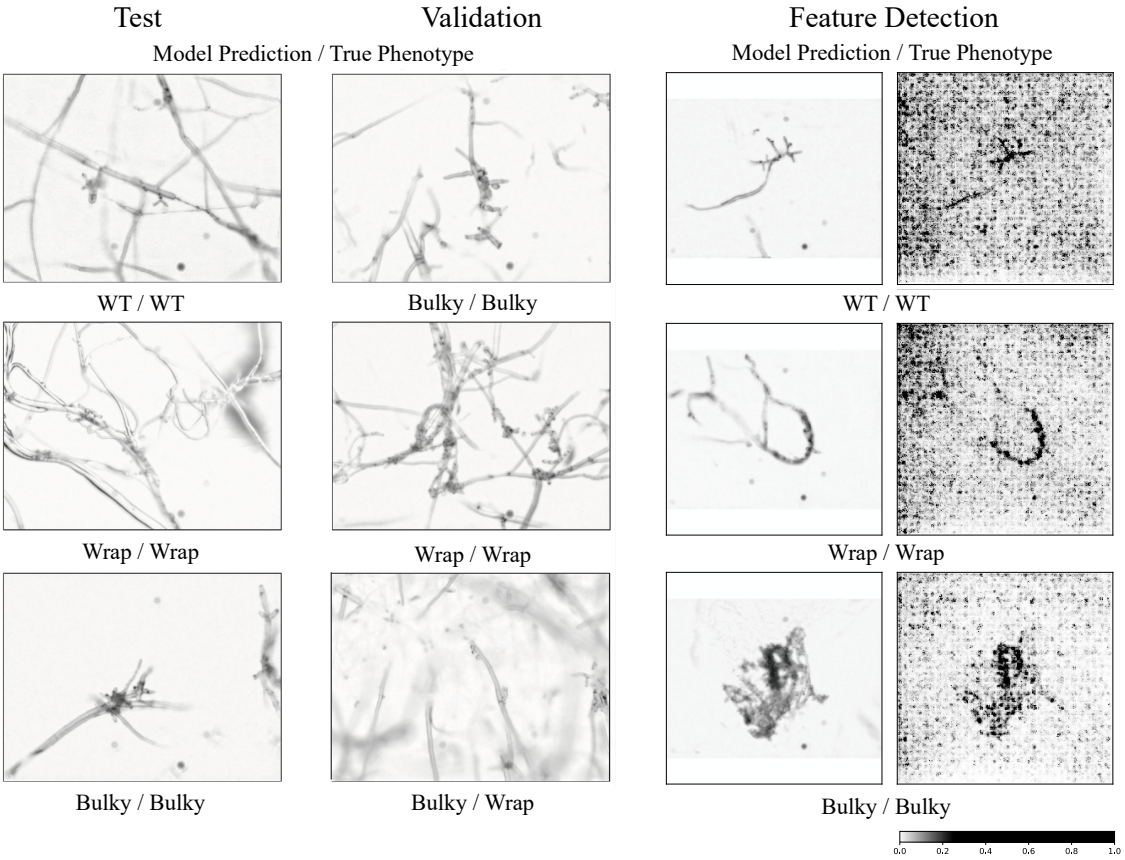

Figure 2.7. Automatic classification of phenotypes. Model performance on test and validation sets is depicted in the first two columns. The far left column shows a selected test set, followed by an example validation set in the second column. The third and fourth

columns show feature importance evaluation for a few test samples. The third column shows the original image (after padding and resize) with the last column identifying feature importance. A higher value (black) in the last column indicates greater feature importance. All images are labeled with the model predicted phenotype first and manually identified phenotype second.

Crosses suggest at least 2-3 genes involved in conidiophore architectural phenotypes.

Three crosses were performed between representative strains for each architectural phenotype: FGSC8872 x FGSC8876 (WT x Wrap), FGSC8876 x FGSC2229 (Wrap x Bulky), and FGSC 8872 x FGSC3943 (WT x Bulky). 50 progeny were selected from each cross, from which conidiophores were isolated and imaged. For efficiency, these 1,932 images were each assigned a phenotype by automatic classification as described above. These phenotype counts were then used to estimate an inheritance model for this discrete complex trait, described below.

Table 2.5. Inheritance model probabilities. The cell probabilities for the fully epistatic inheritance model with 3 genes in three crosses. The probability of phenotype j from cross i is K_{ij}.

	A (WT)	**B (WRAP)**	**C (BULKY)**
A x B	$K_{11} = e^{\lambda}e^{\alpha}e^{-\beta}e^{\alpha\beta}$	$K_{12} = e^{\lambda}e^{-\alpha}e^{\beta}e^{\alpha\beta}$	$K_{13} = e^{\lambda}e^{-\alpha}e^{-\beta}e^{-\alpha\beta}$
B x C	$K_{21} = e^{\lambda}e^{-\beta}e^{-\gamma}e^{-\beta\gamma}$	$K_{22} = e^{\lambda}e^{\beta}e^{-\gamma}e^{\beta\gamma}$	$K_{23} = e^{\lambda}e^{-\beta}e^{\gamma}e^{\beta\gamma}$
A x C	$K_{31} = e^{\lambda}e^{\alpha}e^{-\gamma}e^{\alpha\gamma}$	$K_{32} = e^{\lambda}e^{-\alpha}e^{-\gamma}e^{-\alpha\gamma}$	$K_{33} = e^{\lambda}e^{-\alpha}e^{\gamma}e^{\alpha\gamma}$

The inheritance model is summarized in Table 2.5 above and motivated by classic models for quantitative traits (Falconer 1981). In this model, each cross contributes the effect of one dominant allele at each of three loci. For example, in *Emericella (Aspergillus) nidulans*, at least three genes control conidiophore development (Timberlake 1990). The main effects of the three loci are denoted by $\alpha, \beta, and\ \gamma$ for the A (WT), B (Wrap), and C (Bulky) loci and associated phenotype, respectively. In each cross there are two dominant alleles (one from each parent) being contributed that epistatically interact to determine the conidiophore architectural phenotype. In principle, these pairwise interactions could result from environmental interactions among progeny in the cross and/or developmental interactions within developing progeny. By isolating progeny in their own agar droplet (see Materials and Methods), the former possibility could be eliminated. The pairwise interactions are denoted by $\alpha\beta, \beta\gamma, and\ \alpha\gamma$. In addition, in this model there is one grand mean λ that is adjusted so that all these probabilities of a progeny phenotype, K_{ij}, sum to 1. The data tabled below are the multinomial counts of progeny from each of the three crosses:

Table 2.6. Progeny phenotype counts. Multinomial counts of progeny phenotypes from each of the three crosses.

	A (WT)	B (WRAP)	C (BULKY)
A x B	$N_{11} = 156$	N_{12}=205	$N_{13} = 253$
B x C	$N_{21} = 94$	N_{22}=155	N_{23}=275
A x C	$N_{31} = 202$	N_{32}=230	N_{33}=198

The A denotes an allele associated with the WT phenotype. The B denotes an allele associated with the Wrap phenotype, and C denotes an allele associated with the Bulky phenotype. These counts are stored in a 9 x 1 vector $\underline{N}$, the "dependent variable" to be explained by the allelic and epistatic effects. The sum of these 9 progeny counts is N. Under this model the log of the expectations of these counts E(Y) are linear in the parameters of the model, such as the allelic effects, and thus the model is sometimes referred to as a loglinear model (Williams 1989). Much as in a probit model, the goal for this discrete trait model is to associate an underlying quantitative trait through the log of the expected counts with the allelic and epistatic effects. Under the simplest hypothesis all 9 of these cell probabilities are equal. Departures from this hypothesis (H0) summarize the variation in the counts as measured by the Pearson X_0^2. Departures from the next simplest hypothesis (H1) summarize the additive variation in the counts as measured by the Pearson X_1^2. Departures from the last, most complicated hypothesis (H2) with all 3 interactions summarizes the additive and epistatic variation by the Pearson X_2^2. The heritability is summarized by the ratio of the additive variation to the total variation: H2 = $(X_0^2 - X_1^2)/X_0^2$.

Many intervening models can be envisioned in a hierarchy of possible inheritance models (Figure 2.8).

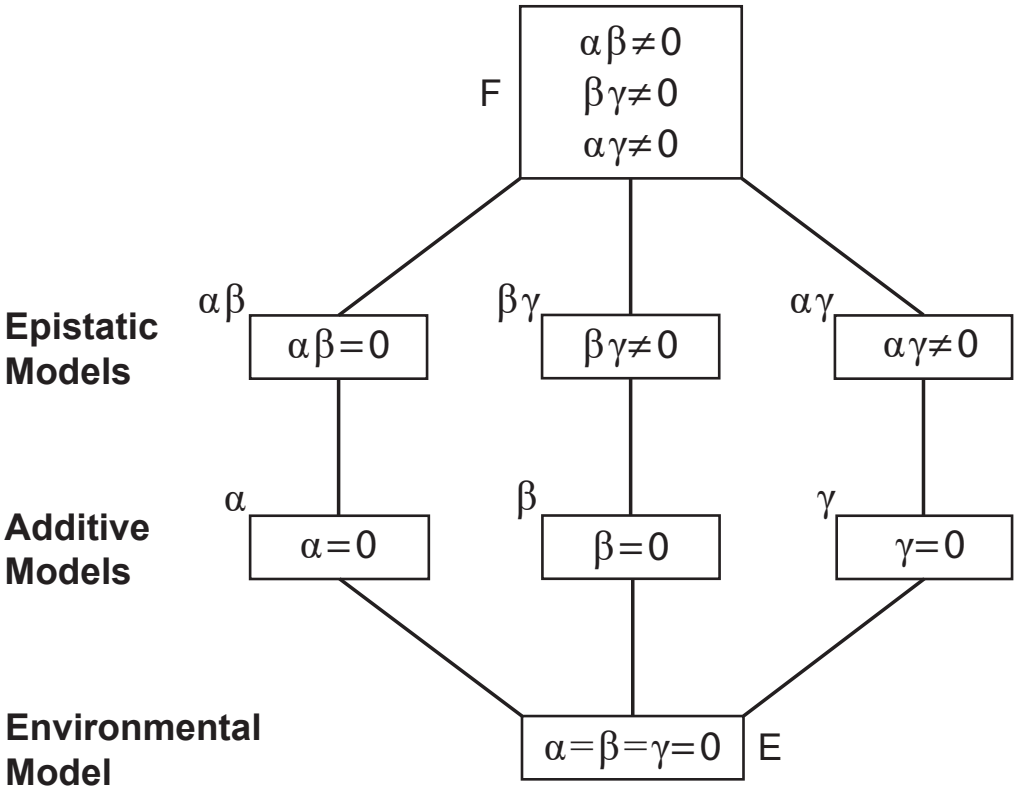

Figure 2.8. Hierarchy of models. The following hierarchy contains particular models that fit the phenotypic counts on three crosses between parents with different conidiophore phenotypes. At the top of the model hierarchy is the full epistatic model (F) with a grand mean, three additive allelic effects, and three epistatic interactions. At the bottom of the hierarchy is an environmental model with no genetic effects on conidiophore phenotype (E). Intervening models in the hierarchy drop one or more parameters describing the additive and epistatic effects of genes A, B, and C associated with the conidiophore phenotypes, A, B, and C.

Each model was fitted by the Method of Maximum Likelihood using Iteratively Reweighted Least Squares (IRLS) (Asmussen, Arnold, and Avise 1987; Kendall and Stuart 1979). Under this approach the Information A about the counts is denoted by A, and the derivatives of the cell probabilities in the model above are stored in the array X tabled below. The matrix NX'AX is the information about the parameters in the model. The score vector S represents the derivatives of the log of the cell probabilities and can be written as S = AY, where A is a 9 x 9 diagonal matrix where A(i,i) = 1/K(i,i).

Table 2.7. Derivative matrix. The derivatives of the model cell probabilities are stored in the following 9 x 7 derivative matrix X. Each row captures the parameters present in an expected cell probability K_{ij} of one of the three phenotypes j in cross i (Table 2.6). The X matrix captures the structure of the model. Dropping/adding columns corresponds to dropping/adding parameters in a model.

Parameters/K	$\boldsymbol{\lambda}$	$\boldsymbol{\alpha}$	$\boldsymbol{\beta}$	$\boldsymbol{\gamma}$	$\boldsymbol{\alpha\beta}$	$\boldsymbol{\beta\gamma}$	$\boldsymbol{\alpha\gamma}$
K_{11}	1	1	1	0	1	0	0
K_{12}	1	1	1	0	1	0	0
K_{13}	1	1	1	0	1	0	0
K_{21}	1	0	1	1	0	1	0
K_{22}	1	0	1	1	0	1	0
K_{23}	1	0	1	1	0	1	0
K_{31}	1	1	0	1	0	0	1
K_{32}	1	1	0	1	0	0	1
K_{33}	1	1	0	1	0	0	1

The fitting of this model with 7 parameters or simplifications of this inheritance model was obtained from solving the following weighted least squares problem where Y = S + NAX$\underline{N}$ is the provisional quantitative dependent variable, X is the regression matrix of independent variables, such as allelic effects, A is the weight matrix, and the parameters are $\beta' = (\lambda, \alpha, \beta, \alpha\beta, \beta\gamma, \alpha\gamma)$. The parameters are found by solving the following normal equations iteratively:

$$\mathrm{N}X'AX\beta^* = \mathrm{X'Y}.$$

The matrix A and vector Y are evaluated with the current provisional parameter estimate β, and then the normal equations are solved for the updated parameter vector β^*.

The process is repeated until the relative error is less than 10^{-8}. The process is initialized by solving the multiple regression problem with $\log\left(\frac{N}{\overline{N}}\right) = X\beta + \epsilon$, where ϵ is a normally distributed error vector with 9 independent components. Goodness of Fit was assessed by Pearson X^2. The only thing to be changed for simplified models is the X matrix by removing the appropriate column(s) to eliminate a parameter or parameters not in a simplified model. The results for fitting the models with IRLS (Asmussen, Arnold, and Avise 1987) computed with relative error < 10^{-8} after 9 iterations IRLS are summarized in the table below.

Table 2.8. Fitting of inheritance models. A nested hierarchy of inheritance models were successfully fitted with at least two genes controlling the conidiophore architectural phenotype to the counts of progeny phenotypes from three crosses (Table 2.6). Nine iterations were necessary to achieve the desired error tolerance of 10^{-8} with IRLS. Recommended models are bolded along with their goodness of fit to the counts of phenotypes in crosses.

Model	X^2	df	P	X^2_{H0}-X^2_{HA}	df	P for HA vs H0	Notes
Full epistatic	0.98	2	**0.61**	-	-	-	H0 = full epistatic
$\alpha\beta = 0$	8.39	3	0.04	8.39-0.98=7.41	1	0.004	H0=full epistatic
$\alpha\beta = \alpha = 0$	25.31	5	0.001	25.31-0.98=24.33	2	<0.00001	H0=full epistatic
$\boldsymbol{\alpha\beta = \beta = 0}$	9.96	5	**0.08**	9.96-0.98=8.98	2	0.01	H0=full epistatic
$\beta\gamma = 0$	9.32	3	0.02	9.32-0.98=8.34	1	0.004	H0=full epistatic
$\alpha\gamma = 0$	84.57	3	<0.0001	84.57-0.98=83.59	1	<0.00001	H0=full epistatic
$\alpha\beta = \beta\gamma = \alpha\gamma = 0$ additive	95.76	4	<0.0001	95.76-0.98=94.78	3	<0.00001	H0=full epistatic
environmental	124.46	8	<0.0001	124.46-0.98=123.48	7	<0.00001	H0=full epistatic
heritability							H^2=(124.46-95.76)/124.46= 0.23 H0=environmental model H1=full additive model

The full epistatic model with three genes fitted the ratios from three crosses (Table 2.8). The only epistatic interaction that could possibly be dropped was between the A (WT) and B (Wrap) genes ($\alpha\beta$). This raised the question of whether or not any one of the additive allelic effects could be dropped altogether. This turned out to be the β allelic effect (for

Wrap). A model without the B gene for Wrap did fit the progeny counts of the three crosses (X^2 = 9.96, df = 5, P = 0.08). The conclusion was that at least two genes control conidiophore phenotype. An additive model and the model without gene effects was then used to assess the heritability. The heritability of H^2 was typical for quantitative traits (Falconer 1981), namely about 0.23.

The maximum likelihood estimates of parameters for the inheritance model are tabled. The two promising models are fairly consistent across model parameters. One of these models has three loci, and the other has only two loci.

Table 2.9. Maximum likelihood estimates of allelic effects and epistatic effects in a two or three locus model of inheritance. The full epistatic model with three genes has three allelic effects and three epistatic interactions. The two-gene model with gene B (Wrap) removed has two allelic effects for A (WT) and C (Bulky) and two epistatic interactions between A (WT) and C (Bulky) and between B (Wrap) and C (Bulky). The standard errors were obtained from the square roots of the diagonal elements of the inverse of the information matrix N$X'AX$.

Parameters	**Full epistatic** **3 genes**	$\boldsymbol{\alpha\beta = \beta = 0}$ **2 genes**
λ	5.32 +/- 0.0040	5.32 +/- 0.0030
α	-0.08 +/- 0.0048	0.02 +/- 0.0048
β	0.05 +/- 0.0061	0
γ	0.53 +/- 0.0047	0.53 +/- 0.0044
$\alpha\beta$	-0.15 +/- 0.0060	0
$\beta\gamma$	.20 +/- 0.0067	0.23 +/- 0.0061
$\alpha\gamma$	-0.60 +/- 0.0064	-0.58 +/- 0.0062

The allelic and epistatic effects are fairly stable between the two models. The C (Bulky) gene appears to have the largest effect both additively and epistatically with both B (Wrap) and A (WT). There also appears to be a strong epistatic interaction between B (Wrap) and C (Bulky) alleles.

Architectural phenotype may impact colonization capacity in N. crassa.

Previous work conducted in *Aspergillus* has shown that conidiophore architecture impacts colonization capability of the organism (Wang et al. 2015). To investigate whether this may also be true in *N. crassa*, we quantified the average number of conidia produced by each conidiophore phenotype, using a representative strain for each. There was no statistically significant difference in number of conidia produced by each phenotype when

suspended in liquid culture (Figure 2.9). Additionally, we found no statistically significant difference in average conidium diameter produced by each phenotype (Figure 2.10).

We also explored sporulation behavior on SFG medium, where mature conidiophores were placed at the center of a plate to allow for sporulation and subsequent colonial growth. Interestingly, fewer WT colonies (n=334) developed compared to Wrap and Bulky (n=1,113 and n=1,252, respectively), suggesting a difference in sporulation behavior in an aerial versus aqueous environment. We quantified the distance from the center of each nitrocellulose membrane to the center of each colony. The distribution of these distanced will be referred to as the spore shadow. Two replicate datasets were combined, as there was no significant difference between replicates of a phenotype following a two-sample Kolmogorov-Smirnov test (Kendall and Stuart 1979). Sporulation by Wrap conidiophores resulted in colonies at a significantly closer distance when compared to that of Bulky colonies ($P=3.101e^{-05}$) (Figure 2.11). No significant sporulation distance difference was found by the other pair combinations; however, differences in the distribution of colony distances are found between pairs WT and Wrap (D=0.090973, P=0.02849) and Wrap and Bulky (D=0.09624, $P=3.702e^{-05}$) by two-sample Kolmogorov-Smirnov tests (Figure 2.12).

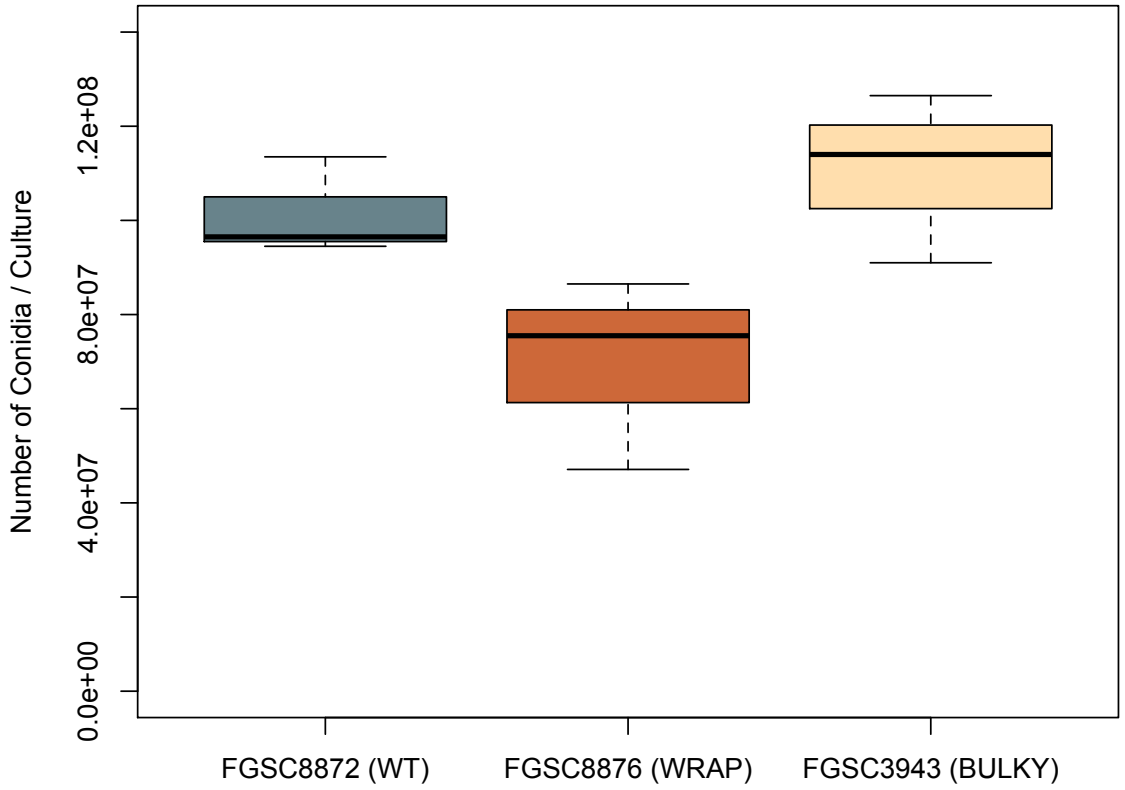

Figure 2.9. Conidia counts generated by each conidiophore phenotype. Number of conidia suspended in water from an 82 mm diameter nitrocellulose membrane by each conidiophore phenotype. Dataset includes three biological replicates. The box shows 25th and 75th percentiles, with the median denoted as a line inside. The whiskers represent the range of data. T-test results for pairs are as follows: WT-Wrap, P=0.09541; Wrap-Bulky, P=0.06079; WT-Bulky, P=0.505.

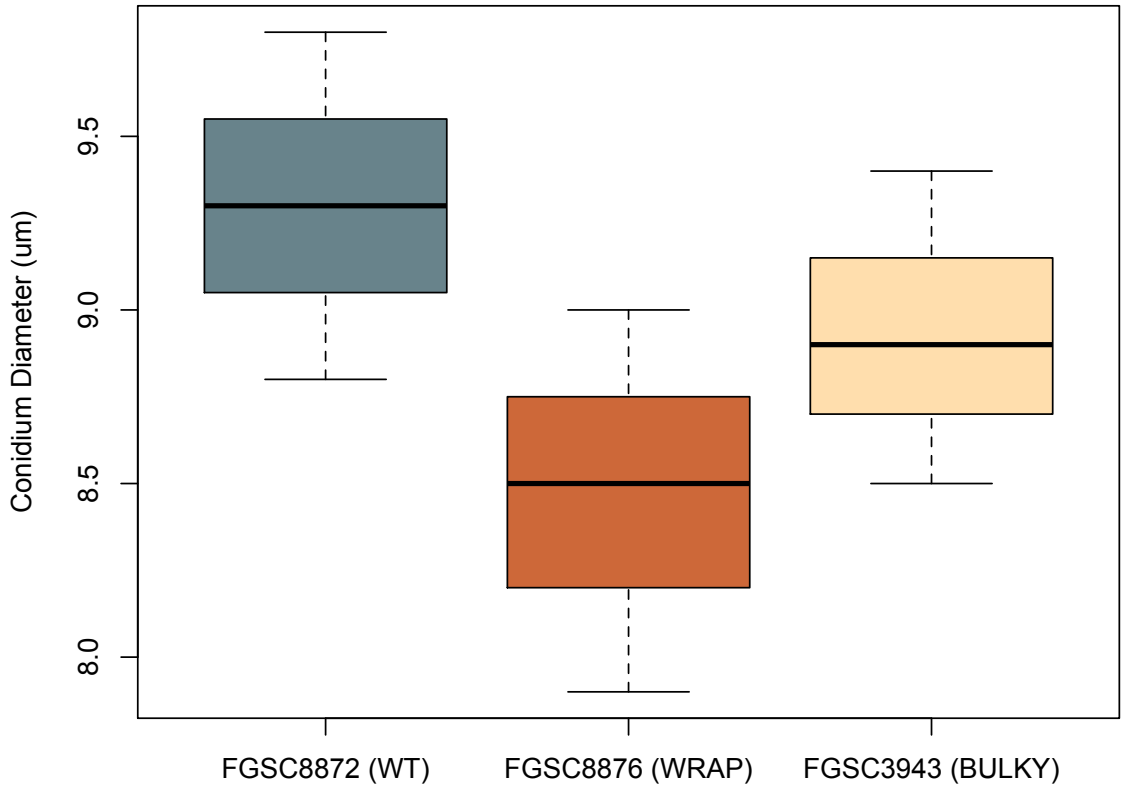

Figure 2.10. Conidium diameters generated by each conidiophore phenotype. Average conidium diameter in microns when suspended in water for each architectural phenotype. Dataset includes three biological replicates. Dataset includes three biological replicates. The box shows 25th and 75th percentiles, with the median denoted as a line inside. The whiskers represent the range of data. T-test results for pairs are as follows: WT-Wrap, P=0.125; Wrap-Bulky, P=0.3219; WT-Bulky, P=0.3995.

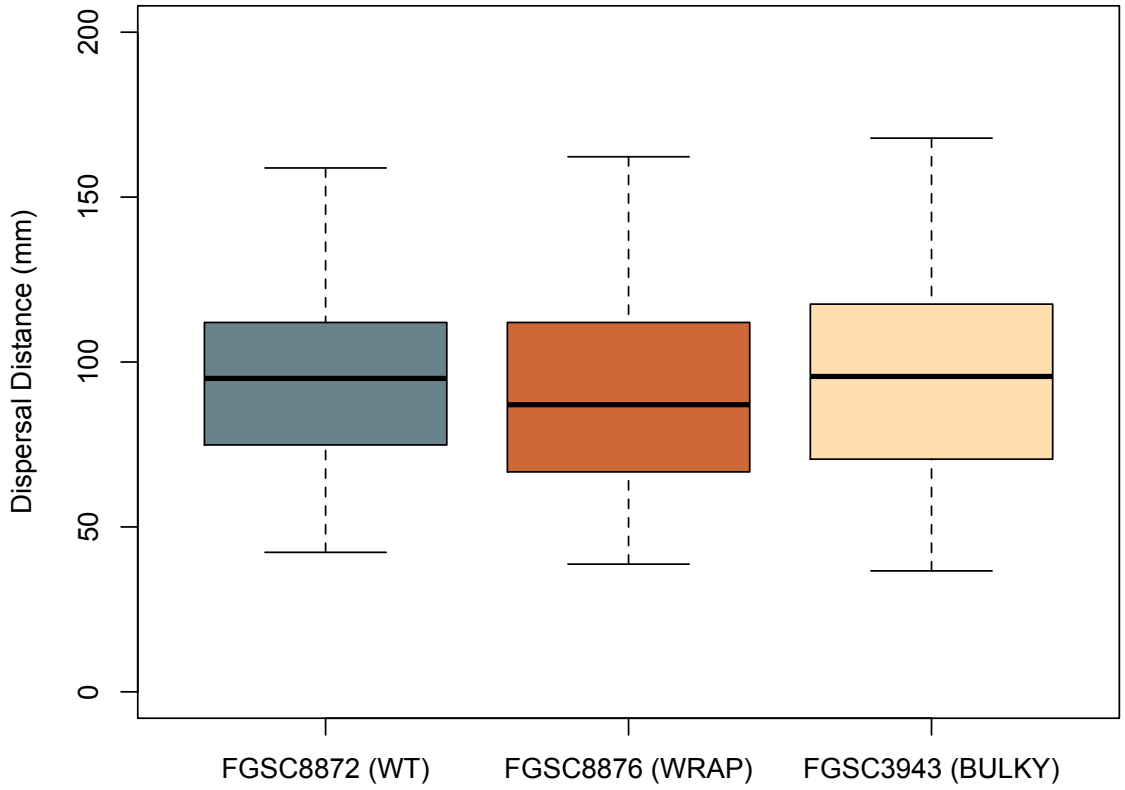

Figure 2.11. Dispersal distances of conidia generated by each conidiophore phenotype. Distance in mm to the center of each colony on SFG medium from the center of each nitrocellulose membrane. Dataset includes two biological replicates. Dataset includes three biological replicates. The box shows 25th and 75th percentiles, with the median denoted as a line inside. The whiskers represent the range of data. T-test results for pairs are as follows: WT-Wrap, P=0.0587; Wrap-Bulky, P=3.101e^{-05}; WT-Bulky, P=0.3466.

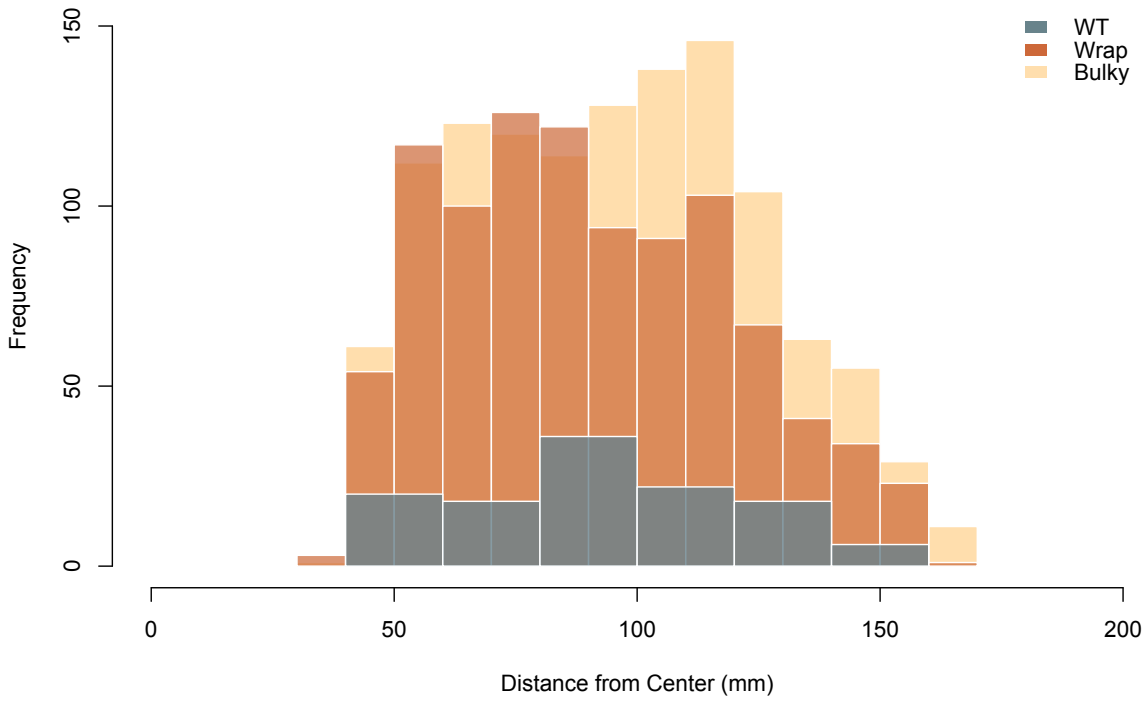

Figure 2.12. Distributions of dispersal distances by conidia from each conidiophore phenotype. Histogram of distances in mm to the center of each colony from the center of each nitrocellulose membrane. Total colony counts combining two replicates are as follows: WT=334, Wrap=1,113, Bulky=1,252. Results of two-sample Kolmogorov-Smirnov tests for each pair are as follows: WT-Wrap D=0.090973, P=0.02849; Wrap-Bulky D=0.09624, P=3.702e^{-05}; WT-Bulky D=0.055465, P=0.3922.

Discussion

Conidiophore development in *N. crassa* has been thoroughly documented over decades of study (Park and Yu 2012). Genetic, temporal, and environmental signals guiding this process are well understood (Springer and Yanofsky 1989; Park and Yu 2012); however, little is known about conidiophore morphological variation, particularly in natural populations. The *N. crassa* collection of Louisiana isolates provides a convenient tool for characterizing variation in a natural population, and has previously been used to describe local adaptations and reveal novel gene functions (Ellison et al. 2011; Ellison et al. 2014; Palma-Guerrero et al. 2013). Following their collection from nature, these strains underwent conidial plating to remove possible fungal contaminants and were maintained vegetatively at the FGSC (Turner, Perkins, and Fairfield 2001). It is entirely likely that these isolates are heterokaryotic, reflective of the genetic variation observed in the wild. By using these populations as is, we aimed to capture the full spectrum of natural variation in conidiophore architecture.

By utilizing this population set of 21 wild strains to explore morphological variation in the conidiophore, we identified three novel architectural phenotypes: Wild Type, Bulky, and Wrap. These three phenotypes are consistently displayed throughout conidiophore development and are likely not the result of temporal disparity along the same growth trajectory. Interestingly, no clear dependence of phenotype on collection location or substrate was observed, suggesting a genetic component to this variation. To further explore this, we conducted crosses between representative strains for each phenotype. By quantifying the subsequent progeny conidiophores of these crosses, we were able to fit a

model for inheritance. Our resulting model suggests that at least two genes control conidiophore architectural phenotype with an estimated heritability of 0.23.

Future work should seek to identify these genetic variants and characterize transcriptional profiles for conidiophores of different architectural phenotypes. Many key genetic players of conidiophore development have already been identified and thoroughly characterized, most notably the *con* genes (Berlin and Yanofsky 1985), and transcriptomic data has elucidated gene expression profiles throughout wild type conidiophore development (Greenwald et al. 2010). Interestingly, the Bulky conidiophore phenotype resembles that of the *attenuated (at)* knockout mutant, where conidia form in dense aggregates (Perkins, Radford, and Sachs 2000). However, we do not observe slowed growth and pigmentation in the Bulky wild isolates as is seen in *at* mutants. Identifying and characterizing additional genes possibly underlying WT, Bulky, and Wrap phenotypes would provide greater understanding of conidiophore development through a morphological lens, and perhaps lend insight to the natural population structure of these wild isolates.

To investigate a potential environmental impact of conidiophore architecture, we evaluated the effect of conidiophore phenotype on sporulation in both an aqueous suspension and aerial environment. No significant effect was detected on the number of conidia or average conidium diameter when suspended in water, nor was there any difference in wettability of conidia while washing off a plate. This indicates that conidiophore architectural phenotype is not due to difference in hydrophobicity of the conidia. In an aerial environment, fewer conidia from Wrap conidiophores germinated compared to Bulky. Additionally, spore shadows by conidia from Wrap conidiophores fit

a different distribution compared to that of both WT and Bulky groups. This suggests that conidiophore architectural phenotype may impact colonization capacity of the organism. Sporulation experiments should be conducted at a larger scale to more effectively determine the maximum dispersal distance of each conidiophore phenotype, and hence effective population size and neighborhood size (Powell and Dobzhansky 1976; Lemke 1985). Furthermore, it is possible that conidiophore phenotype may contribute to microspatial variation through altering effective population size and neighborhood size, as some strains exhibiting different architectural phenotypes were collected from the same substrate in the same location (Powell et al. 2003).

It remains a challenge to relate complex traits describing growth and form to their underlying genes (Davis 2000). Doing so requires genomics (Palma-Guerrero et al. 2013; Galagan et al. 2003), transcriptomics (Ellison et al. 2014), and/or metabolomics (Judge et al. 2019), as well as high-throughput approaches to phenotyping. Morphological diversity presents an attractive opportunity for image analyses and phenotyping at a large-scale, as has been shown in other model fungal systems, like yeast (Ohya et al. 2005; Levy and Siegal 2008). Phenomics tools like Digital Imaging of Root Traits (DIRT) have been developed specifically to quantify architectural features in plant root systems (Das et al. 2015). Though filamentous fungi bear some similarities to roots, the unique morphology of conidiophores is best characterized with a tool specifically designed for their structure. We present a novel method to classify brightfield images of conidiophores into three architectural phenotypes and extract important features for their classification. This same approach can be applied to characterize conidiophores of other filamentous fungi, and may even be used in conjunction with DIRT to characterize morphology in the symbiotic

relationship between roots and arbuscular mycorrhiza (Parniske 2008; Johnson et al. 2006). To further improve our method, automation in sample collections and blurred region removal could be implemented. Performance in the model training was also limited by the sample size in our study and domain specific features.

Acknowledgments

We acknowledge Mary E. Case for suggesting the two-gene hypothesis in the heritability model. We also thank James Griffith and the UGA GACRC.

References

Adebayo, Julius, Justin Gilmer, Michael Muelly, Ian Goodfellow, Moritz Hardt, and Been Kim. 2018. *Sanity Checks for Saliency Maps*.

Asmussen, M. A., J. Arnold, and J. C. Avise. 1987. 'Definition and properties of disequilibrium statistics for associations between nuclear and cytoplasmic genotypes', *Genetics*, 115: 755-68.

Bailey-Shrode, L., and D. J. Ebbole. 2004. 'The fluffy gene of Neurospora crassa is necessary and sufficient to induce conidiophore development', *Genetics*, 166: 1741-9.

Berlin, V., and C. Yanofsky. 1985. 'Protein changes during the asexual cycle of Neurospora crassa', *Mol Cell Biol*, 5: 839-48.

Brunson, J. K., J. Griffith, D. Bowles, M. E. Case, and J. Arnold. 2016. 'lac-1 and lag-1 with ras-1 affect aging and the biological clock in Neurospora crassa', *Ecol Evol*, 6: 8341-51.

Case, M. E., J. Griffith, W. Dong, I. L. Tigner, K. Gaines, J. C. Jiang, S. M. Jazwinski, and J. Arnold. 2014. 'The aging biological clock in Neurospora crassa', *Ecol Evol*, 4: 3494-507.

Das, Abhiram, Hannah Schneider, James Burridge, Ana Karine Martinez Ascanio, Tobias Wojciechowski, Christopher N. Topp, Jonathan P. Lynch, Joshua S. Weitz, and Alexander Bucksch. 2015. 'Digital imaging of root traits (DIRT): a high-throughput computing and collaboration platform for field-based root phenomics', *Plant Methods*, 11: 51.

Davis, R. H. 2000. *Contributions of a Model Organism* (Oxford University Press: New York).

Deng, Z., S. Arsenault, C. Caranica, J. Griffith, T. Zhu, A. Al-Omari, H. B. Schüttler, J. Arnold, and L. Mao. 2016. 'Synchronizing stochastic circadian oscillators in single cells of Neurospora crassa', *Sci Rep*, 6: 35828.

Ellison, C. E., C. Hall, D. Kowbel, J. Welch, R. B. Brem, N. L. Glass, and J. W. Taylor. 2011. 'Population genomics and local adaptation in wild isolates of a model microbial eukaryote', *Proc Natl Acad Sci U S A*, 108: 2831-6.

Ellison, C. E., D. Kowbel, N. L. Glass, J. W. Taylor, and R. B. Brem. 2014. 'Discovering functions of unannotated genes from a transcriptome survey of wild fungal isolates', *mBio*, 5: e01046-13.

Falconer, D.S. 1981. 'Introduction to Quantitative Genetics'.

Galagan, James, Sarah Calvo, Katherine Borkovich, Eric Selker, Nick Read, David Jaffe, William Fitzhugh, Li-Jun Ma, Serge Smirnov, and Seth Purcell. 2003. 'The genome sequence of the filamentous fungus Neurospora crassa', *Nature*, 422: 859-68.

Greenwald, C. J., T. Kasuga, N. L. Glass, B. D. Shaw, D. J. Ebbole, and H. H. Wilkinson. 2010. 'Temporal and spatial regulation of gene expression during asexual development of Neurospora crassa', *Genetics*, 186: 1217-30.

He, K., X. Zhang, S. Ren, and J. Sun. 2016. "Deep Residual Learning for Image Recognition." In *2016 IEEE Conference on Computer Vision and Pattern Recognition (CVPR)*, 770-78.

Johnson, Nancy Collins, Jason D. Hoeksema, James D. Bever, V. Bala Chaudhary, Catherine Gehring, John Klironomos, Roger Koide, R. Michael Miller, John Moore, Peter Moutoglis, Mark Schwartz, Suzanne Simard, William Swenson, James Umbanhowar, Gail Wilson, and Catherine Zabinski. 2006. 'From Lilliput to Brobdingnag: Extending Models of Mycorrhizal Function across Scales', *BioScience*, 56: 889-900.

Judge, M. T., Y. Wu, F. Tayyari, A. Hattori, J. Glushka, T. Ito, J. Arnold, and A. S. Edison. 2019. 'Continuous in vivo Metabolism by NMR', *Front Mol Biosci*, 6: 26.

Kendall, Maurice, and Alan Stuart. 1979. *The advanced theory of statistics. Vol.2: Inference and relationship*.

Lau, G. W., and J. E. Hamer. 1998. 'Acropetal: a genetic locus required for conidiophore architecture and pathogenicity in the rice blast fungus', *Fungal Genet Biol*, 24: 228-39.

Lemke, Klaus. 1985. 'Dispersal Models for Drosophila'.

Levy, Sasha F., and Mark L. Siegal. 2008. 'Network Hubs Buffer Environmental Variation in Saccharomyces cerevisiae', *PLOS Biology*, 6: e264.

Maheshwari, R. 1999. 'Microconidia of Neurospora crassa', *Fungal Genet Biol*, 26: 1-18.

McCluskey, K. 2003. 'The Fungal Genetics Stock Center: from molds to molecules', *Adv Appl Microbiol*, 52: 245-62.

Mir-Rashed, N., D. J. Jacobson, M. R. Dehghany, O. C. Micali, and M. L. Smith. 2000. 'Molecular and functional analyses of incompatibility genes at het-6 in a population of Neurospora crassa', *Fungal Genet Biol*, 30: 197-205.

Mukund Sundararajan, Ankur Taly, Qiqi Yan. 2017. 'Axiomatic Attribution for Deep Networks', *ArXiv*.

Ohya, Yoshikazu, Jun Sese, Masashi Yukawa, Fumi Sano, Yoichiro Nakatani, Taro L. Saito, Ayaka Saka, Tomoyuki Fukuda, Satoru Ishihara, Satomi Oka, Genjiro Suzuki, Machika Watanabe, Aiko Hirata, Miwaka Ohtani, Hiroshi Sawai, Nicolas Fraysse, Jean-Paul Latgé, Jean M. François, Markus Aebi, Seiji Tanaka, Sachiko Muramatsu, Hiroyuki Araki, Kintake Sonoike, Satoru Nogami, and Shinichi Morishita. 2005. 'High-dimensional and large-scale phenotyping of yeast mutants', *Proceedings of the National Academy of Sciences of the United States of America*, 102: 19015.

Olmedo, M., C. Ruger-Herreros, and L. M. Corrochano. 2010. 'Regulation by blue light of the fluffy gene encoding a major regulator of conidiation in Neurospora crassa', *Genetics*, 184: 651-8.

Palma-Guerrero, J., C. R. Hall, D. Kowbel, J. Welch, J. W. Taylor, R. B. Brem, and N. L. Glass. 2013. 'Genome wide association identifies novel loci involved in fungal communication', *PLoS Genet*, 9: e1003669.

Park, H. S., and J. H. Yu. 2012. 'Genetic control of asexual sporulation in filamentous fungi', *Curr Opin Microbiol*, 15: 669-77.

Parniske, Martin. 2008. 'Arbuscular mycorrhiza: the mother of plant root endosymbioses', *Nature Reviews Microbiology*, 6: 763-75.

Paszke, Adam, S. Gross, Francisco Massa, A. Lerer, J. Bradbury, G. Chanan, T. Killeen, Z. Lin, N. Gimelshein, L. Antiga, Alban Desmaison, Andreas Kˆpf, E. Yang, Zach DeVito, Martin Raison, Alykhan Tejani, Sasank Chilamkurthy, B.

Steiner, Lu Fang, Junjie Bai, and Soumith Chintala. 2019. 'PyTorch: An Imperative Style, High-Performance Deep Learning Library', *ArXiv*, abs/1912.01703.

Perkins, D., A. Radford, and M. Sachs. 2000. "The Neurospora Compendium: Chromosomal Loci." In.

Powell, A. J., D. J. Jacobson, L. Salter, and D. O. Natvig. 2003. 'Variation among natural isolates of Neurospora on small spatial scales', *Mycologia*, 95: 809-19.

Powell, Jeffrey R., and Theodosius Dobzhansky. 1976. 'How Far Do Flies Fly? The effects of migration in the evolutionary process are approached through a series of experiments on dispersal and gene diffusion in Drosophila', *American Scientist*, 64: 179-85.

Russakovsky, Olga, Jia Deng, Hao Su, Jonathan Krause, Sanjeev Satheesh, Sean Ma, Zhiheng Huang, Andrej Karpathy, Aditya Khosla, Michael Bernstein, Alexander C. Berg, and Li Fei-Fei. 2015. 'ImageNet Large Scale Visual Recognition Challenge', *International Journal of Computer Vision*, 115: 211-52.

Sargent, M. L., and S. H. Kaltenborn. 1972. 'Effects of medium composition and carbon dioxide on circadian conidiation in neurospora', *Plant Physiol*, 50: 171-5.

Schneider, Caroline A., Wayne S. Rasband, and Kevin W. Eliceiri. 2012. 'NIH Image to ImageJ: 25 years of image analysis', *Nature Methods*, 9: 671-75.

Sokolova, Marina, and Guy Lapalme. 2009. 'A systematic analysis of performance measures for classification tasks', *Information Processing & Management*, 45: 427-37.

Springer, M. L., and C. Yanofsky. 1989. 'A morphological and genetic analysis of conidiophore development in Neurospora crassa', *Genes Dev*, 3: 559-71.

Sturmfels, Pascal and Lundberg, Scott. 2020. 'Visualizing the Impact of Feature Attribution Baselines', *Distill*, 5: e22.

Timberlake, William E. 1990. 'MOLECULAR GENETICS OF ASPERGILLUS DEVELOPMENT', *Annual Review of Genetics*, 24: 5-36.

Turner, Barbara C., David D. Perkins, and Ann Fairfield. 2001. 'Neurospora from Natural Populations: A Global Study', *Fungal Genetics and Biology*, 32: 67-92.

Wang, F., J. Dijksterhuis, T. Wyatt, H. A. Wösten, and R. J. Bleichrodt. 2015. 'VeA of Aspergillus niger increases spore dispersing capacity by impacting conidiophore architecture', *Antonie Van Leeuwenhoek*, 107: 187-99.

Williams, C.J. et al. 1989. 'An Analysis of Density-Dependent Viability Selection', *Journal of the American Statistical Association*, 84: 662-68.

CHAPTER 3

CHARACTERIZING THE GENE-ENVIRONMENT INTERACTION UNDERLYING NATURAL MORPHOLOGICAL VARIATION IN *NEUROSPORA CRASSA* CONIDIOPHORES USING HIGH-THROUGHPUT PHENOMICS AND TRANSCRIPTOMICS[1]

[1] Krach, E.K., M. Skaro, Y. Wu, and J. Arnold. Submitted to *G3: Genes, Genomes, Genetics,* 11/05/2021

Abstract

Neurospora crassa propagates through dissemination of conidia, which develop through specialized structures called conidiophores. Recent work has identified striking variation in conidiophore morphology, using a wild population collection from Louisiana, United States of America (USA) to classify three distinct phenotypes: Wild-Type (WT), Wrap, and Bulky. Little is known about the impact of these phenotypes on sporulation or germination later in the *N. crassa* life cycle, or about the genetic variation that underlies them. In this study, we show that conidiophore morphology likely affects colonization capacity of wild *N. crassa* isolates through both sporulation distance and germination on different carbon sources. We generated and crossed homokaryotic strains belonging to each phenotypic group to more robustly fit a model for and estimate heritability of the complex trait, conidiophore architecture. Our fitted model suggests at least three genes and two epistatic interactions contribute to conidiophore phenotype, which has an estimated heritability of 0.47. To uncover genes contributing to these phenotypes, we performed RNA-Sequencing (RNA-Seq) on mycelia and conidiophores of strains representing each of the three phenotypes. Our results show that the Bulky strain had a distinct transcriptional profile from that of WT and Wrap, exhibiting differential expression patterns in *clock-controlled genes* (*ccgs*), the conidiation-specific gene *con-6*, and genes implicated in metabolism and communication. Combined, these results present novel ecological impacts of and differential gene expression underlying natural conidiophore morphological variation, a complex trait that has not yet been thoroughly explored.

Introduction

The classic filamentous fungus *Neurospora crassa* reproduces vegetatively through the development of macroconidiophores (conidiophores). These specialized structures serve to generate haploid macroconidia (conidia) that sporulate and germinate to propagate the asexual life cycle throughout an environment. Conidiophore development in *N. crassa* is well understood following decades of study in the laboratory. Briefly, the conidiation process begins with perpendicular growth of an aerial hypha. The filament undergoes minor and major constriction budding to generate spores that will eventually break off as mature conidia (Springer and Yanofsky, 1989). Environmental cues such as desiccation, aeration, nutrient deprivation, and light are required for induction of this process, which is under strict circadian regulation (Sargent and Kaltenborn 1972; Nelson et al 1975; Loros and Dunlap 2001). Many genes guiding conidiophore development have been identified and their expression has been characterized throughout the roughly 12-hour developmental timeline (Springer and Yanofsky, 1989; Greenwald et al, 2010). While these environmental, temporal, and genetic signals of conidiophore development are well understood, little is known about the morphological variation of these structures, particularly in natural populations.

Conidiophore architectural variation has just recently been explored in a wild population collection of *N. crassa* isolates from Louisiana, United States of America (USA) (Krach et al, 2020). This work identified three novel and distinct phenotypes, named Wild-Type (WT), Wrap, and Bulky, where WT conidiophores formed linear chains of conidia, Wrap conidiophores wrapped around and/or stuck to hyphal filaments, and Bulky conidiophores formed tight clusters (Krach et al, 2020). These phenotypes were

found to be upheld throughout the duration of their development and had a significant impact on resulting "spore shadows," or distributions of spore dispersal distances. This suggests that conidiophore architectural phenotype may affect colonization capacity of the organism, a hypothesis further explored in this study.

Here, using the same wild population collection of 21 strains, we reinforce that conidiophore morphology impacts spore dispersal distances on a larger scale, also affecting the maximum distance a conidium may travel. Furthermore, we show that conidiophore phenotype influences both germination rates and germination times of conidia on growth media containing different carbon sources, particularly in the Bulky strain. Applying methods developed in Krach et al (2020), we crossed homokaryotic strains for each phenotype and classified conidiophores of the resulting progeny. These phenotypic counts were used to fit a model where at least three genes and two epistatic interactions contributed to conidiophore morphology, a complex trait with an estimated heritability of 0.47. To identify genes underlying these conidiophore phenotypes, we performed RNA-Sequencing on both mycelia and conidiophores of a representative strain for each phenotypic group. Our results show that the Bulky strain has a unique transcriptional profile from WT and Wrap, exhibiting the most striking differential expression patterns in *clock-controlled genes* (*ccg-1*, *ccg-2*, *ccg-14*), metabolic genes responsive to starvation (*acu-6*, NCU04482), genes involved in communication (*doc-1*, *doc-2*, *plp-1*, *plp-2*), and the conidiation-specific gene, *con-6*. To our knowledge, this is the first report of genes implicated in natural morphological variation of *N. crassa* conidiophores. Together, this work lends insight to phenotypic variation of the conidiophore and its robustness to

environmental perturbations, as well as genetic differences underlying this variation in natural populations.

Materials and Methods

Strains and Media

Wild Louisiana isolates were obtained from the Fungal Genetics Stock Center (FGSC, Manhattan, KS, USA) and are listed below in Table 3.1. Strains were maintained on 1.8% glucose/1.8% fructose/1.5% agar slants with 1X Vogel's media and recommended biotin and trace element supplements (Davis and de Serres 1970).

Table 3.1. Wild isolates used in this study.

Strain Number	FGSC	Perkins	Mat	Strain provenance	Collection site	Substrate/Annotation
Wild Strains						
D110	8870	4448	A	Dettman, J.	Franklin, LA	sugarcane
D111	8871	4449	a	Dettman, J.	Franklin, LA	sugarcane
D112	8872	4453	A	Dettman, J.	Franklin, LA	sugarcane
D114	8874	4464	A	Dettman, J.	Franklin, LA	sugarcane
D116	8876	4481	a	Dettman, J.	Franklin, LA	sugarcane
D118	8878	4491	a	Dettman, J.	Franklin, LA	sugarcane
JW09	2229		A	Welch, J.	Welsh, LA	burned grass
JW10	2229		A	Welch, J.	Welsh, LA	burned grass
JW59	3200		a	Welch, J.	Coon, LA	burned stumps
JW66	3211		a	Welch, J.	Sugartown, LA	pine burn
JW70	3199		A	Welch, J.	Coon, LA	burned stumps
JW75	3943		a	Welch, J.	Houma, LA	sugarcane burn
	847		A	Lein	Louisiana	sugarcane burn
D113	8873	4454	a	Dettman, J.	Franklin, LA	sugarcane
D119	8879	4500	a	Dettman, J.	Franklin, LA	sugarcane
JW20	3212		A	Welch,J	Ravenswood, LA	bonfire
JW76	3943		a	Welch,J	Houma, LA	sugarcane burn
JW159	2221		a	Welch,J	Houma, LA	sugarcane burn
JW160	2222		A	Welch,J	Iowa, LA	grass burn
JW162	2223		a	Welch,J	Iowa, LA	grass burn
JW164	2224		a	Welch,J	Marrero, LA	wood burn
JW167	2228		a	Welch,J	Roanoke, LA	grass burn
OR74A	2489		A	FGSC	Marrero, LA	Unknown

Sporulation Experiment

Representative strains for each phenotypic class (FGSC8872, FGSC8876, and FGSC3943) were inoculated on 1.8% glucose 1.8% fructose 1.5% agar plates with 1X Vogel's Media, Biotin, and trace element supplements and incubated at 30°C for 30 hours. Mycelia was then harvested onto a 60 mm diameter nitrocellulose membrane with 0.45 μm pore size (Whatman Protran BA-85, Maidstone, England), inverted onto a new plate with media as described above, and set under the light for 20 hours before being transferred to a new environment for sporulation.

To explore sporulation on a larger scale, this "new environment" was 18x18 inch plastic cake platters repurposed as petri dishes (Fineline Settings, Middletown, NY, USA). The platters and their clear plastic lids were sterilized with ethanol and UV light before use. The nitrocellulose membranes containing isolated conidiophores were placed at the center of each cake platter, where SFG medium surrounded a 60 mm diameter blank space now occupied by the membrane. Each platter was covered with a lid through which light could penetrate and placed under the light for 4 days to allow sporulation, germination, and subsequent colonial growth. Pictures of each plate were taken with an iPhone XS, and ImageJ (Schneider et al 2012) was used to measure the distance from the center of each nitrocellulose membrane to the center of a colony, sampling up to 75 colonies per platter. Three biological replicates of each strain were performed.

Germination Assay

Representative strains used for each phenotypic group were FGSC8872 for Wild Type, FGSC8876 for Wrap, and FGSC2229 for Bulky. Cultures were grown up on 1.8%

glucose/1.8% fructose/1.5% agar slants with 1X Vogel's media and recommended biotin and trace element supplements for 5 days under light (Davis and de Serres 1970). Conidia were then suspended in water, counted using a Cellometer Auto 2000 (Nexcelom, Inc. Lawrence, MA USA), and diluted to roughly 1.00 x 10^3 cells/mL (Case et al 2014). 100 μl of conidial suspensions were pipetted onto 1.5% agar plates with 1% sorbose, 1X Vogels medium, recommended biotin and trace element supplements, and various carbon sources as follows: fructose and glucose (0.1% and 0.01%), mannose (1%, 0.1%, 0.01%), and xylose (1%, 0.1%, 0.01%). Plates were kept at 30°C for up to seven days and checked daily for colony germination, as germination time often varied with strain and medium. Colonies were counted once they germinated. Each strain was plated in triplicate for each medium condition, always alongside a positive control plate with 1.8% glucose/ 1.8% fructose/ 1.5% agar Vogel's medium.

We counted the number of colonies on each plate and calculated the average among three replicates. To calculate germination rates, we divided the average number of colonies per strain and condition by the expected colony count (based on conidial suspension concentration) x 100%.

To image conidiophores on 0.1% Mannose and 0.1% Xylose media (recipes described above), we left plates at 30℃ for an additional three days after counting colonies to allow sufficient conidiation. Brightfield images were taken at 20X using the microscope and augmentation methods described below (Microscopy and Image Deconvolution).

Crosses and Progeny Screening

Crosses were performed in the dark on cornmeal crossing medium, after which ascospores were plated on sorbose + fructose + glucose (SFG) media (Davis and de Serres 1970). Colonies were subsequently picked to isolate random ascospore progeny. Wild strains selected for initial crossing are tabled below in Table 3.2. Crosses were conducted in duplicate with 25 progeny selected from each cross.

Table 3.2. Wild isolates selected for crossing.

PARENT (A)	PHENOTYPE		PARENT (a)	PHENOTYPE		OFFSPRING
FGSC8872	WT 77.78%	x	FGSC3943	Bulky 48.78%	→	#42, 43
FGSC8872	WT 77.78%	x	FGSC8876	Wrap 53.85%	→	#151, 156
FGSC2229	Bulky 46.55%	x	FGSC8876	Wrap 53.85%	→	#83, 91

Because the original wild strains may possibly be heterokaryotic, we crossed representative strains from each phenotypic group (FGSC8872 for WT, FGSC8876 for Wrap, FGSC2229 and FGSC3943 for Bulky) to generate homokaryotic F1s. We then crossed F1s that represented each phenotypic group with the highest penetrance. F1s selected for crossing are tabled below in Table 3.3. F2 ascospores were plated on SFG medium as described above and picked to isolate 30 random ascospore progeny from each cross.

Table 3.3. F1s selected for crossing.

PARENT (A)	PENETRANCE		PARENT (a)	PENETRANCE
WT #151	100%	x	Bulky #91	100%
WT #151	100%	x	Wrap #43	80%
Wrap #156	83%	x	Bulky #91	100%

To isolate and image conidiophores in a high-throughput manner while preventing fusion of different progeny sharing a plate, each F2 strain was inoculated on a 1 mL 1.5% agar droplet containing 1.8% glucose/1.8% fructose with 1× Vogel's media and recommended biotin and trace element supplements (Davis and de Serres 1970). Each 150 × 15 mm petri dish contained eight agar droplets evenly spaced roughly 2.5 cm apart. Each droplet was inoculated with progeny conidia and incubated at 30 °C for 20 h to allow sufficient mycelial growth without hyphal fusion between droplets. Each droplet was then harvested onto a separate nitrocellulose membrane with 0.45 μm pore size (Whatman Protran BA-85, Maidstone, England). Each membrane was inverted onto a new agar droplet as described above and placed under light for aerial hyphae to penetrate the membrane. After 25 h, membranes were removed from the agar and secured on a flat surface for imaging of conidiophores (Krach et al 2020; adapted from Bailey-Shrode and Ebbole 2004).

Microscopy and Image Deconvolution

Nitrocellulose membranes containing conidiophores were visualized on an inverted microscope (Axio Observer A1, Carl Zeiss Microscopy, LLC, Thornwood, NY, USA) at

20X magnification and brightfield images were taken with a charge-coupled device (CCD) camera (AxioCam HRm, Carl Zeiss Microscopy, LLC, Thornwood, NY, USA). Multiple z-slices were captured and overlaid in ImageJ (Schneider et al 2012) to convey a complete representation of the three-dimensional conidiophore structure. Augmentation including contrast enhancement and noise and background subtraction was conducted on image stacks to isolate conidiophores from underlying mycelia and/or aerial hyphae. Classification of conidiophores was carried out through a convolutional neural network (Krach et al. 2020).

RNA Extraction

Previous work has shown that growing fungi on solid medium overlayed with a nylon membrane facilitates harvest of the mycelium, produces sufficient biomass, and enhances RNA quality (Schumann et al, 2013). Large petri dishes (150 x 15 mm) with 1.8% glucose, 1.8% fructose, 1.5% agar, 1X Vogel's media and recommended biotin and trace elements were covered with a Hybond XL Nylon membrane (Amersham, Buckinghamshire, UK). Membranes were inoculated with conidia from representative wild strains (FGSC8872, FGSC8876, FGSC2229) and placed at 30°C for 30 hours to allow for mycelial growth. Mycelia was then harvested with a sterile razor blade into a microcentrifuge tube and immediately frozen with liquid nitrogen for later RNA extraction. Four biological replicates of each strain were grown and harvested.

Conidiophore cultures were first grown following the protocol above. At the 30 hour time point, mycelia was covered with a 0.45 μm pore size nitrocellulose membrane (Whatman Protran BA-85, Maidstone, England) and placed under the light for 20 hours.

Aerial hyphae penetrated the nitrocellulose membrane, allowing conidiophore isolation from this top layer. Conidiophores were then harvested with a sterile razor blade and immediately frozen with liquid nitrogen for RNA extraction. Four biological replicates of each strain were grown and harvested. The method was adapted from Krach et al (2020) and Schumann et al (2013).

Mycelia and conidiophore samples were later ground to fine powder using the Cellcrusher tissue pulverizer (Cellcrusher, Cork, Ireland) submerged in liquid nitrogen. Samples were transferred to a new microcentrifuge tube and kept frozen. Total RNA was later isolated and suspended in RNase-free water using the Qiagen RNeasy Plant Mini Kit (QIAGEN, Inc., Valencia, CA) following the protocol outlined by the manufacturer. RNA integrity was assessed using the Agilent Bioanalyzer and RNA concentration was quantified using the fluorometric Qubit analyzer at the Georgia Genomics and Bioinformatics Core.

RNA Library Preparation

Libraries were prepared according to the KAPA Stranded RNA-Seq Kit. The libraries were then pooled and sequenced on a NextSeq2000 instrument to generate paired end reads. Library preparation, pooling, and sequencing was conducted at the Georgia Genomics and Bioinformatics Core.

RNA-Seq Data Analysis

Sequencing reads were demultiplexed by BaseSpace (Illumina). Reads were trimmed from the adaptor sequences using the cutadapt software (Martin 2011) and aligned

to the *Neurospora crassa* genome (NC12) following star quantification mRNA-seq pipeline. Gene expression data was analyzed in R version (4.0.3). The differentially expressed genes were measured using Bioconductor: DeSeq2 (Love et al, 2014). Differential gene expression was measured between cell type and strain. Power estimation for differential expression analysis was conducted using the Vanderbilt power calculation for RNA-Seq experiment Shiny app (Guo et al, 2014). Genes were filtered for an adjusted *p*-value and absolute fold change of $10e^{-5}$ and absolute $\log_2FC > 3.0$, respectively.

Differentially expressed genes were extracted from the res table generated in the DESeq2 pipeline. Expression values for the top 500 most significantly differentially expressed genes were used to hierarchically cluster samples. The DESeq2 package was used to conduct principal component analysis (PCA) and generate PCA plots. Hierarchical clustering was used to discriminate sample phylogeny in the experimental setting. Pretty Heatmaps package (Kolde 2018) was used to visualize the expression patterns of the most significantly differentially expressed genes for each experimental design.

Results

Conidiophore architectural phenotype may impact colonization capacity of N. crassa by affecting the maximum dispersal distance of released conidia.

Previous work showed that conidiophore architectural phenotype may play a role in colonization capacity of the organism by affecting spore dispersal distance (Krach et al, 2020). Dispersal experiments to measure gene flow have been extensively used in population genetics (Dobzhansky and Wright, 1943; Trapnell and Hamrick, 2005; Hamrick and Trapnell, 2011). A key element to the design of these experiments is the size of the

grid on which dispersal is measured. We wanted to scale up our previous spore shadow experiment to explore spore dispersal over a larger area (Powell and Dobzhansky, 1976). Limiting the boundaries of a dispersal experiment to measure gene flow introduces biases in specifying the distribution of dispersal distances of the organism (Lemke, 1985). To expand these boundaries, we allowed conidiophores of each architectural phenotype to sporulate and germinate on 0.1% SFG medium, reinventing an 18x18 inch plastic cake platter as a large petri dish.

Consistent with the findings in Krach et al 2020, fewer colonies developed from WT conidiophores (n=35) compared to that of Wrap and Bulky (n=195 and n=104, respectively). The distribution of spore dispersal distances by the Wrap conidiophores was significantly different from that of both WT ($p=0.04926$) and Bulky ($p=0.004794$) phenotypes, found by two-sample Kolmogorov-Smirnov tests (Kendall and Stuart 1979). No significant difference was found in spore dispersal distance distributions between the WT and Bulky groups ($p=0.2734$). Both findings are consistent with sporulation patterns observed at a smaller scale, indicating that the spore shadows displayed by each conidiophore phenotype are upheld in this new, larger environment (Krach et al, 2020). Taking advantage of this larger controlled environment, we then sought to investigate whether the conidiophore architectural phenotype had an impact on the maximum distance a conidium could travel and subsequently germinate.

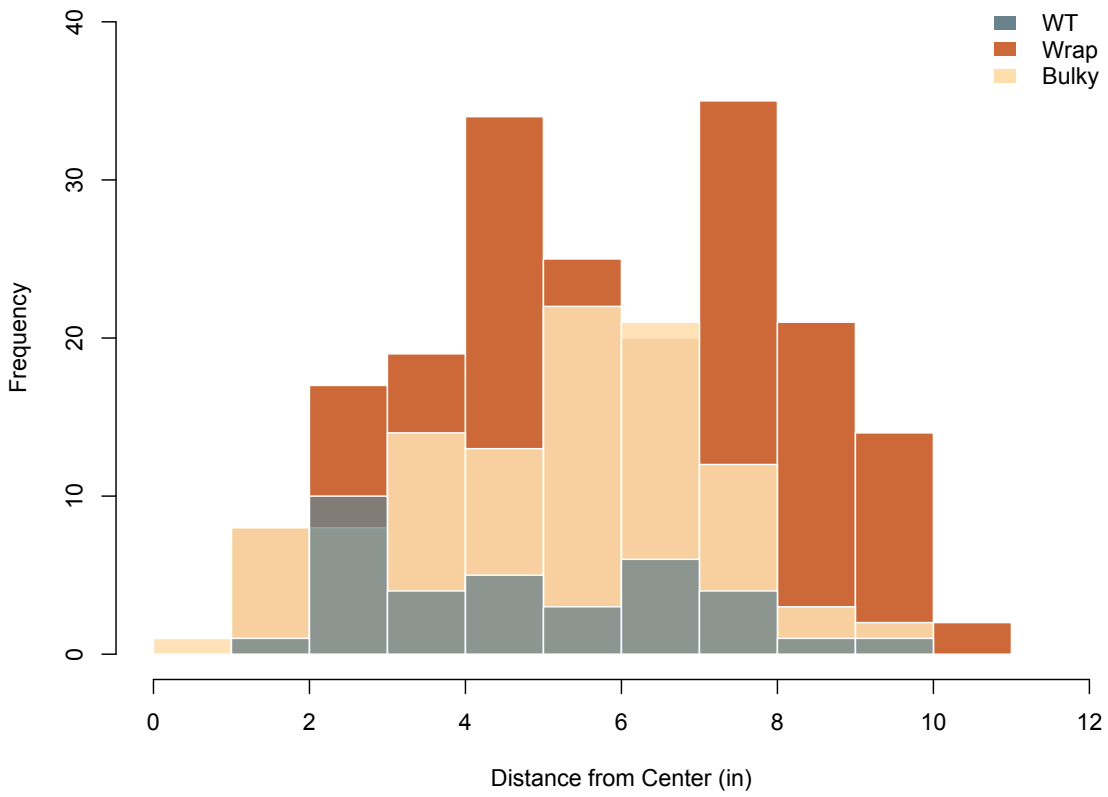

Figure 3.1. Distribution of spore dispersal distances, scaled up. Histogram of distances in inches to the center of each colony from the center of each nitrocellulose membrane. Total colony counts combining three replicates are as follows: WT = 35, Wrap = 195, Bulky = 104. Results of two-sample Kolmogorov–Smirnov tests for each phenotype pair are as follows: WT-Wrap D=0.24982, p=0.04926; Wrap-Bulky D=0.2109, p=0.004794; WT-Bulky D=0.18709, p=0.2734.

Previous work showed that WT spores traveled the least distance following dispersal (Krach et al, 2020). The null hypothesis examined is whether the maximum distance traveled by Wrap and Bulky could be considered to be drawn from the same distribution of the maximum distance squared traveled by WT (Table 3.4). It is reasonable to suppose that spore dispersal coordinate is normally distributed (Powell and Dobzhansky,

1976). The distribution of standardized distance squared is then chi-squared with one degree of freedom. The largest distance traveled has a known distribution, and the probability that the largest distances seen in Wrap and Bulky are drawn from the dispersal distribution of WT is extremely unlikely (David 1981).

Table 3.4. Maximum spore dispersal distances traveled by Wrap and Bulky are significantly different from WT. Maximum distance in inches among three biological replicates traveled by a germinating conidium of each phenotype. For all three values, the mean movement ($\bar{X}$ = 4.729) was subtracted, the sample variance (S^2 = 2.165) was used to standardize, and the resulting z-value ($z = (X-\bar{X})/s$), squared. The resulting z^2 is then chi-squared in distribution with one degree of freedom. The tail probability for the distribution of the largest rank from this chi-squared distribution was then computed as if these z^2 values were all order statistics from the same distribution (David 1981).

Strain (Phenotype)	**Maximum Distance**	**Tail Probability of the WT distribution of the largest rank of distance squared**
FGSC8872 (WT)	9.25 inches	-
FGSC8876 (Wrap)	10.15 inches	3.80×10^{-64}
FGSC3943 (Bulky)	9.51 inches	2.15×10^{-51}

Spores from conidiophores with different architectural phenotypes show distinct germination patterns on different carbon sources.

We sought to further explore the potential impact of conidiophore phenotype on environmental colonization through the lens of germination. To do this, we plated known amounts of conidia from a WT, Wrap, and Bulky strain (FGSC8872, FGSC8876, and FGSC2229, respectively) onto media containing 1% sorbose, a monosaccharide known to limit the organism to colonial growth. Each colony on a plate represents germination of one conidium. We varied the media to assess the germination behavior of each conidiophore phenotype on different carbon sources: Fructose/Glucose, Mannose, and Xylose. In addition to the different carbon sources, we also explored varying concentrations of each. Germination rates were determined from colonies counted / expected colonies x 100% and are depicted below in Figure 3.2.

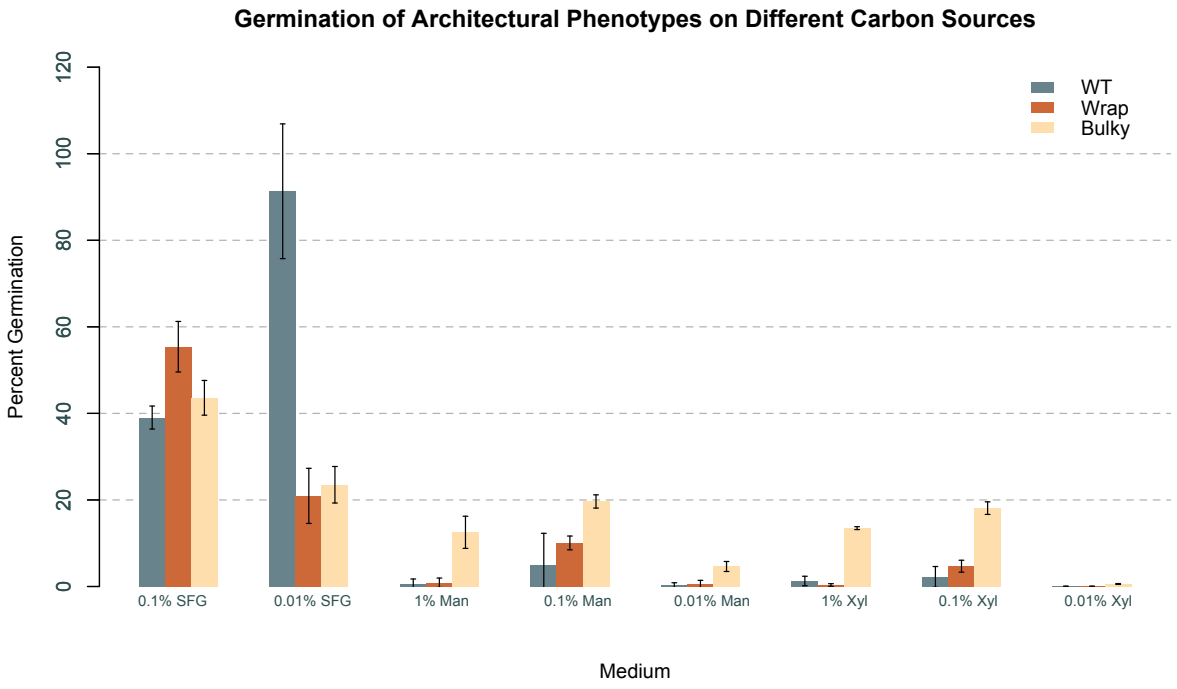

Figure 3.2. Germination rates of architectural phenotypes on different carbon sources. Germination rates of conidia from each phenotypic group (FGSC8872 for WT, FGSC8876 for Wrap, FGSC2229 for Bulky) on media containing varying concentrations of different carbon sources (SFG = fructose and glucose, Man = mannose, Xyl = xylose).

When compared to different concentrations of the same carbon source, all strains show the highest germination rate with a sugar concentration of 0.1%, with the one exception of WT on 0.01% SFG. Interestingly, spores from WT conidiophores show a jump in germination from 39% to 91% when fructose and glucose are decreased by an order of magnitude, whereas Wrap and Bulky groups both show lower germination rates. This pattern exhibited by WT indicates a starvation response that is unique to this phenotypic group on SFG medium.

In all concentrations of media containing mannose and xylose, Bulky spores consistently show a significantly elevated germination rate compared to the other two groups. This is a pattern unique to these two carbon sources and is not observed at either concentration of SFG medium.

In addition to germination rate, germination time also varies with conidiophore phenotype under some medium conditions (Figure 3.3). All three phenotypic groups germinated synchronously on SFG medium, as well as on the positive control of 1.8% Glucose Vogel's Medium. However, on all concentrations of mannose and xylose, Bulky conidia germinated earlier than the other two phenotypic groups, which remained synchronous. Interestingly, this unique temporal behavior exhibited by Bulky conidia is

consistent with the uniqueness of higher germination rates observed by Bulky on these same carbon sources.

On all carbon sources, germination of each strain is delayed as concentration of the sugar decreases. This is true in all cases, except for Bulky on 0.1% and 1% Mannose where germination occurs on Day 3 under both conditions.

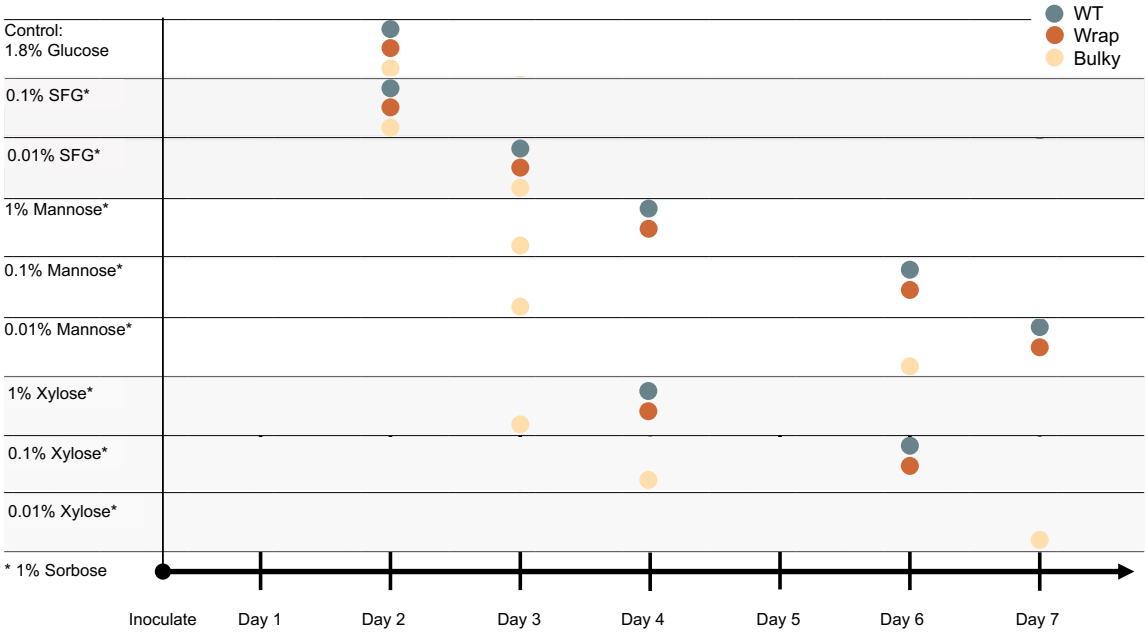

Figure 3.3. Germination timeline of architectural phenotypes on different carbon sources. Germination times of conidia from each conidiophore phenotype (FGSC8872 for WT, FGSC8876 for Wrap, FGSC2229 for Bulky) on different media conditions at 30°C.

After characterizing germination on these new carbon sources, we were curious if conidiophore architectural phenotype was upheld once conidiation occurred. We imaged conidiophores of each strain on 0.1% mannose and 0.1% xylose, as germination rates were

highest with this sugar concentration for all three strains. On both 0.1% mannose and 0.1% xylose, WT, Wrap and Bulky architectural phenotypes were upheld in the conidiophores (Figure 3.4).

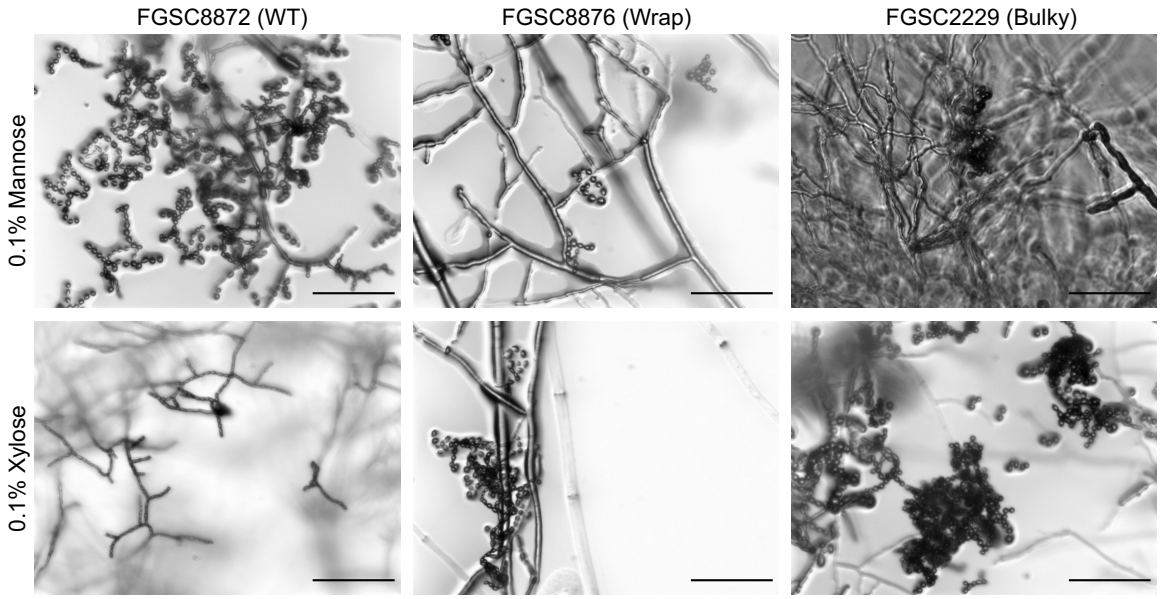

Figure 3.4. Conidiophore phenotypes on media containing mannose and xylose. Conidiophore architectural phenotypes are upheld on media containing 0.1% mannose (top row) and 0.1% xylose (bottom row) as a carbon source. Representative strains used were FGSC8872 for WT, FGSC8876 for Wrap, and FGSC2229 for Bulky. Scale bar, 100 μm.

Crosses between homokaryotic F1s suggest at least three genes contribute to conidiophore architectural phenotype.

Previous work has shown that at least two genes contribute to the conidiophore architectural phenotype, and the trait has an estimated heritability of 0.23 (Krach et al, 2020). This model was based on progeny phenotype counts from crosses between original Louisiana wild isolates. Because wild strains may possibly be heterokaryotic, this

inheritance model would be more robust by crossing homokaryotic F1s, quantifying conidiophore phenotypes of the resulting F2, and fitting the model to those phenotypic ratios.

We selected F1 parents with the greatest penetrance of each conidiophore phenotype and conducted crosses between groups. We then selected 30 random ascospore progeny from each cross. Conidiophores from these F2 were isolated, imaged, and classified using the automated classification method developed and successfully applied in Krach et al 2020. The phenotypic ratios of each F1 parent and the resulting F2 progeny are depicted below in Figure 3.5 and summed in Table 3.5.

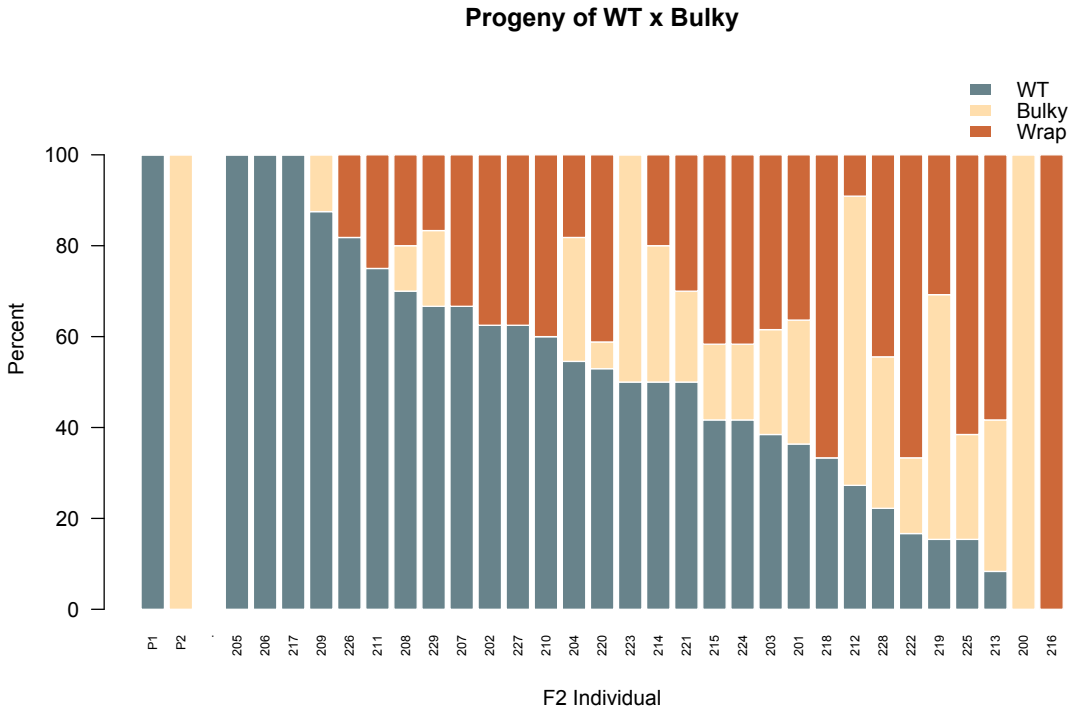

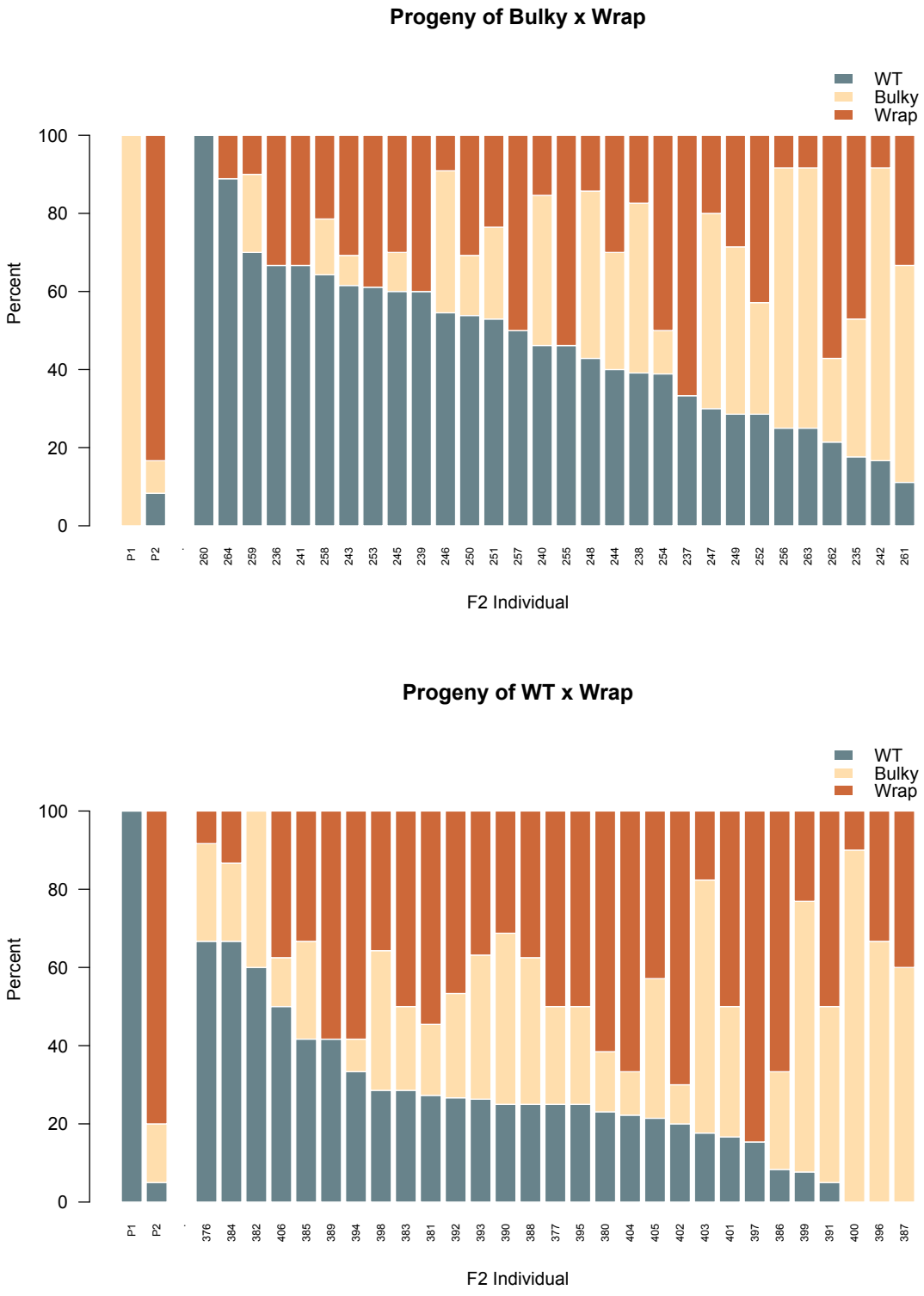

Figure 3.5. Percent of conidiophore phenotypes observed in F1 parents and resulting F2 progeny. Crosses were conducted between majority WT x Bulky (top), Bulky x Wrap

(middle), and WT x Wrap (bottom) F1s, whose phenotypic ratios are depicted as the two left most bars on each plot. Phenotype ratios of the resulting F2 progeny are plotted as the following 30 bars.

Table 3.5. F2 phenotype counts. Multinomial counts of progeny phenotypes from each of the three crosses.

	A (WT)	**B (Wrap)**	**C (Bulky)**
A × B	$N_{11} = 103$	N_{12}=167	$N_{13} = 126$
B × C	$N_{21} = 142$	N_{22}= 86	N_{23}= 58
A × C	$N_{31} = 170$	N_{32}=108	N_{33}=88

Conidiophore phenotype counts were used to estimate an inheritance model successfully fitted in Krach et al 2020. The model was fitted by the Method of Maximum Likelihood (ML) using iteratively reweighted least squares (IRLS) (Asmussen et al 1987; Kendall and Stuart 1979). The results for ML fitting the model computed with IRLS computed with a relative error < 10^{-8} after nine iterations are summarized below in Table 3.6. The full epistatic model with three genes fitted the phenotypic ratios, and the only epistatic interaction that could be dropped was between the A (WT) and C (Bulky) genes. We concluded that at least three genes contribute to conidiophore phenotype. Using an additive model and the model without gene effects, we were able to estimate a heritability (H^2) of 0.47 for this complex trait. This is an increase from our previously estimated H^2 of 0.23, suggesting that using homokaryotic F2s reduced noise in the model (Krach et al 2020).

Table 3.6. Fitting of inheritance models. A nested hierarchy of inheritance models was successfully fitted with at least three genes controlling the conidiophore architectural phenotype to the counts of progeny phenotypes from three crosses (Table 3.5), in which the number of offspring from each cross is fixed. Nine iterations were necessary to achieve the desired error tolerance of 10^{-8} with iteratively reweighted least square (IRLS). Recommended model was bolded along with its goodness of fit to the counts of phenotypes in crosses. A null hypothesis (H0) is tested against an alternative (HA) with the chi-squared test having degrees of freedom (df).

Model	**X^2**	**df**	***p***	**$X^2_{HA} - X^2_{H0}$**	**df**	***p* for HA vs. H0**	**Notes**
Full epistatic	9.12	3	-	-	-	0.03	H0 = full epistatic
$\alpha\beta = 0$	13.37	1	<0.0001	13.37 – 9.12 = 4.25	1	0.04	H0 = full epistatic
$\alpha\beta = \alpha = 0$	16.27	2	<0.0001	16.27 – 9.12 = 7.15	2	0.03	H0 = full epistatic
$\alpha\beta = \beta = 0$	29.88	2	<0.0001	29.88 – 9.12 = 20.76	2	<0.0001	H0 = full epistatic
$\beta\gamma = 0$	43.42	1	<0.0001	43.42 – 9.12 = 34.30	1	<0.001	H0 = full epistatic
$\boldsymbol{\alpha\gamma = 0}$	11.11	1	<0.0001	11.11 – 9.12 = 11.11	1	0.16	H0 = full epistatic
$\alpha\beta = \beta\gamma = \alpha\gamma = 0$ additive	44.61	3	<0.0001	44.61 – 9.12 = 35.49	3	<0.0001	H0 = full epistatic
environmental	84.27	6	<0.0001	84.27 – 9.12 = 75.15	6	<0.0001	H0 = full epistatic
heritability							H^2=(84.27– 44.61)/84.27 = 0.47 H0=environmental model H1 = full additive model

Table 3.7. Maximum likelihood estimates of allelic effects and epistatic effects in a three-locus model of inheritance. The full epistatic model with three genes has three allelic effects and two epistatic interactions. The standard errors were obtained from the square roots of the diagonal elements of the inverse of the information matrix N$X'AX$.

Parameters	$\alpha\gamma = 0$ **3 Genes**
α	0.14 ± 0.0130
β	0.38 ± 0.0182
γ	-0.28 ± 0.0085
$\alpha\beta$	-0.24 ± 0.0175
$\beta\gamma$	-0.55 ± 0.0175
$\alpha\gamma$	0.00

Bulky mycelia and conidiophore samples display different transcriptional profiles from that of the WT and Wrap strains.

Our inheritance model estimated at least three genes are involved in conidiophore architectural phenotype. To explore loci that may contribute to this complex trait, we performed RNA-sequencing (RNA-seq) on both mycelia and conidiophores from strains representing each conidiophore architectural phenotype (FGSC8872 for WT, FGSC8876 for Wrap, FGSC2229 for Bulky). Clustering by principal component analysis (PCA) showed a clear grouping by cell type, as expected by previous work identifying genes differentially expressed in *N. crassa* vegetative cell types (Nelson et al 1997; Greenwald et al 2010; Sachs and Yanofsky 1991). Interestingly, the clustering suggests striking similarity between expression patterns of WT and Wrap mycelia, and WT and Wrap conidiophores, while Bulky cell types cluster to groups of their own (Figure 3.6).

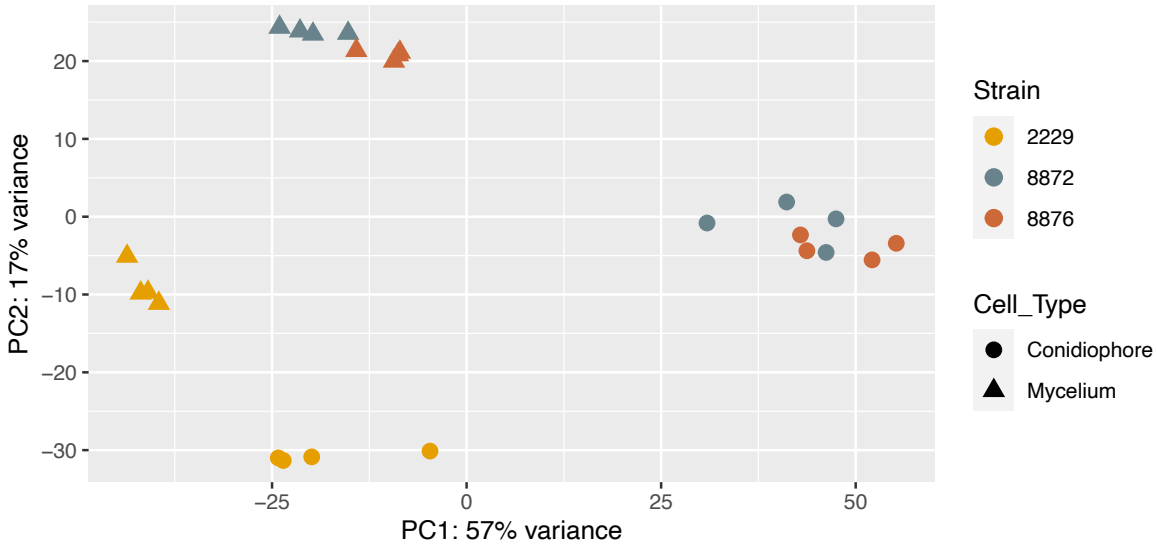

Figure 3.6. Principal component analysis (PCA) of all samples characterized by RNA-seq. Principal component analysis. A 2D PCA plot was generated using normalized and variance stabilized transcript expression data (vst transformation, DESeq2) for the top 500 most variant transcripts in the dataset (measured by row variance). The percent of variance explained by each principal component is displayed on each axis. 2229 samples (Hexcode: E69F00), 8872 samples (Hexcode: 68838B), and 8876 (Hexcode CD6839) cluster into two distinct groups on PC1 where conidiophore of 8872 and 8876 form a clear cluster away from 2229. Within the mycelium clusters, samples of 8872 and 8876 cluster together on PC2. 74 % of the total variance can be distinguished by cell type. Samples are assigned a color by strain and shape by cell type. Representative strains used were FGSC8872 for WT, FGSC8876 for Wrap, and FGSC2229 for Bulky. Four biological replicates were measured per condition.

Expression patterns for the twenty most differentially expressed genes are presented in Figure 3.7. Of these twenty loci, five are *clock-controlled genes* (*ccgs*): NCU08457 (*ccg-2*), NCU03753 (*ccg-1*), NCU07787 (*ccg-14*), NCU08936 (*ccg-15*), and NCU05495 (*ccg-16*). Interestingly, Bulky mycelia have lower *ccg-2* expression compared to WT and Wrap mycelia, just as Bulky conidiophores have lower *ccg-2* expression than both WT and Wrap conidiophores. *ccg-2* is allelic with easily wettable (*eas*) and encodes a hydrophobin critical for maintaining cell wall hydrophobicity in the conidium (Bell-Pedersen et al 1992). The Bulky samples also show a unique expression pattern of *ccg-1*, where transcription is higher in the mycelium than in the conidiophore. This contrasts with both WT and Wrap, where *ccg-1* expression is higher in the conidiophore than in the mycelium. Expression of *ccg-14* is higher in both Bulky mycelia and conidiophores when compared to the corresponding cell types of WT and Wrap samples.

Another interesting expression pattern is observed with NCU09873 (*acu-6*) and NCU04482 (uncharacterized). Both loci show strikingly lower expression in Bulky mycelia compared to all other strains and cell types. *acu-6* encodes the structural gene for phosphoenolpyruvate carboxykinase (PEPCK), and NCU04482 encodes a hypothetical protein that plays a role in amino acid metabolism (Flavell and Fincham 1968; Schmoll et al 2012).

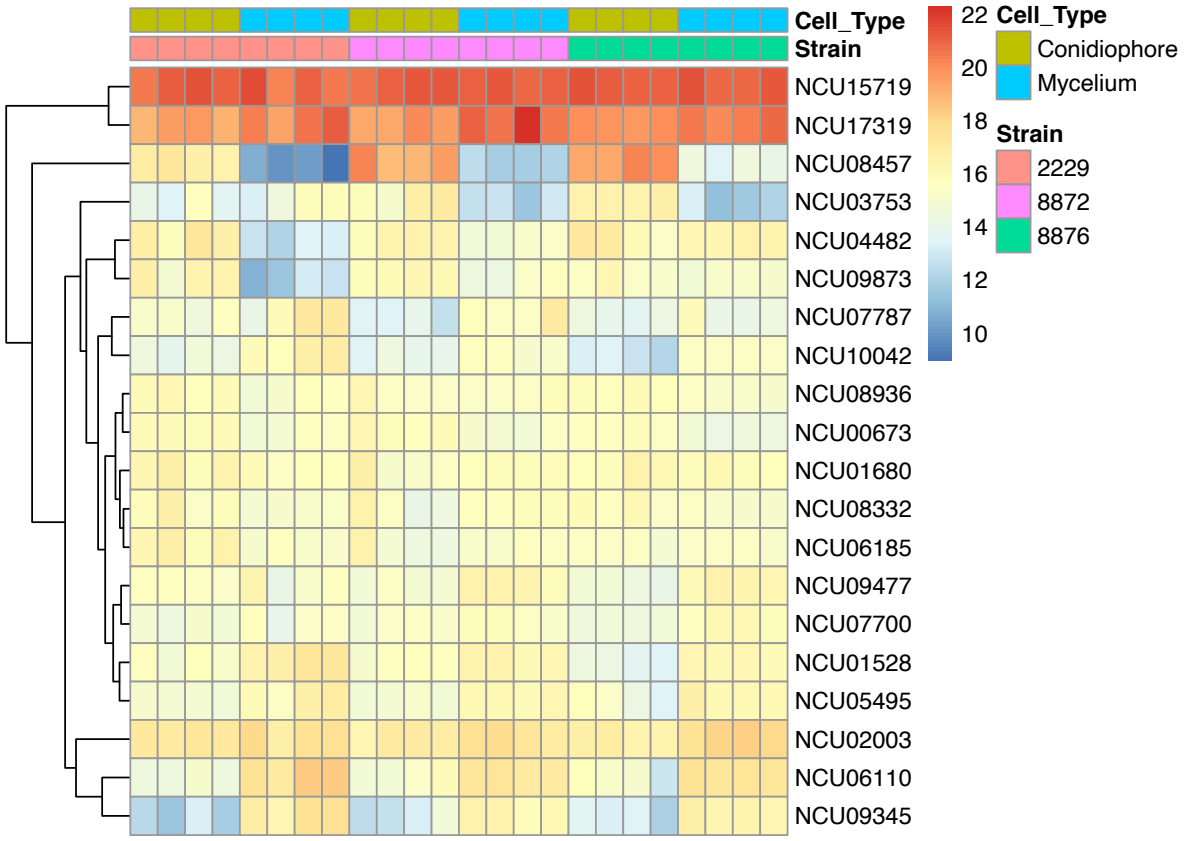

Figure 3.7. Heatmap of normalized counts. Reads were normalized in DESeq2 by the median of ratios method (Love et al, 2014) and are depicted for the 20 most differentially expressed genes for all strains and cell types. Each column represents a biological sample and each row a gene. There are four biological replicates per condition.

To further explore the genes driving separation of the Bulky strain by PCA (Figure 3.6), we examined genes differentially expressed when comparing WT to Bulky and Wrap to Bulky (Figure 3.8). There were genes significantly up- and down-regulated in both strain comparisons. Of these significantly differentially expressed genes, only five loci were shared by both strain comparisons, all of which were more highly expressed in Bulky

than WT or Wrap. These shared genes are NCU07191 (*doc-1*), NCU07192 (*doc-2*), NCU09244 (*plp-1*), NCU09245 (*plp-2*), and NCU05035 (*vad-12*).

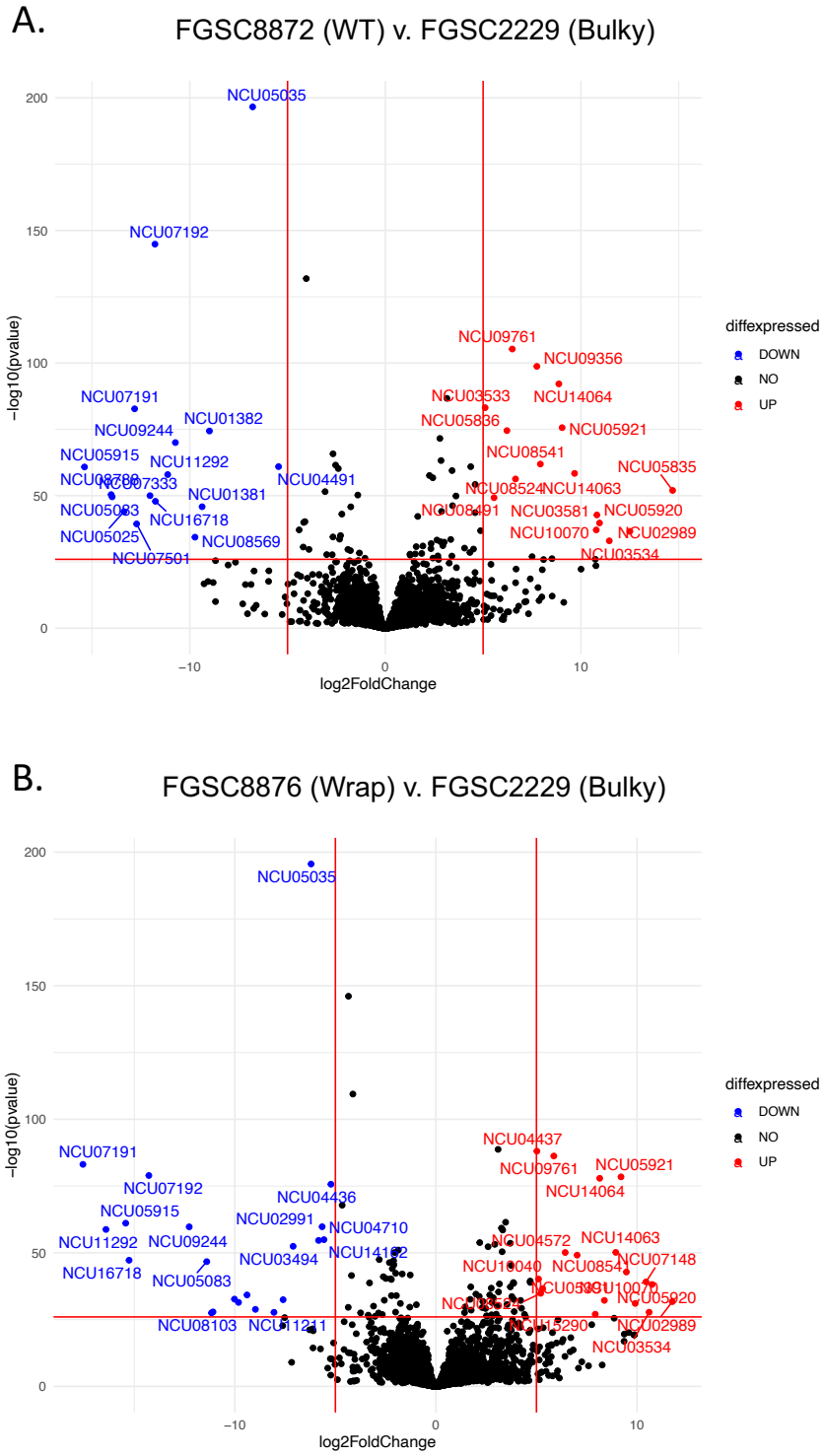

Figure 3.8. Volcano plots of significantly differently expressed genes between strains. Genes differentially expressed in WT versus Bulky strains are plotted in the left panel, and genes from the Wrap versus Bulky comparison are on the right. The log2 fold change signifies normalized expression of a gene, each represented by a dot. Each gene is color coded according to its significance, where blue genes are significantly down-regulated in WT/Wrap, red genes are significantly up-regulated in WT/Wrap, and black genes are not significant.

The *doc* (*determinant of communication*) genes mediate long-distance kind-recognition, where filaments belonging to the same communication group are more likely to interact (Heller et al 2016). Increased expression of *doc-1* and *doc-2* in the Bulky strain sparked the hypothesis that perhaps there was a relationship between communication group and conidiophore phenotype. Previous work has characterized the communication groups (CG) of 110 wild *N. crassa* isolates, including the Louisiana collection employed in this work (Heller et al 2016). While the representative strains selected for RNA-Seq do belong to different CGs, this pattern is not upheld when examining the complete population collection (Figure 3.9). The *plp* (*palatin-like phospholipase*) genes also contribute to *N. crassa* self-recognition, triggering germling-regulated death following heterokaryon incompatibility (Heller et al 2018). The final gene more expressed in Bulky than in both WT and Wrap is *vad-12*, a locus involved in vegetative asexual development that is not well characterized (Carrillo et al 2017).

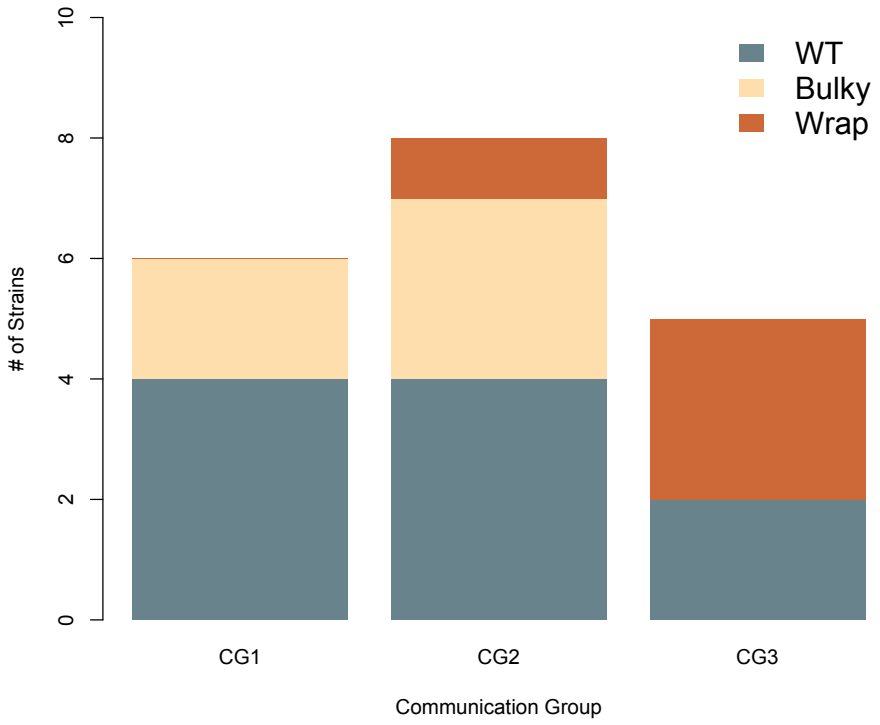

Figure 3.9. Communication groups (CG) of wild isolates and their conidiophore architectural phenotype. Strains are color coded by their conidiophore phenotype. There is no significant relationship between CG assignment and conidiophore phenotype determined by Chi-square test of independence (X^2=7.3388, df=4, p=0.119).

To more specifically examine genes contributing to these morphological phenotypes, we compared expression patterns between strains for the conidiophore samples alone. Principal component analysis showed clear clustering between conidiophore samples from each of the three strains (Figure 3.10).

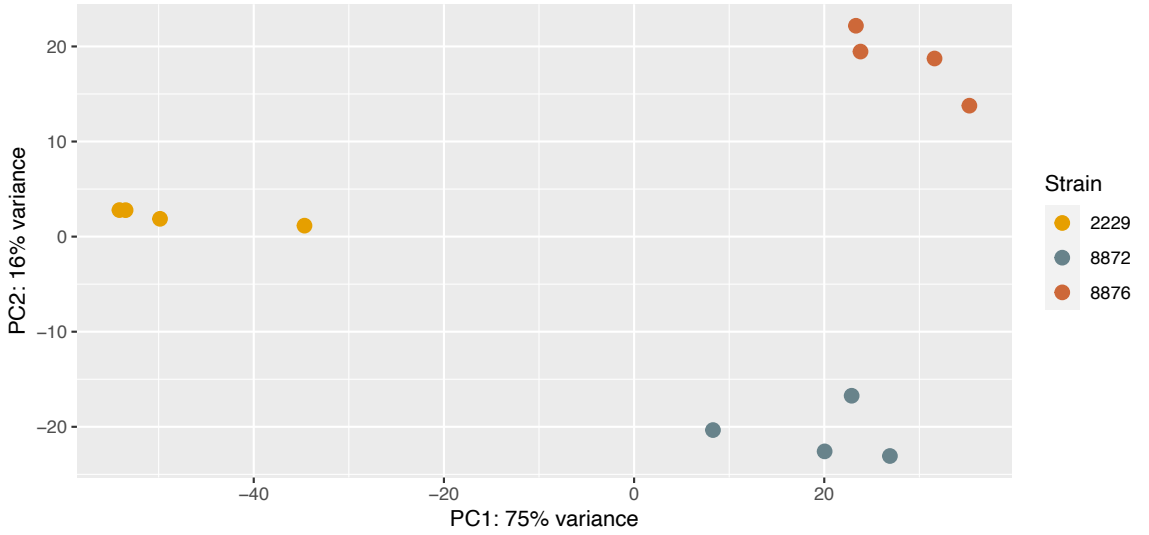

Figure 3.10. Principal component analysis (PCA) of conidiophore samples characterized by RNA-seq. PCA explains 91% of the variance between the three strains representing conidiophore phenotypes. Samples are assigned a color according to strain. Four biological replicates were measured per condition.

Expression patterns for the twenty genes most differentially expressed in the conidiophore are presented in Figure 3.11. Fourteen of these genes are consistent with those presented in Figure 3.7, including the previously mentioned *ccg-2*, *ccg-1*, *ccg-15*, *acu-6*, and NCU04482. However, analyzing the conidiophore samples revealed two additional genes displaying striking differential expression patterns: NCU08769 (*con-6*) and NCU00265 (uncharacterized). The conidiation specific gene *con-6* is also under clock control and is down-regulated in Bulky conidiophores. NCU00265 encodes a predicted secreted protein and is upregulated in Bulky conidiophores.

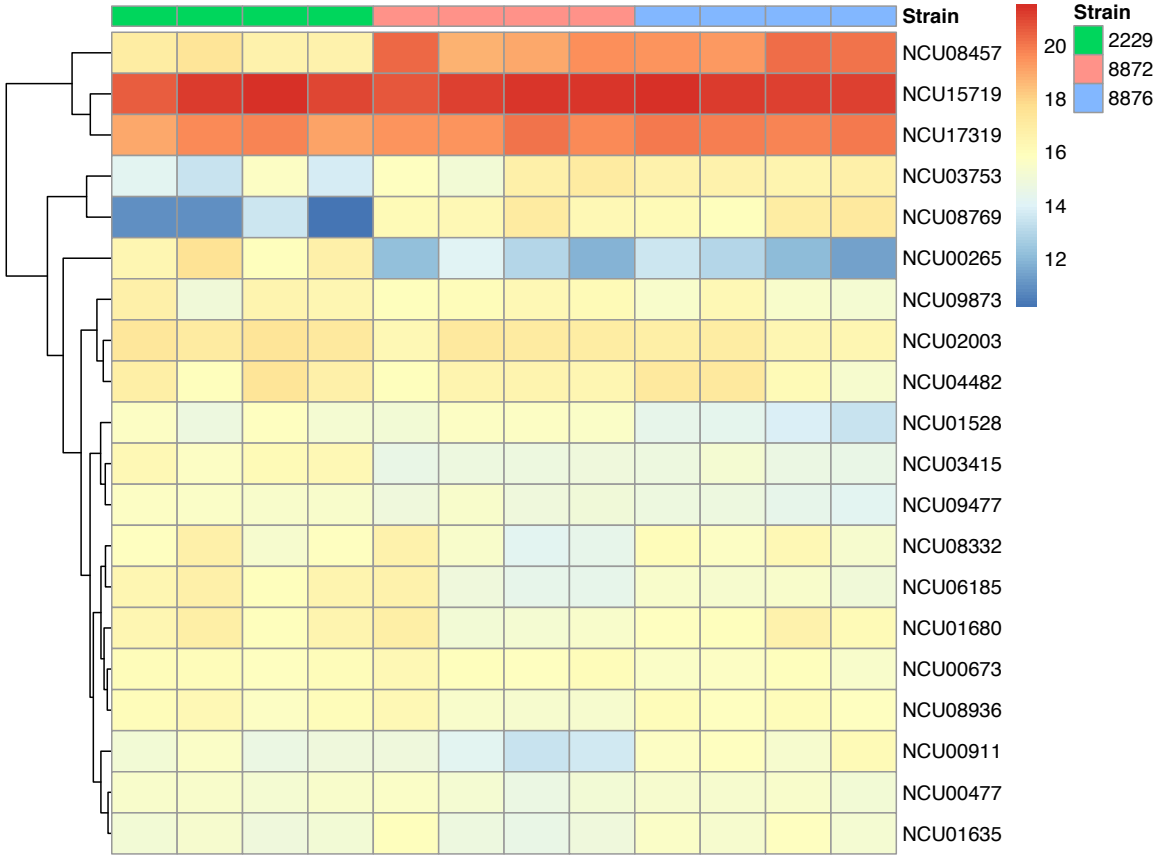

Figure 3.11. Heatmap of normalized counts in conidiophores. Read counts were normalized in DESeq2 using the median of ratios method (Love et al, 2014) and are depicted for the 20 most differentially expressed genes for conidiophores of all strains. Each column represents a biological sample and each row a gene. There are four biological replicates per condition.

Discussion

Conidiation in *N. crassa* has been thoroughly investigated over the course of decades of study. While much work has been done to characterize the genetic, temporal, environmental, and circadian signals guiding conidiophore development, we lack a complete understanding of the morphological variation of these structures (Springer and

Yanofsky 1989; Sargent and Kaltenborn 1972; Loros and Dunlap 2001). Recent work has begun to explore natural conidiophore variation, using a collection of wild isolates to identify three architectural phenotypes: Wild-Type, Wrap, and Bulky (Krach et al 2020). We continued this exploration by investigating the impact of these phenotypes on sporulation and germination, developing a more robust model to estimate heritability of the trait, and identifying genes differentially expressed in representative strains for each conidiophore shape.

Previous work has demonstrated that conidiophore morphology impacts the distribution of distances traveled by sporulating conidia, or the "spore shadow" (Krach et al, 2020). Similar studies have revealed that dispersal patterns impact gene flow between natural populations of *Drosophila* and *Laelia rubescens*, for example (Powell and Dobzhansky, 1976; Trapnell and Hamrick, 2005). Modeled at a small scale, fewest WT conidia germinated and the maximum distance a spore traveled and germinated was the least in WT (Krach et al, 2020). Here, we showed that both patterns were upheld at a larger scale, indicating that WT populations may not have as wide a colonization capacity, and thus as large of gene flow, as Wrap and Bulky. Additional studies could be conducted to explore spore shadows from each conidiophore phenotype in different environments, such as on various plant substrates or in different climates. We also demonstrated that conidiophore phenotype impacted germination rate and germination time of conidia on different carbon sources. Germination of conidia from WT conidiophores drastically increased by 52% when fructose and glucose concentration decreased from 1% to 0.1%, presumably a stress response that was not observed in the other two phenotypes. On medium containing mannose or xylose as a carbon source, conidia from Bulky

conidiophores showed a striking response, consistently germinating earlier and at significantly higher rates than the other two phenotypes. This suggests that Bulky is much more responsive than the other two strains to the stress of these unfavorable carbon sources.

Implementing tools previously developed in Krach et al (2020), we used homokaryotic strains to more robustly estimate heritability of conidiophore phenotype. Our model suggested that at least three genes contribute to this complex trait with two epistatic interactions (Table 3.6). The fitted model revealed an estimated heritability of 0.47, an increase from the heritability previously estimated using the original, possibly heterokaryotic, wild isolates. To further explore the genes contributing to conidiophore morphology, we conducted RNA-Seq on mycelia and conidiophores from each phenotype.

Our RNA-seq results demonstrate that the Bulky (FGSC2229) transcriptional profile is unique from that of WT and Wrap, clearly separating it from the other two strains by PCA (Figure 3.6). Five of the twenty most differentially expressed genes were *clock controlled genes* (*ccgs*), three of which showed distinctive expression patterns in the Bulky cell types: *ccg-2*, *ccg-1*, and *ccg-14*. Notably, both *ccg-2* and *ccg-14* encode proteins that localize to the conidium cell wall. The CCG-2 protein, a hydrophobin, maintains hydrophobicity of the conidium cell wall (Bell-Pedersen et al, 1992). The protein encoded by *ccg-14* (*snodprot1*) bears sequence similarity to cerato-platanin, a phytotoxin prevalent in other ascomycetes that has both hydrophobin and expansin properties (Jeong et al 2007). It is known that the cell wall plays a critical role in fungal morphology, growth rate, and viability, and several mutations affecting *N. crassa* cell wall components have been associated with a compact growth phenotype (Patel and Free, 2019). Our study shows that compared to both WT and Wrap, Bulky mycelia and conidiophores have increased

expression of *ccg-14* and decreased expression of *ccg-2*. It is possible that the Bulky cell wall is comprised of different proportions of the CCG-2 and CCG-14 proteins, potentially affecting polarity of the structure and conidiophore morphology. An alternative hypothesis is that the Bulky strain has up-regulated expression of the cerato-platanin phytotoxin as an evolved defense mechanism, another potential explanation for the compactness of the Bulky phenotype. Additional research should be conducted on known cell wall mutants and the role of CCG-14 in *Neurospora* to better assess the impact of these genes on morphology of the conidiophore.

Two genes with roles in metabolism were also differentially expressed in the Bulky strain: *acu-6* and NCU04482. *acu-6* is the structural gene for PEPCK, which converts oxaloacetate to phosphoenolpyruvate in gluconeogenesis (Flavell and Fincham, 1968). Previous work has demonstrated that *acu-6* is upregulated under starvation and is responsive to quinic acid, an unfavorable carbon source (Tang et al, 2011). NCU04482 encodes a hypothetical protein and is upregulated by amino acid starvation (Schmoll et al 2012). We observed that both loci are strikingly downregulated in Bulky mycelia and upregulated in Bulky conidiophores compared to corresponding cell types of the other two strains. This provides evidence that the Bulky strain is more metabolically responsive to unfavorable carbon sources, such as quinic acid. This hypothesis is upheld by our germination assay results, where conidia from Bulky conidiophores had higher germination rates and earlier germination times on medium containing mannose or xylose as a carbon source (Figure 3.2, Figure 3.3).

Comparisons between strain pairs revealed five loci consistently upregulated in Bulky, four of which are involved in communication: *doc-1*, *doc-2*, *plp-1*, and *plp-2*. The

doc genes identify communication group compatibility prior to hyphal fusion, and the *plp* genes trigger germling-regulated death following an incompatible fusion (Heller et al, 2016; Heller et al, 2018). We did not find a correlation between communication group assignment and conidiophore phenotype. It is reasonable to suppose that more communication takes place in the Bulky conidiophore, where there is a higher density of cells than in WT or Wrap. Enrichment of these *doc* and *plp* genes could simply be a result of this increased communication. Alternatively, the Bulky strain may be more heterokaryotic than the WT or Wrap strain, requiring more communication and germling-regulated death following heterokaryon incompatibility. This hypothesis is supported by the fact that this Bulky strain has lower penetrance of the phenotype (46.55%) than the WT (77.78%) and Wrap (53.85%) strains selected for RNA-Seq (Krach et al, 2020). To test this hypothesis, RNA-Seq could be conducted on homokaryotic F1s representing each conidiophore phenotype.

Identifying genes differentially expressed in just the conidiophore samples revealed many of the same loci differentially expressed according to both cell type and strain (Figure 3.7, Figure 3.11). Among the fourteen shared loci are *ccg-2*, *ccg-1*, *ccg-15*, *acu-6*, and NCU04482. This provides evidence that these genes were not solely identified by differences between cell types, but showed significant differential expression in the conidiophores and may play a role in the morphological differences observed. Analyzing differential expression patterns in the conidiophore samples did reveal two additional loci: *con-6* and NCU00265. Bulky conidiophores showed much lower expression of *con-6* and higher expression of NCU00265 than WT and Wrap conidiophores. While *con-6* has been well characterized as a light-responsive, clock-controlled, conidiation-specific gene, *Δcon-*

6 shows no obvious phenotype and the function of the CON-6 protein remains unknown (White and Yanofsky 1993; Olmedo et al 2010). Additional work should be conducted to characterize the function of this protein and explore the possible connection of *con-6* down-regulation and a Bulky phenotype. Further research should also be conducted on NCU00265 to better identify and characterize the predicted secreted protein it encodes. This protein has been detected alongside known cell wall proteins following their secretion by hyphae into growth medium (Maddi and Free, 2020). If NCU00265 does encode a cell wall protein that is enriched in Bulky conidiophores, it provides additional evidence, alongside *ccg-2* and *ccg-14*, that the Bulky phenotype may in part be due to a difference in its cell wall components.

High-throughput phenotyping has been recently applied in other fungal systems, such as *Saccharomyces cerevisiae*, to attribute genes to novel morphological phenotypes (Ohya et al, 2005). This study illustrates how high-throughput methods of phenotyping complex traits using machine learning applied to natural populations can be successfully combined with omics approaches, such as RNA-Seq, to implicate the genes underlying complex traits. These studies not only provide insights into the genetic basis of complex traits in natural populations, but they also provide potential insights into the robustness of genetic systems to both environmental and genetic perturbations (Levy and Siegal, 2008).

Acknowledgments

We acknowledge Mary E. Case for contributing feedback on the sporulation and germination assays and Leidong Mao for providing access to the microscope. We thank the Georgia Genomics and Bioinformatics Core for library preparation and sequencing.

References

Asmussen, M. A., J. Arnold, and J. C. Avise. 1987. 'Definition and properties of disequilibrium statistics for associations between nuclear and cytoplasmic genotypes', *Genetics*, 115: 755-68.

Bailey-Shrode, L., and D. J. Ebbole. 2004. 'The fluffy gene of Neurospora crassa is necessary and sufficient to induce conidiophore development', *Genetics*, 166: 1741-9.

Bell-Pedersen, D., J. C. Dunlap, and J. J. Loros. 1992. 'The Neurospora circadian clock-controlled gene, ccg-2, is allelic to eas and encodes a fungal hydrophobin required for formation of the conidial rodlet layer', *Genes Dev*, 6: 2382-94.

Carrillo, A. J., P. Schacht, I. E. Cabrera, J. Blahut, L. Prudhomme, S. Dietrich, T. Bekman, J. Mei, C. Carrera, V. Chen, I. Clark, G. Fierro, L. Ganzen, J. Orellana, S. Wise, K. Yang, H. Zhong, and K. A. Borkovich. 2017. 'Functional Profiling of Transcription Factor Genes in Neurospora crassa', *G3 (Bethesda)*, 7: 2945-56.

Case, M. E., J. Griffith, W. Dong, I. L. Tigner, K. Gaines, J. C. Jiang, S. M. Jazwinski, and J. Arnold. 2014. 'The aging biological clock in Neurospora crassa', *Ecol Evol*, 4: 3494-507.

David, Herbert Aaron. 1981. *Order statistics* (J. Wiley: New York; Toronto).

Davis, Rowland H., and Frederick J. de Serres. 1970. '[4] Genetic and microbiological research techniques for Neurospora crassa.' in, *Methods in Enzymology* (Academic Press).

Dobzhansky, T., and S. Wright. 1943. 'Genetics of Natural Populations. X. Dispersion Rates in Drosophila Pseudoobscura', *Genetics*, 28: 304-40.

Flavell, R. B., and J. R. Fincham. 1968. 'Acetate-nonutilizing mutants of Neurospora rassa. II. Biochemical deficiencies and the roles of certain enzymes', *Journal of bacteriology*, 95: 1063-68.

Greenwald, C. J., T. Kasuga, N. L. Glass, B. D. Shaw, D. J. Ebbole, and H. H. Wilkinson. 2010. 'Temporal and spatial regulation of gene expression during asexual development of Neurospora crassa', *Genetics*, 186: 1217-30.

Guo, Y., S. Zhao, C. I. Li, Q. Sheng, and Y. Shyr. 2014. 'RNAseqPS: A Web Tool for Estimating Sample Size and Power for RNAseq Experiment', *Cancer Inform*, 13: 1-5.

Hamrick, J. L., and Dorset W. Trapnell. 2011. 'Using population genetic analyses to understand seed dispersal patterns', *Acta Oecologica*, 37: 641-49.

Heller, J., J. Zhao, G. Rosenfield, D. J. Kowbel, P. Gladieux, and N. L. Glass. 2016. 'Characterization of Greenbeard Genes Involved in Long-Distance Kind Discrimination in a Microbial Eukaryote', *PLoS Biol*, 14: e1002431.

Heller, Jens, Corinne Clavé, Pierre Gladieux, Sven J. Saupe, and N. Louise Glass. 2018. 'NLR surveillance of essential SEC-9 SNARE proteins induces programmed cell death upon allorecognition in filamentous fungi', *Proceedings of the National Academy of Sciences*, 115: E2292-E301.

Jeong, Jun Seop, Thomas K. Mitchell, and Ralph A. Dean. 2007. 'The Magnaporthe grisea snodprot1 homolog, MSP1, is required for virulence', *FEMS Microbiology Letters*, 273: 157-65.

Kendall, Maurice, and Alan Stuart. 1979. *The advanced theory of statistics. Vol.2: Inference and relationship*.

Kolde, Raivo. 2018. 'pheatmap: Pretty Heatmaps'.

Krach, E. K., Y. Wu, M. Skaro, L. Mao, and J. Arnold. 2020. 'Wild Isolates of Neurospora crassa Reveal Three Conidiophore Architectural Phenotypes', *Microorganisms*, 8.

Lemke, Klaus. 1985. 'Dispersal Models for Drosophila', *M.S. Dissertation in Statistics. University of Georgia, Athens, GA.*

Levy, Sasha F., and Mark L. Siegal. 2008. 'Network Hubs Buffer Environmental Variation in Saccharomyces cerevisiae', *PLOS Biology*, 6: e264.

Loros, J. J., and J. C. Dunlap. 2001. 'Genetic and molecular analysis of circadian rhythms in Neurospora', *Annu Rev Physiol*, 63: 757-94.

Love, Michael I., Wolfgang Huber, and Simon Anders. 2014. 'Moderated estimation of fold change and dispersion for RNA-seq data with DESeq2', *Genome Biology*, 15: 550.

Maddi, Abhiram, and Stephen J. Free. 2010. 'α-1,6-Mannosylation of N-Linked Oligosaccharide Present on Cell Wall Proteins Is Required for Their Incorporation into the Cell Wall in the Filamentous Fungus Neurospora crassa', *Eukaryotic Cell*, 9: 1766-75.

Martin, Marcel. 2011. 'Cutadapt removes adapter sequences from high-throughput sequencing reads', *2011*, 17: 3.

Nelson, M. A., S. Kang, E. L. Braun, M. E. Crawford, P. L. Dolan, P. M. Leonard, J. Mitchell, A. M. Armijo, L. Bean, E. Blueyes, T. Cushing, A. Errett, M. Fleharty, M. Gorman, K. Judson, R. Miller, J. Ortega, I. Pavlova, J. Perea, S. Todisco, R. Trujillo, J. Valentine, A. Wells, M. Werner-Washburne, D. O. Natvig, and et al.

1997. 'Expressed sequences from conidial, mycelial, and sexual stages of Neurospora crassa', *Fungal Genet Biol*, 21: 348-63.

Nelson, R. E., C. P. Selitrennikoff, and R. W. Siegel. 1975. 'Mutants of Neurospora deficient in nicotinamide adenine dinucleotide (phosphate) glycohydrolase', *Journal of bacteriology*, 122: 695-709.

Ohya, Yoshikazu, Jun Sese, Masashi Yukawa, Fumi Sano, Yoichiro Nakatani, Taro L. Saito, Ayaka Saka, Tomoyuki Fukuda, Satoru Ishihara, Satomi Oka, Genjiro Suzuki, Machika Watanabe, Aiko Hirata, Miwaka Ohtani, Hiroshi Sawai, Nicolas Fraysse, Jean-Paul Latgé, Jean M. François, Markus Aebi, Seiji Tanaka, Sachiko Muramatsu, Hiroyuki Araki, Kintake Sonoike, Satoru Nogami, and Shinichi Morishita. 2005. 'High-dimensional and large-scale phenotyping of yeast mutants', *Proceedings of the National Academy of Sciences of the United States of America*, 102: 19015.

Olmedo, M., C. Ruger-Herreros, E. M. Luque, and L. M. Corrochano. 2010. 'A complex photoreceptor system mediates the regulation by light of the conidiation genes con-10 and con-6 in Neurospora crassa', *Fungal Genet Biol*, 47: 352-63.

Patel, Pavan K., and Stephen J. Free. 2019. 'The Genetics and Biochemistry of Cell Wall Structure and Synthesis in Neurospora crassa, a Model Filamentous Fungus', *Frontiers in Microbiology*, 10.

Powell, Jeffrey R., and Theodosius Dobzhansky. 1976. 'How Far Do Flies Fly? The effects of migration in the evolutionary process are approached through a series of experiments on dispersal and gene diffusion in Drosophila', *American Scientist*, 64: 179-85.

Sachs, M. S., and C. Yanofsky. 1991. 'Developmental expression of genes involved in conidiation and amino acid biosynthesis in Neurospora crassa', *Dev Biol*, 148: 117-28.

Sargent, M. L., and S. H. Kaltenborn. 1972. 'Effects of medium composition and carbon dioxide on circadian conidiation in neurospora', *Plant Physiol*, 50: 171-5.

Schmoll, Monika, Chaoguang Tian, Jianping Sun, Doris Tisch, and N. Louise Glass. 2012. 'Unravelling the molecular basis for light modulated cellulase gene expression - the role of photoreceptors in Neurospora crassa', *BMC genomics*, 13: 127-27.

Schneider, Caroline A., Wayne S. Rasband, and Kevin W. Eliceiri. 2012. 'NIH Image to ImageJ: 25 years of image analysis', *Nature Methods*, 9: 671-75.

Schumann, U., N. A. Smith, and M. B. Wang. 2013. 'A fast and efficient method for preparation of high-quality RNA from fungal mycelia', *BMC Res Notes*, 6: 71.

Springer, M. L., and C. Yanofsky. 1989. 'A morphological and genetic analysis of conidiophore development in Neurospora crassa', *Genes Dev*, 3: 559-71.

Tang, Xiaojia, Wubei Dong, James Griffith, Roger Nilsen, Allison Matthes, Kevin B. Cheng, Jaxk Reeves, H. Bernd Schuttler, Mary E. Case, Jonathan Arnold, and David A. Logan. 2011. 'Systems Biology of the qa Gene Cluster in Neurospora crassa', *PLOS ONE*, 6: e20671.

Trapnell, D. W., and J. L. Hamrick. 2005. 'Mating patterns and gene flow in the neotropical epiphytic orchid, Laelia rubescens', *Mol Ecol*, 14: 75-84.

White, B. T., and C. Yanofsky. 1993. 'Structural characterization and expression analysis of the Neurospora conidiation gene con-6', *Dev Biol*, 160: 254-64.

CHAPTER 4

CONCLUSIONS AND FUTURE DIRECTIONS

Conidiophore development in *N. crassa* has been thoroughly characterized over decades of study in the laboratory (reviewed in Park and Yu, 2012 and Ruger-Herreros and Corrochano, 2020). While much is known about the environmental, genetic, and circadian signals regulating this process, minimal work has explored the natural morphological variation of conidiophores, until now. Wild populations of *N. crassa* are readily available through the Fungal Genetics Stock Center and provide an excellent tool through which to study natural variation. The Louisiana collection is a particularly attractive tool as it shows no population subdivision, unlike other wild collections, and has been previously used to reveal environmental adaptations and uncover novel gene functions (Ellison et al, 2011; Ellison et al, 2014; Palma-Guerrero et al, 2013). We explored conidiophore morphological variation in this wild population collection of 21 strains, identifying three novel and distinct architectural phenotypes. These phenotypes were named Wild-Type (WT), Wrap, and Bulky, and were shown to be upheld throughout the duration of conidiophore development (Krach et al, 2020). While we did not find that conidiophore phenotype impacted the size or amount of conidia produced, it did affect sporulation distance. In our initial "spore shadow" experiment, the distribution of distances traveled by germinating Wrap conidia was shifted significantly leftward, suggesting a more contained dispersal pattern by this phenotypic group. We did not observe a clear relationship between primary conidiophore

phenotype and the site or substrate from which each strain was collected, suggesting a genetic component to this trait.

To estimate the heritability of conidiophore architecture, we first conducted crosses between wild isolates representing each phenotype and classified conidiophores of the resulting progeny. Doing this manually would be incredibly time-consuming while introducing bias. So, we developed an automatic image classifier specifically designed to assign conidiophore phenotype in a high-throughput manner. We used the resulting phenotype counts to fit a model for inheritance, indicating that at least two genes contributed to conidiophore morphology with an estimated heritability of 0.23. While this heritability was typical for quantitative traits (Falconer, 1981), it could be more robustly estimated by conducting crosses between homokaryotic strains. We addressed this concern in Chapter 3, where we conducted crosses with homokaryotic F1s representing each phenotypic group and quantified conidiophore phenotypes of the resulting progeny using the same image classification method. Using these counts to fit an inheritance model resulted in a much higher heritability estimate of 0.47.

In Chapter 3, we also conducted experiments to further evaluate the impact of conidiophore morphology on propagation of the *N. crassa* vegetative life cycle. We evaluated the "spore shadow" produced by each conidiophore phenotype at a larger scale, finding that the Wrap strain still exhibited a unique distribution of dispersal distances. We also observed that the maximum distance traveled and germinated by WT spores was less than that of the other two phenotypes. While these assays show that conidiophore morphology likely does affect sporulation reach, additional experiments should be conducted to assess this in different environments more reflective of the *N. crassa* natural

habitat (such as on plant substrates and/or in warmer temperatures). This would provide greater insight into how conidiophore architecture affects colonization capacity of the organism and thus the gene flow taking place between populations in nature (Dobzhansky and Wright, 1943). We then evaluated the impact of conidiophore architecture on subsequent germination of conidia, finding that the phenotypes responded differently to various carbon sources and concentrations of them. Decreasing the concentration of glucose and fructose by an order of magnitude resulted in a striking 52% jump in germination rate of conidia from only WT conidiophores. However, on medium containing mannose or xylose as a carbon source, conidia from Bulky conidiophores exhibited the more notable stress response. The Bulky conidia consistently germinated at least one day earlier and at significantly higher rates than conidia from the other two phenotypes, suggesting a greater sensitivity to these unfavorable conditions. Future work should seek to characterize germination behavior of the three conidiophore phenotypes under additional environmental perturbations, such as temperature variation or osmotic stress.

To identify genes differentially expressed in each conidiophore phenotype, we performed RNA-Seq on mycelia and conidiophores of a strain representing each phenotypic group. While we observed clear separation of cell type by PCA, as expected, we also found separation of the Bulky strain from the WT and Wrap strains, which clustered together. Some of the genes most differentially expressed in the Bulky group encode proteins that localize to the cell wall (*ccg-2*, *ccg-14*, and possibly NCU00265) (Bell-Pedersen et al, 1992; Jeong et al, 2007; Maddi and Free, 2020). This presented a hypothesis that the compactness of the Bulky phenotype could in part be due to a difference in cell wall composition, a phenomenon that has previously been observed in *N. crassa* cell

wall mutants (Patel and Free, 2019). Additional experiments should be conducted to better characterize the cell wall composition in conidiophores of each phenotype. Known cell wall mutants should also be screened for variation in their conidiophore morphology. Combined, these experiments would better illuminate the role that cell wall composition plays in conidiophore architectural variation.

Our RNA-Seq results also revealed differential expression of two genes implicated in starvation (*acu-6* and NCU04482) in the Bulky strain (Flavell and Fincham, 1968; Schmoll et al, 2012). Both loci were upregulated in Bulky conidiophores, providing additional evidence for the heightened sensitivity to metabolic stress we postulated from our germination assay results. We also observed differential expression of four genes involved in communication (*doc-1, doc-2, plp-1,* and *plp-2*) in the Bulky strain compared to both the WT and Wrap strains. Though the *doc* genes contribute to communication group recognition prior to hyphal fusion, we did not find a correlation between communication group assignment and primary conidiophore phenotype (Heller et al, 2016). The *plp* genes trigger germling-regulated death following an incompatible fusion (Heller et al, 2018). Taken together, enrichment of these four genes in the Bulky strain may just be due to increased communication taking place in a more densely populated environment. Alternatively, the Bulky strain selected for RNA-Seq could be more heterokaryotic than the WT and Wrap strains selected. While this could explain the lower penetrance of the Bulky phenotype compared to penetrance of the primary phenotype in the other two strains, heterokaryon incompatibility often results in slowed growth, altered hyphal morphology, and an aconidiate mycelium, alongside rapid cell death (Saupe, 2000; Glass and Kaneko, 2003). We did not observe any of these characteristics in the Bulky

cultures. Lastly, the gene *con-6* was downregulated in Bulky conidiophores. While *con-6* is recognized as a conidiation-specific gene under clock control, *Δcon-6* shows no obvious phenotype and the function of the CON-6 protein remains unknown (White and Yanofsky 1993; Olmedo et al 2010). Future studies should seek to characterize the function of this protein to better understand how its downregulation may be related to a Bulky phenotype.

To our knowledge, this dissertation work is the first investigation into natural morphological variation of *N. crassa* conidiophores, and the first report of the WT, Wrap, and Bulky conidiophore phenotypes. It would be beneficial to extend this study into other wild populations to determine whether these architectural phenotypes are found elsewhere, and if additional morphological phenotypes exist. Differences in environmental conditions and organism life histories could provide critical insight into how and why these phenotypes evolved. In general, there is a need to incorporate observations of natural variation into model organism biology, particularly when exploring complex traits like the conidiophore (Gasch et al, 2016). This study illustrates how a survey on natural variation can be combined with high-throughput phenotyping and transcriptomics to implicate genes underlying a complex trait in nature. Not only does this work explore the genetic basis of conidiophore morphology, but it also provides potential insight into the robustness of this variation to both environmental and genetic perturbations. Together, these findings help us to better understand how natural variation of conidiophore morphology impacts colonization capacity in the wild, and potentially, if conserved in other filamentous fungi, presents a novel opportunity through which to target pathogenicity.

References

Bell-Pedersen, D., Dunlap, J. C., & Loros, J. J. (1992). The Neurospora circadian clock-controlled gene, ccg-2, is allelic to eas and encodes a fungal hydrophobin required for formation of the conidial rodlet layer. *Genes Dev, 6*(12a), 2382-2394. doi:10.1101/gad.6.12a.2382

Dobzhansky, T., & Wright, S. (1943). Genetics of Natural Populations. X. Dispersion Rates in Drosophila Pseudoobscura. *Genetics, 28*(4), 304-340. doi:10.1093/genetics/28.4.304

Ellison, C. E., Hall, C., Kowbel, D., Welch, J., Brem, R. B., Glass, N. L., & Taylor, J. W. (2011). Population genomics and local adaptation in wild isolates of a model microbial eukaryote. *Proc Natl Acad Sci U S A, 108*(7), 2831-2836. doi:10.1073/pnas.1014971108

Ellison, C. E., Kowbel, D., Glass, N. L., Taylor, J. W., & Brem, R. B. (2014). Discovering functions of unannotated genes from a transcriptome survey of wild fungal isolates. *mBio, 5*(2), e01046-01013. doi:10.1128/mBio.01046-13

Falconer, D. S. (1981). Introduction to Quantitative Genetics.

Flavell, R. B., & Fincham, J. R. (1968). Acetate-nonutilizing mutants of Neurospora rassa. II. Biochemical deficiencies and the roles of certain enzymes. *Journal of bacteriology, 95*(3), 1063-1068. doi:10.1128/jb.95.3.1063-1068.1968

Gasch, A. P., Payseur, B. A., & Pool, J. E. (2016). The Power of Natural Variation for Model Organism Biology. *Trends in genetics : TIG, 32*(3), 147-154. doi:10.1016/j.tig.2015.12.003

Glass, N. L., & Kaneko, I. (2003). Fatal attraction: nonself recognition and heterokaryon incompatibility in filamentous fungi. *Eukaryotic Cell, 2*(1), 1-8. doi:10.1128/EC.2.1.1-8.2003

Heller, J., Zhao, J., Rosenfield, G., Kowbel, D. J., Gladieux, P., & Glass, N. L. (2016). Characterization of Greenbeard Genes Involved in Long-Distance Kind Discrimination in a Microbial Eukaryote. *PLoS Biol, 14*(4), e1002431. doi:10.1371/journal.pbio.1002431

Jeong, J. S., Mitchell, T. K., & Dean, R. A. (2007). The Magnaporthe grisea snodprot1 homolog, MSP1, is required for virulence. *FEMS Microbiology Letters, 273*(2), 157-165. doi:10.1111/j.1574-6968.2007.00796.x

Krach, E. K., Wu, Y., Skaro, M., Mao, L., & Arnold, J. (2020). Wild Isolates of Neurospora crassa Reveal Three Conidiophore Architectural Phenotypes. *Microorganisms, 8*(11). doi:10.3390/microorganisms8111760

Maddi, A., & Free, S. J. (2010). α-1,6-Mannosylation of N-Linked Oligosaccharide Present on Cell Wall Proteins Is Required for Their Incorporation into the Cell Wall in the Filamentous Fungus Neurospora crassa. *Eukaryotic Cell, 9*(11), 1766-1775. doi:doi:10.1128/EC.00134-10

Olmedo, M., Ruger-Herreros, C., Luque, E. M., & Corrochano, L. M. (2010). A complex photoreceptor system mediates the regulation by light of the conidiation genes con-10 and con-6 in Neurospora crassa. *Fungal Genet Biol, 47*(4), 352-363. doi:10.1016/j.fgb.2009.11.004

Palma-Guerrero, J., Hall, C. R., Kowbel, D., Welch, J., Taylor, J. W., Brem, R. B., & Glass, N. L. (2013). Genome Wide Association Identifies Novel Loci Involved in Fungal

Communication. *PLOS Genetics, 9*(8), e1003669. doi:10.1371/journal.pgen.1003669

Park, H. S., & Yu, J. H. (2012). Genetic control of asexual sporulation in filamentous fungi. *Curr Opin Microbiol, 15*(6), 669-677. doi:10.1016/j.mib.2012.09.006

Patel, P. K., & Free, S. J. (2019). The Genetics and Biochemistry of Cell Wall Structure and Synthesis in Neurospora crassa, a Model Filamentous Fungus. *Frontiers in Microbiology, 10*(2294). doi:10.3389/fmicb.2019.02294

Ruger-Herreros, C., & Corrochano, L. M. (2020). Conidiation in Neurospora crassa: vegetative reproduction by a model fungus. *International Microbiology, 23*(1), 97-105. doi:10.1007/s10123-019-00085-1

Saupe, S. J. (2000). Molecular genetics of heterokaryon incompatibility in filamentous ascomycetes. *Microbiology and molecular biology reviews : MMBR, 64*(3), 489-502. doi:10.1128/MMBR.64.3.489-502.2000

Schmoll, M., Tian, C., Sun, J., Tisch, D., & Glass, N. L. (2012). Unravelling the molecular basis for light modulated cellulase gene expression - the role of photoreceptors in Neurospora crassa. *BMC genomics, 13*, 127-127. doi:10.1186/1471-2164-13-127

White, B. T., & Yanofsky, C. (1993). Structural characterization and expression analysis of the Neurospora conidiation gene con-6. *Dev Biol, 160*(1), 254-264. doi:10.1006/dbio.1993.1303